Micro-Scale Flood Hazard Assessment in Phnom Penh, Cambodia

Miss Naichy Sea

จุฬาลงกรณ์มหาวิทยาลัย
CHULALONGKORN UNIVERSITY

A Thesis Submitted in Partial Fulfillment of the Requirements
for the Degree of Master of Engineering in Water Resources Engineering
Department of Water Resources Engineering
Faculty of Engineering
Chulalongkorn University
Academic Year 2018
Copyright of Chulalongkorn University

การประเมินภัยน้ำท่วมในพื้นที่ขนาดเล็กในพนมเปญ ประเทศกัมพูชา

น.ส.นายชี ซี

Thesis Title   Micro-Scale Flood Hazard Assessment in Phnom Penh,
                      Cambodia
By   Miss Naichy Sea
Field of Study   Water Resources Engineering
Thesis Advisor   Assistant Professor Supattra Visessri, Ph.D.
Thesis Co Advisor   Sokchhay Heng, Ph.D.

        Accepted by the Faculty of Engineering, Chulalongkorn University in Partial
Fulfillment of the Requirement for the Master of Engineering

                                               Dean of the Faculty of Engineering
        (Professor SUPOT TEACHAVORASINSKUN, D.Eng.)

THESIS COMMITTEE
                                               Chairman
        (Assistant Professor Anurak Sriariyawat, Ph.D.)
                                               Thesis Advisor
        (Assistant Professor Supattra Visessri, Ph.D.)
                                               Thesis Co-Advisor
        (Sokchhay Heng, Ph.D.)
                                               Examiner
        (Pongsak Suttinon, Ph.D.)
                                               External Examiner
        (Assistant Professor Chaiwat Ekkawatpanit, Ph.D.)

จุฬาลงกรณ์มหาวิทยาลัย
CHULALONGKORN UNIVERSITY

นายซี ซี : การประเมินภัยน้ำท่วมในพื้นที่ขนาดเล็กในพนมเปญ ประเทศกัมพูชา. (Micro-Scale Flood Hazard Assessment in Phnom Penh, Cambodia) อ.ที่ปรึกษาหลัก : สุภัทรา วิเศษศรี, อ.ที่ปรึกษาร่วม : ซกเซย์ เฮง

  ภัยน้ำท่วมเป็นพิบัติด้านน้ำที่พบในเขตเมืองซึ่งเกิดขึ้นบ่อยครั้งและทวีความรุนแรงมากยิ่งขึ้นเรื่อยๆ ก่อให้เกิดความเสียหายต่อชีวิตและทรัพย์สิน โครงสร้างการพัฒนา การดำเนินธุรกิจ รวมถึงการประกอบกิจกรรมในชีวิตประจำวัน พนมเปญเป็นเมืองหลวงของประเทศกัมพูชาซึ่งประสบเหตุการณ์น้ำท่วมครั้งใหญ่ในช่วงฤดูฝนอยู่บ่อยครั้ง และยังมีความเสี่ยงในการเผชิญภัยพิบัติด้านน้ำในปัจจุบันและอนาคตหากยังไม่มีมาตรการป้องกันและบรรเทาภัยน้ำท่วมรวมถึงการบริหารจัดการที่เหมาะสม การใช้แบบจำลองน้ำท่วมเพื่อการวิเคราะห์และสร้างแผนที่ภัยน้ำท่วมเป็นวิธีหนึ่งที่ช่วยให้เห็นภาพความรุนแรงของภัยน้ำท่วมได้ง่ายขึ้นและเป็นข้อมูลสนับสนุนการบริหารจัดการและการวางแผนการใช้ที่ดิน เพื่อจำกัดการพัฒนาในพื้นที่ที่มีความเสี่ยงต่อภัยน้ำท่วม การศึกษานี้มีจุดมุ่งหมายเพื่อจำลองเหตุการณ์น้ำท่วมในตัวเมืองพนมเปญ โดยใช้แบบจำลอง FLO-2D การสอบเทียบและตรวจสอบแบบจำลองโดยใช้ข้อมูลระดับน้ำตรวจวัดในปี พ.ศ.2561 และการประมาณความสูงของระดับน้ำท่วมจากภาพถ่ายที่ได้จากสื่อสังคมออนไลน์ในปี พ.ศ.2558 พบว่า แบบจำลองมีสามารถจำลองเหตุการณ์น้ำท่วมอยู่ในระดับที่ยอมรับได้ โดยมีค่า NSE, RMSE และ R^2 เท่ากับ 0.76, 0.13 และ 0.91 ตามลำดับ แบบจำลองที่สอบเทียบแล้วถูกนำไปใช้จำลองการไหลในทางน้ำพื้นที่น้ำท่วม และความสูงน้ำท่วมโดยใช้รอบการเกิดซ้ำของปริมาณฝน 2, 5, 10 และ 25 ปี สำหรับช่วงเวลาน้ำท่วมนั้น จะกำหนดจากการซ้อนทับของแผนที่น้ำท่วมที่พิจารณาจาก 3 ช่วงเวลาของไฮโดรกราฟ ได้แก่ ช่วงเพิ่มขึ้น ช่วงสูงสุด ช่วงลดลง การสร้างแผนที่ภัยน้ำท่วมจะใช้นำผลจากการประเมินความสูงของระดับน้ำท่วมมาพิจารณาร่วมกับช่วงเวลาน้ำท่วมโดยแบ่งระดับของภัยเป็น 5 ระดับ ตั้งแต่ระดับต่ำมากถึงระดับสูงมาก ผลจากการวิเคราะห์ภัยน้ำท่วมพบว่า ภัยที่เกิดขึ้นในพื้นที่น้ำท่วมส่วนใหญ่อยู่ในระดับต่ำมากและมักจะพัฒนาระดับของภัยสูงขึ้นสู่กับในระดับกลางเมื่อจำลองด้วยรอบการเกิดซ้ำของฝนที่สูงขึ้น จากผลการวิเคราะห์พบว่า พื้นที่ที่มีความเสี่ยงต่อภัยน้ำท่วมสูงที่สุดอยู่บริเวณรอบสนามกีฬาโอลิมปิค รอบพระราชวังที่อยู่ริมแม่น้ำ และตำบลบึงตระแบก ผลจากแบบจำลองแสดงให้เห็นว่าระบบระบายน้ำที่มีอยู่สามารถรองรับน้ำท่วมในพื้นที่ศึกษาได้ที่รอบการเกิดซ้ำของปริมาณฝน 2 ปี

สาขาวิชา วิศวกรรมแหล่งน้ำ   ลายมือชื่อนิสิต ....
ปีการศึกษา 2561   ลายมือชื่อ อ.ที่ปรึกษาหลัก ....
                 ลายมือชื่อ อ.ที่ปรึกษาร่วม ....

6070407021 : MAJOR WATER RESOURCES ENGINEERING
KEYWORD: Floods, Urban floods, Flood hazard, FLO-2D, Phnom Penh, Flood event,
           Flood hazard index, IDF curve
           Naichy Sea : Micro-Scale Flood Hazard Assessment in Phnom Penh, Cambodia.
           Advisor: Asst. Prof. Supattra Visessri, Ph.D. Co-advisor: Sokchhay Heng, Ph.D.

Water-related disasters in urban area, especially urban floods have become more frequent and severe. This leads to loss of life, infrastructure damage, business interruption as well as difficulties in conducting daily activities. Phnom Penh, the capital city of Cambodia, has frequently experienced significant rainfall-flood events during rainy season. Without proper prevention and mitigation and management of urban drainage system, Phnom Penh is expected to confront with the current and future challenge of water-related disaster. To address this urban flood issue, flood modeling could be used to assess flood severity and make a visual representation of the urban flood hazard as basic information for land-use planning and limiting development in flood-prone areas. This study, therefore, aims to simulate flood events in a downtown area with the complex storm drainage system in Phnom Penh using FLO-2D model. The model was successfully calibrated and validated with time series data of water level in 2018 and estimated flood depth based on photo visualization through social media in 2015. The values of NSE, RMSE, and R^2 were 0.76, 0.13, and 0.91 respectively. After model calibration, the model was used to simulate the flood flow through the channels, and floodplain within the study area in terms of flooding depth for 2-, 5-, 10-, and 25-year return periods of rainfall. The flood duration was determined by overlaying three flooding maps considered based on hydrograph components: rising flood, peak flood, and receding flood map. The result was delineated into flood hazard map defined by five categories, ranging from very low to very high. The result of flood hazard assessment shows that the floodplain under very low hazard category is constantly the highest one among all categories. However, with higher return period the flooding area under very low hazard category decreases while other hazard categories increase, especially medium hazard category increases significantly. The areas were found to have highest level of hazard are areas around Olympic stadium, areas around Royal Palace (along the river side), and areas in Beoung Trabek district. Besides, the simulated results show that the drainage system improved by JICA is capable to deal with the flood problem from the rainfall of 2-year return period in the study area.

Field of Study:	Water Resources Engineering	Student's Signature ....
Academic Year:	2018	Advisor's Signature ....
		Co-advisor's Signature ....

ACKNOWLEDGEMENTS

TABLE OF CONTENTS

Page

จุฬาลงกรณ์มหาวิทยาลัย

CHULALONGKORN UNIVERSITY

LIST OF TABLES

จุฬาลงกรณ์มหาวิทยาลัย
CHULALONGKORN UNIVERSITY

LIST OF FIGURES

CHAPTER 1

INTRODUCTION

1.1 Background

Flooding is one of the most serious natural disasters in the world in terms of its frequency and severity. Due to the severe effect of climate change it is expected that flooding will occur more often and increase in magnitude in the future (Kvočka et al., 2016). In the world index, Cambodia ranked 9th among the most 15 disaster prone countries in the world (Birkmann et al., 2014). Furthermore, the rate of urbanization of Cambodia was the highest one in the region, averaging about 3.5% per year between 1990 and 2013. This rapid urbanization over the past two decades has brought severe water-related disaster to Cambodia's population. Phnom Penh capital, located at the confluence of the Mekong River, Tonle Sap River and Bassac River, is the political, economic and cultural center of Cambodia. According to recent studies of Phnom Penh, it was found that 42% of urban poor residents were affected by flooding from polluted water bodies (Meg, 2014), and 23% lived on the banks of rivers (Capital, 2012). Poor quality housing, lack of sanitation facilities and high rates of poverty are also characteristics of urban poor areas that increase their vulnerability to disasters. More importantly, a network of wetlands, streams and ponds in Phnom Penh which are the temporary flood storage, are currently being filled with earth to create developable land (Shelby, 2012). Without proper mitigation and management of urban drainage system, Phnom Penh is expected to face with the current and future challenge of water-related disaster. In such context, Molyvann (2003) stated that the development with little planning or control resulted in flooding problems, informal settlement along drainage ways, increased landfill and poor urban infrastructure.

There are two significant cases of flood events in Phnom Penh – daily rainy season flood events and episodic larger scale flood plain events (Shelby, 2012). During rainy season, some low-lying streets are flooded with water level around 1.5 m deep adversely affecting normal daily lives, society, and environment. To deal with such problem, The Royal Government of Cambodia (RGC) made an urgent request to the

Government of Japan (GOJ) to formulate an integrated plan for urban drainage and flood control. The feasibility study of the flood control project was carried out between March 1998 and August 1999. Later, the Japan International Cooperation Agency (JICA) dispatched by GOJ has conducted over $325 million of infrastructure upgrades in Phnom Penh including drinking water supply facilities, flood protection, drainage improvements and the rehabilitation of the Phnom Penh port. As a result of JICA's work, flooding in some area of Phnom Penh has been decreased. However, it cannot be relied upon JICA's project outcome to eliminate all of Phnom Penh's drainage problems or to prevent future flooding in the areas developed without flood protection. Also, due to growing development of urban area, the improved drainage system and flood projection built approximately a decade ago are less likely to accommodate higher degree of flooding.

Since flood hazard, an estimation of the probability of flooding caused by particular intensity over a period of time (Wright, 2015), plays an important role in supporting for a range of decision-making process such as improving flood management, land-use planning, infrastructure design, and response planning, it is important to conduct flood hazard assessment to identify the priority areas for flood mitigation. Meanwhile, flood modeling, a technique of imitating a real flood phenomenon with a set of mathematical principles, can make a visual representation of the urban flood hazard as information basis for land-use planning, limiting development in flood-prone areas. In this study, FLO-2D, a flood modeling is used to simulate flood hazard.

1.2 Research questions

As indicated above, Phnom Penh, the capital city of Cambodia, has frequently experienced significant rainfall-events during rainy season. The flood hazard assessment framework in this study can be used as a guideline to identify the spatial and temporal distribution of flooding hazard in the study area. An attempt to answer following research questions will be carried out.

a. What are the flood parameters that can be used to represent the hazard in the study area?

b. Is flood modeling, FLO-2D, applicable to simulate flood in urban area in Phnom Penh?

c. What is the performance of improved storm drainage system and magnitude of flood under different return period of rainfall?

1.3 Objectives

The overall objective of this study is to evaluate flood hazard of flood events in a micro-scale in Phnom Penh. Detailed objectives contributing to the overall objective are:

a. To develop a flood hazard methodology for the selected area based on two parameters namely: flood depth, and flood duration

b. To calibrate FLO-2D model for simulating urban flood

c. To assess flood hazard under different magnitudes of flood

1.4 Scopes and limitations

The scopes of this study are:

a. Flood hazard assessments is carried out using the results from FLO-2D model.

b. Flood hazard assessment are done by considering two parameters: flood depth and flood duration and these two parameters are given equal influence.

c. Rainfall data used for this study are from two stations namely: Pochentong and ITC station which are located nearby the study area.

d. The rainfall data used in this study are daily data from Pochentong station (1985 – 2013) and 5-min data from ITC station (2010 – 2016).

The limitations of this study are:

a. Information of drainage system set up in the model is based on JICA's project design.

b. All storm drain inlets on the ground surface are assumed to be curb opening inlet type.

c. Groundwater is not included in modeling.

d. The initial flow in the pipe network conveyance is assumed to be zero.

e. This study was done based on polder system concept by assuming that the inflow to the study area is from the accumulation of rainfall within the study area only.

f. Average uniform rainfall is applied in the study area.

1.5 Expected outputs and outcomes

The expected outputs are:

a. Modeled flood depth and duration

b. Flood hazard maps for different return periods

The expected outcomes are:

a. Understanding the process of flood

b. Ability to produce flood hazard map

c. Ability to identify the area and the degree affected by floods.

CHAPTER 2
LITERATURE REVIEW

This chapter focuses on conducting a review of relevant knowledges, important information, and existing available tools and previous research studies which could possibly be applied to this thesis. In other words, carrying out a comprehensive literature review aims to deeply understand the facts of the problems and to explore practical techniques to deal with the matters. The main contents of this chapter are: flood perspective, urban rainfall-runoff, urban drainage system, urban modeling, model performance evaluation, and flood hazard assessment.

2.1 Flood perspectives

2.1.1 Flood definition

Many definitions exist for floods. Floods have defined as natural catastrophe resulting from rising of waterflow that exceeds river and reservoir capacities or a result in response to increasing in runoff from snowmelt or heavy rainfall in watershed (Burrel et al., 2007). According to Commission (2007) on the assessment and management of flood risk, flood is a state of the temporary covering by water of land not normally covered by water. Floods are included from rivers, mountain torrents, water courses, and floods from the sea in coastal areas, and may exclude floods from storm drain systems. Definition given by Ozga-Zielinska (1989) flood can be defined as a period when discharges Q are equal or larger than flood threshold Q_f (Figure 2-1) where threshold discharge is the acceptable flow, i.e. the highest discharge which still does not cause flood losses.

Based on the flood definitions above, the definition of Ozga-Zielinska (1989) was adopted in this study by considering the threshold flood depth instead of threshold discharge. However, the concept is the same. The flood is defined when the flood depth can cause damage and disturb human lives.
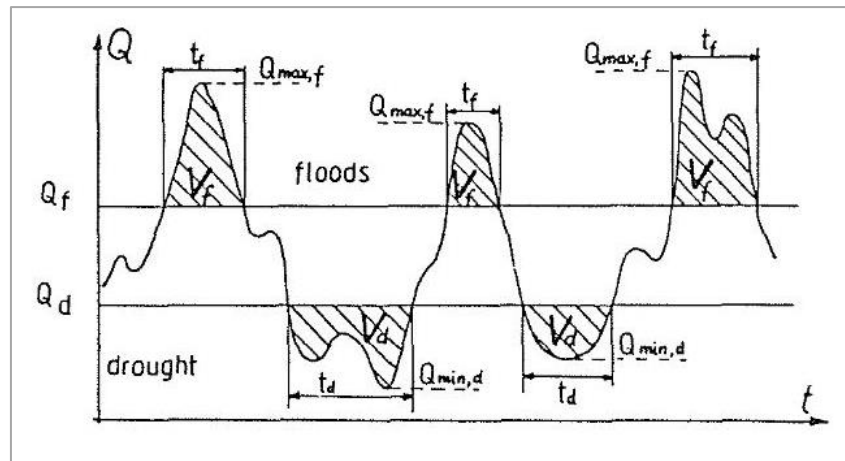
Figure 2-1: Flood and drought characteristics (Ozga-Zielinska, 1989)

2.1.2 Types of floods

Wright (2015) has divided floods into three main types: natural floods, coastal floods and anthropogenic floods (Figure 2-2) based on its causes. However, Ivan (2014) states that there are three main common flood types: coastal flood, fluvial flood, and pluvial flood.

Coastal flood which occurs in the area of low elevation coastal zone, is typically driven by the extreme sea level events, such as high tides, storm surge, and large waves. High tides known as "perigean spring tides" appear when the moon is at the closest point to the Earth. This phenomenon increases a few inches or approximately 20% to normal spring tides height. Storm surge is a large-scale of water level rise which is resulted from the variations of atmospheric pressure and wind circulation of hurricane or tropical cyclone moving towards the coastline. The result of coastal flooding will be more serious if high tides meet storm surge and/or large waves.

Fluvial flood called river flood is the result of intense rainfall causing water level in river exceeds its bank and overflows toward the floodplain. This kind of flood can be subdivided into two types: overbank flood and flash flood.

Pluvial flood is defined as rain-related flood which occurs when heavy rainfall cannot be drained by the drainage system and absorbed by soil into the ground. Generally, this kind of flood occurs in urban area lacking proper drainage network.

This study centers on modeling pluvial flood which commonly occurs in urban area.
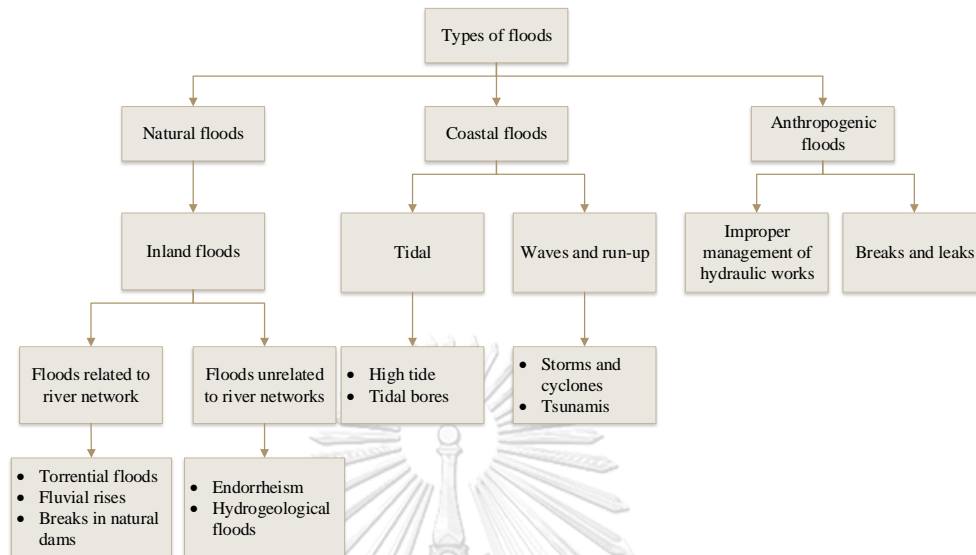
Figure 2-2: Types of floods (Wright, 2015)

2.2 Rainfall-runoff in urban environment

This part focusses on previous studies of the impact of urbanization on rainfall, important terms of rainfall, and hydrological processes starting from rainfall hyetograph up till the runoff hydrograph in urban environment.

2.2.1 Rainfall

Rainfall plays an important role in hydrology process especially in urban hydrology context, since it is the main driving contributor of creating runoff on the ground surface. Numerous studies attempted to evaluate the impact of urbanization on precipitation and found that the expansion of urban size tends to increase the spatial average air temperature (Takebayashi and Senoo, 2018). Sheebe and Alka (2016) conducted a study to prove that the temperature in cities is 5.6 °C higher than surrounding area. According to Salvadore et al. (2015), land use and land cover change with interaction of human activities effect energy balance, create urban heat island effect, and have impact on wind circulation. As a consequence, there is a significant change in rainfall pattern and rainfall intensity.

Not only does rainfall variation depend on time but rainfall also changes in space. Time and space parameters are inter-dependent (Loucks et al., 2005). The fact is that small changes exist when the time is short, and the scale is small. However, the changes become bigger when time and scale increase. More importantly, Loucks et al. (2005) also stated that the great size of rainfall cells connected with large weather system will extend storm period and minor changes of rainfall intensity in space occurs in this case. In contrast, this spatial variation will be significant when short storms created by small rain cells pass quickly over the catchment. To interpret the statistics of rainfall depths, three parameters such as rainfall intensity, the length of the period over which rainfall intensity occurs, and the occurrence frequency in any particular year are used. Those parameters can be expressed in Intensity-Duration-Frequency (IDF) curves as shown in Figure 2-3. Intensity and duration are inversely related. It can be seen that increasing rainfall duration leads to decreasing rainfall intensity. Similar relationship is found between frequency and intensity; when rainfall event is less frequent, the intensity becomes more intense. IDF curves are common tool for creating hyetographs (design rainfall events) which can be used as the input for flood model simulation.
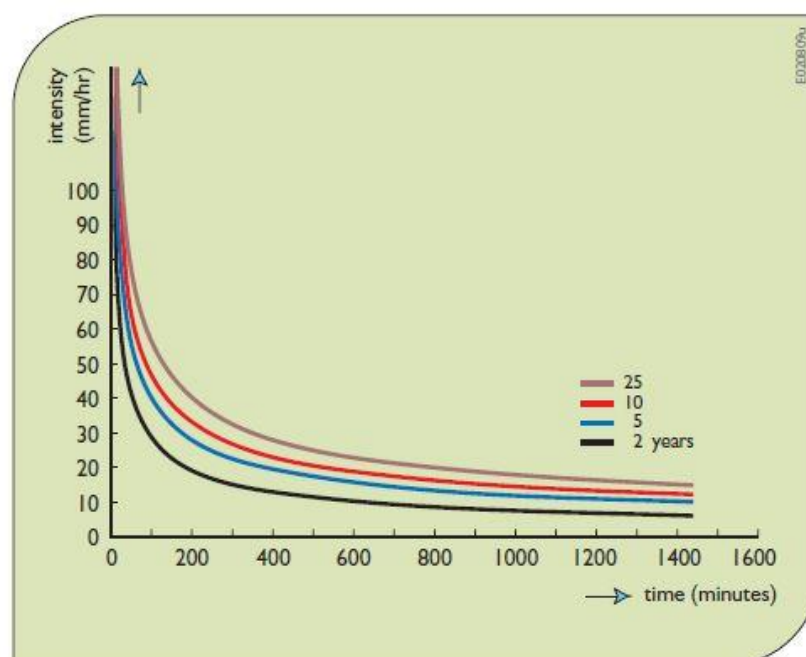
Figure 2-3: Rainfall Intensity-duration-frequency (IDF) curves (Loucks et al., 2005)

2.2.2 Urban rainfall-runoff processes

In urban area, the rainfall-runoff processes differ from those in rural area due to some conditions. The notable difference involves small spatial and temporal scales required for studying rainfall-runoff processes in urban area. Another difference is that the natural pathways of draining water in rural area is taken place by artificial one in urban area. Therefore, it implies that urban rainfall-runoff processes are more complicated than that in rural region since it is required site-specific data and rigorous principles to model surface runoff, and flow in storm drainage systems.

Before generating surface runoff or overland flow, rainfall normally loses through the interception, infiltration, and depression. The prediction of rainfall volume is crucial for obtaining streamflow data which is needed for various purposes such as water resources planning and disaster prevention and mitigation. Amount of runoff is strongly determined by rainfall and catchment characteristics. Hence, insufficiency of catchment physical data e.g. land use, land cover, slope data, soil condition, etc. may lead to high uncertainty in runoff prediction. Figure 2-4 shows urban rainfall-runoff processes starting from rainfall hyetograph up to the runoff hydrograph in urban environment.
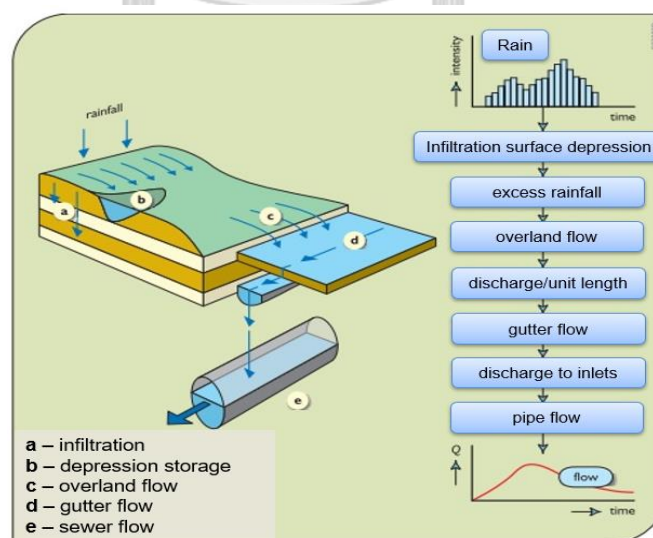
Figure 2-4: Schematic representation of urban rainfall-runoff processes (Loucks et al., 2005)

Urbanization leading to expansion of impervious surfaces such as building, roads, and other paved areas is a main factor to reduce infiltration and increase significant amount of surface runoff. More importantly, due to the smooth surface and low permeability of impervious surfaces, these two factors tend to produce higher flow velocity, shorter lag time which result in higher flood peaks and lower baseflow in post-urbanized conditions (Lerner, 2002, Jacobson, 2011, Salvadore et al., 2015). Ragab et al. (2003), who investigated infiltration and runoff processes in three car parks, a road and a grass site in Crowmarsh Gifford, Wallingford, found that between 6% and 9% of rainfall infiltrates through the road surfaces, 21% - 24% of annual rainfall evaporates. The ratio of runoff to rainfall was found to be 0.7, 0.9 and 0.5 for annual, winter and summer respectively. Similarly, Ramier et al. (2011) conducted a research on the hydrological behavior on two street stretches over a 38 month-period and concluded that between 30% and 40% of cumulative rainfall became runoff losses which fell into evaporation around 20% and infiltration between 10% and 20%. i.e. rainfall was mainly transformed into runoff between 60% and 70%.

2.3 Role of drainage system

According to Butler and Davies (2004), two kinds of water in developed urban catchment: storm water and wastewater are produced by the interaction between human activities and natural water cycle processes. This interaction has two main forms: water is withdrawn from natural cycle to support water supply for human, and urban paved surfaces deflect rainwater away from natural drainage system and accelerate surface runoff simultaneously. Thus, drainage system is needed to deal with those types of water. Without drainage network, developed area would face too many issues such as pollution, damage, flooding, and further health threat caused by several kinds of water. In response to these problems, drainage system which is an artificial system taking the place of a natural one, is a key means to reduce effects to public health and environment.

2.4 Urban modeling

In cities, complicated hydraulic systems interacting mutually with heterogeneous and intensively disturbed soil make urban hydrology more complex and it is a must for an urban hydrologist to cope with. To understand and cover the whole system process, it is necessary to develop calculation methods and modeling techniques. Recently, urban hydrology and hydrodynamic models are significantly becoming the important and more commonly practiced tools to support for urban water resources management as well as for environmental assessment. However, it is highly challenging since urban catchments have very specific hydrologic nature and data used must be site specific, which is labor-intensive, costly and time-consuming (Niemczynowicz, 1999, Salvadore et al., 2015, Van de Ven, 1990).

Salvadore et al. (2015) reviewed 43 urban modeling approaches described in 58 publications in the period 1987-2014. The modeling approaches were classified based on spatial and temporal resolutions and grouped into 5 categories based on the spatial discretization as (1) lumped, (2) semi-distributed, (3) Hydrologic Response Unit (HRU) based, (4) grid-based spatially distributed, and (5) Urban Hydrological Element (UHE). However, based on main purpose and methodology of each model, those 43 analyzing modeling approaches can be fallen into 7 categories (Figure 2-5) including: (1) impervious cover and land-use change impact analysis, (2) conceptual integrated water balance, (3) inundation and floods protection, (4) storm drainage design, (5) urban soils and groundwater, (6) urban climate, and (7) integrated physically-based models. Table 2-1 summarizes the urban model characteristics and their limitations for each functional category.
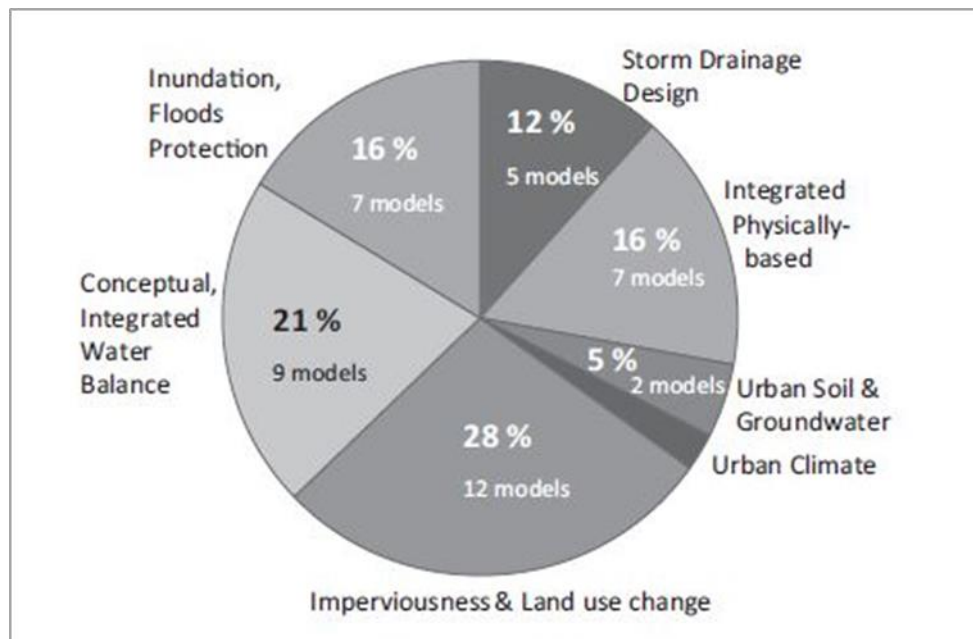
Figure 2-5: Seven functional categories based on approaches applied for defining the
urban environment (Salvadore et al., 2015)

Table 2-1: Main model characteristics and limitations of seven functional categories
approaches (Salvadore et al., 2015)

Model category	Characteristics	Limitations
(1) Impervious cover, Land use change	**MAIN PROCESSES**: Describing the process of urban infiltration and the generation of urban runoff in detail **PURPOSE**: Assessing the impact of land-cover change and comprehensive hydrological simulations **APPLICATION**: Catchment scale	Limited simulation of artificial systems (water supply, stormwater system, sewers, etc.) Simplification of groundwater principle and the urban soil properties
(2) Conceptual, Integrated Water Balance	**MAIN PROCESSES**: Simulating with a complete principle of artificial system, including leakage **PURPOSE**: Assessing pollution, Water resources management **APPLICATION**: Small city-scale	Theorical-empirical formulations, limited applicability for flood assessment and sub-surface water simulation Questionable application for big city-scale

Model category	Characteristics	Limitations
(3) and (4) Inundation, Flood Protection and Storm Drainage Design	**MAIN PROCESSES**: Comprehensive formulas of hydraulic approaches for surface runoff, storm drainage systems, sewers including pollutant simulation. **PURPOSE**: Simulating flood, designing storm drainage system **APPLICATION**: Small city-scale, localized phenomena	Limited treatment of natural hydrological phenomena; pipe leakage Constraint on simulation of water movement in the sub-soil Questionable application for big city-scale
(5) Urban Soils and Groundwater	**MAIN PROCESSES**: Describing the processes of sub-surface, "urban porosity", "urban transmissivity", physically-based leakage in detail **PURPOSE**: Assessing urban groundwater systems, pollutants **APPLICATION**: Small city-area	Limited evaluation of other processes of urban catchments; very specific purpose models; limited applicability Questionable application for big city-scale
(6) Urban climate	**MAIN PROCESSES**: Investigating urban rainfall and urban evapotranspiration. Describing energy balance in detail. **PURPOSE**: Energy balance, urban climate-evapotranspiration **APPLICATION**: Small to medium size catchment	No effect of urbanization on rainfall trends and intensity Lumped description for others hydrological processes
(7) Integrated Physically-based	**MAIN PROCESSES**: Describing the processes of urban hydrological, energy and water balance, physically based equations in detail, including subsurface **PURPOSE**: Assessing hydrological processes in urban catchments **APPLICATION**: Catchment scale, spatially-distributed	High complexity/uncertainty; data demanding; computational heavy; inconsistency of detail level of urban hydrological processes

Due to a large number of flood models, a few models that have widely been used in urban Asian context are reviewed here.

2.4.1 Storm Water Management Model (SWMM)

Storm Water Management Model (SWMM) is a rainfall-runoff model, which was first developed in 1979. It is widely used throughout the world for planning, analysis and design related to storm water runoff, combined sewers, sanitary sewers,

and other drainage systems in urban areas. It is an open-source computer model which can be used for single event or long-term simulations of water runoff quantity and quality primarily in urban areas (Rossman, 2015). SWMM also consists of a flexible set of hydraulic modeling capacities used to route runoff and external inflows through a drainage system network of pipes, channels, storage units and diversion structures. This model forms a drainage system as a series of water and material flows between several major environmental compartments. The compartments of this model are: atmosphere compartment, land surface compartment, groundwater compartment, and transport compartment.

Hsu et al. (2000) used SWMM model coupled with 2D diffusive overland-flow model to simulate urban inundation in the downtown of Taipei. SWMM was adopted for flow computation in storm sewer systems and surcharge flow at manholes in the study. The models were successfully calibrated and validated. To calibrate the model, Manning's roughness coefficient has been adjusted based on land use. Then, the model performance was inspected by comparing inundation zones of model simulation and surveyed inundation zones. Huong and Pathirana (2013) assessed future urban flooding driven by urbanization and climate change impact in Can Tho city, the biggest city in Mekong River Delta, Vietnam. A set of models were used in the study such as: land use simulation model, dynamic limited-area atmospheric model, and SWMM to estimate the change of flood hazard in the city. SWMM was utilized to compute storm-sewer surcharge and surface inundation as the result of the changes of rainfall and climate drivers.

2.4.2 FLO-2D

FLO-2D was developed in 1988 and first known as MUDFLOW. It was first used to simulate an urbanized alluvial flood in Colorado for Federal Emergency Management Agency (FEMA). It is a grid-based physical process model that routes rainfall-runoff and flood hydrographs. It is specifically initiated for delineating flood hazards, managing floodplain zoning or arranning flood mitigation of river overbanks flows and unconventional flooding problem such as unconfined flows surfaces and channel flow. The main utility of the model is for urban flood simulation with building,

streets, walls and storm drains. Figure 2-6 shows the physical processes used in FLO-2D.

Two main fundamental fluid motion equations: the continuity equation (Eq. 2-1) and the momentum equation (Eq. 2-2) are used as governing equations in FLO-2D:

$$\frac{\partial h}{\partial t} + \frac{\partial hV}{\partial x} = i \qquad \text{(Eq. 2-1)}$$

$$S_f = S_0 - \frac{\partial h}{\partial x} - \frac{V}{g}\frac{\partial V}{\partial x} - \frac{1}{g}\frac{\partial V}{\partial t} \qquad \text{(Eq. 2-2)}$$

where: h = the flow depth

V = the average velocity

i = the excess rainfall intensity

S_f and S_0 = the friction bottom slope and bed slop respectively based on Manning's equation.
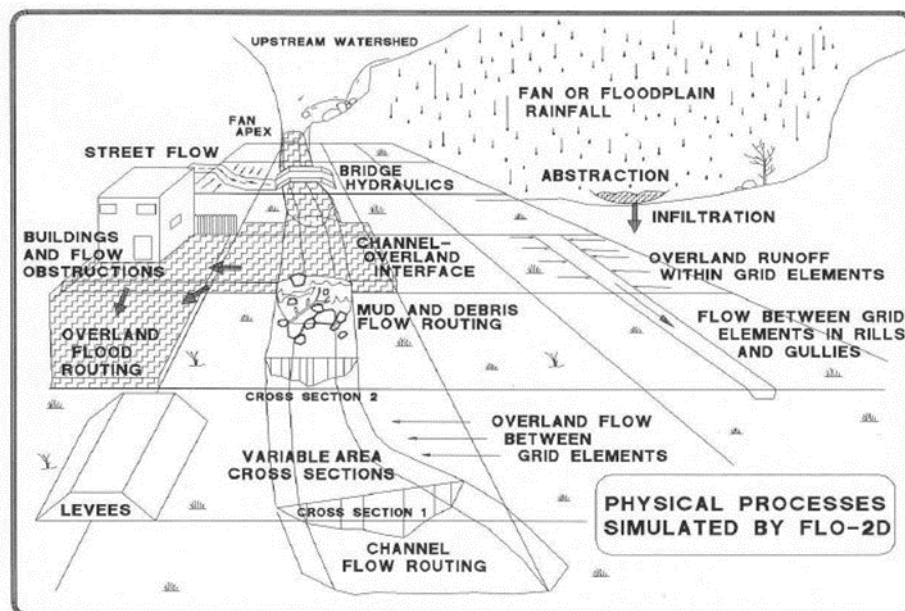
Figure 2-6: Physical processes simulated by FLO-2D (O'Brien, 2009)

The package of FLO-2D software includes a QGIS Plugin Tool, a grid developer system (GDS), a MAPPER++ program and two other processor programs PROFILES and MAXPLOT. The QGIS plugin tool is used to integrate GIS for generating the FLO-2D data files and mapping the model results. The GDS will interpolate the DTM data and spatially develop grid system attributes. MAPPER++ program is used to create flood hazard map delineation and meanwhile the PROFILE and MAXPLOT program corrects channels slope and cross section shape.

Heng et al. (2017) used FLO-2D modeling to simulate flood condition in a downtown in Phnom Penh capital, Cambodia. The flood hazard map was produced based on flood depth. FLO-2D modeling with the grid system of cell size of 30 m x 30 m was used to visualize the computational domain. However, there was no historical flood data to calibrate and validate the model. To deal with such issue, the observed inundation information from JICA team survey (JICA, 2011) and the flood photo visualization obtained from social media such as Facebook, were used to verify overall performance of the model. Moreover, effect of climate change on future annual maximum precipitation was also predicted in the study. The result showed that the inundated water depth is likely to increase between 0.2 m to 0.5 m in the submerged area and spread over the study area in the near future.

Liao and Chang (2011) conducted a research of evaluating the vulnerability of urban flooding based on spatial pattern in Ecological City, Taiwan. The FLO-2D model was firstly utilized to figure out four urban inundation situations in terms of flood depth and flood velocity. Then, geographic information system (GIS) and explore spatial data analysis (ESDA) were used to compare and discuss the degree of flooding based on spatial pattern.

2.4.3 MIKE FLOOD

MIKE FLOOD (DHI, 2017c) developed by the Danish Hydraulic Institute, is a dynamically coupled modeling system that integrates the one-dimensional model MIKE 11 and the two-dimensional model MIKE 21 into single model. MIKE 11 hydrodynamic model (DHI, 2017b) is able to compute spatial and temporal unsteady

flows, water quality in river, and water courses, channels, and other water bodies. This model solves the Saint-Venant equation employing an implicit, finite difference method. MIKE 21 hydrodynamic module (DHI, 2017a) is a tool used to simulate 2D free-surface flow and commonly applied for assessing hydraulic and environmental phenomena in estuaries, lakes, and coastal areas.

Keokhumcheng et al. (2012) conducted a study of flood risk assessment caused by direct rainfall occurring within the study area, in the region surrounding the Bangkok Suvarnabhumi Airport using the MIKE FLOOD hydrodynamic model in conjunction with a geographic information system (GIS). Two main parameters of flood characteristics are flood depth and flood duration were considered in the study to assess flood hazard and produced hazard maps. To assess the flood hazard, a Gumbel probability distribution was applied for rainfall frequency analysis and MIKE 11 and MIKE 21 hydrodynamic models with grid size 200 m x 200 m were set up for flood routing. More interestingly, once two main parameters flood depth and flood duration were calculated, hazard indicators of each parameter were assigned to represent the degree of flood hazard or severity of flood hazard.

In response to the disastrous effects of floods, Thai authorities: the Thai Ministry of Science and Technology, and Hydro Informatics Institute (HII) urged DHI to establish a flood forecasting and management decision support system (DSS) which consists of numerous models such as hydrological models, 1D hydraulic models, coupled 1D and 2D hydraulic models and water management models (Finn et al., 2018). To develop such complex DSS, MIKE OPERATIONS platform of DHI were employed. The MIKE FLOOD model, which was included in MIKE OPERATION platforms, is applied to model the flow between the river band and the floodplain. However, MIKE FLOOD model is considered as challenging tool in a real-time mode since it takes a long time to simulate. Thus, the hardware is considered with care to accelerate the speed of calculation.

2.5 Model selection

It is true that all computer models, which are explained previously have their own limitations. However, they are capable of visualizing and analyzing particular concerns based on their technical descriptions. To choose a proper model, user should select a capable tool in correlation with the study objectives and availability of resources such as data, computer specification, run time. More importantly, it must be well documented and has been used successfully by the practitioners.

FLO-2D model is chosen to reach the objectives in this study, particularly to simulate urban flood in calculating flood depth and flood duration. This model is chosen due to some subsequent reasons:

a. The model is applicable to simulate flooding in urban environment with complex system such as building, streets, walls and storm drains.

b. Track records of the model are well documented with the understandable user's and reference manuals.

c. The license of using this model is provided by Institute of Technology of Cambodia through the project "Elucidation and prediction of urban flooding and its health impact in Asian tropical cities" funded by JSPS Core-to-Core Program, B. Asia-Africa Science Platforms.

d. The model seems to be applicable in Phnom Penh city (study area), even though it was not yet calibrated and validated with historical data (Heng et al., 2017).

2.6 Model performance evaluation

To verify the reliability of mathematical models used for calculating variables or simulating processes in hydrological and other environmental sciences, it is required to perform calibration and validation procedure. Generally, model performance is evaluated by comparing the simulated values and the corresponding observed data by using some statistical error or goodness-of-fit indicators (Ritter and Muñoz-Carpena, 2013, Moriasi et al., 2007) such as Root Mean Square Error (RMSE), Nash-Sutcliff

Efficiency (NSE), Percent Bias (PBIAS), coefficient of determination (R^2). According to Ritter and Muñoz-Carpena (2013), the goodness-of-fit indicators are sometimes misinterpreted. This is due to the fact that, first, the information describing each indicator has different meanings; and second, there is no standard guideline for each indicator range values to state when model performance is acceptable, good or very good. Due to no absolute choices for evaluating the model performance, a few widely-used statistical indices i.e. NSE, RMSE, R^2 will be adopted for this study because they are widely used.

2.7 Flood hazard assessment

According to the report of Nations United (2010), hazard is defined as a natural process or phenomenon with adverse effects on life, health impact, property damage, loss of livelihood and services, and environmental damage. Hazards differ in severity, scale, and frequency and are often classified by causes such as hydro-meteorological or geological. Keokhumcheng et al. (2012) stated that flood hazard assessment is an estimation of the overall adverse effect of flooding, which depends on many parameters (flood depth, flood duration, etc.). One or more parameters can be taken into account, according to the characteristic of the study area and inundation floods.

The main steps to assess flood hazard (Wright, 2015) are: estimation of design rainfall by rainfall frequency analysis or rainfall-runoff modeling, and hydraulic modeling and floodplain mapping. Each step is described below:

Estimation of design rainfall: the two most commonly-applied principles are: statistical rainfall-frequency analysis and rainfall-runoff modeling. Rainfall-frequency analysis principle is applied to obtain the probable maximum precipitation that crosses a certain location during a flood while rainfall-runoff modeling is employed to create a design hydrograph past across a certain location over a period of time.

Statistical rainfall-frequency analysis principle depends on the existing long-term series data of rainfall measurements. Usually, annual maximum rainfall records are adopted in the analysis. For instance, if 30 years of daily rainfall data have been recorded and available at a particular rainfall station, then 30 data points corresponding

to annual maximum daily rainfall records, are used in the rainfall-frequency analysis. Once these data points have been determined, those data must be fitted with statistical distributions such as Gumbel, Log-Normal, Log-Pearson, or generalized extreme value and then choose the most fitted distribution.

Another principle is using rainfall-runoff models (hydrologic models) to produce design hydrographs converted from extreme rainfall. To do so, the water movement crossing the terrain or the process of runoff and flow into the channel, river or storm drains must be delineated. Numerous models used to simulate rainfall-runoff are available. Each model has their own advantages and disadvantages according to different factors such as data availability, application, and geographic.

Hydraulic model and floodplain mapping: once a design time series rainfall has been estimated, hydraulic model (hydrodynamic model) is applied to transform the design rainfall or design hydrograph into flood depth, flood velocity, flood duration, etc. Before, most of the models were small-scale physical models, but nowadays they change to be almost computer-based simulation software. The complexity of each hydraulic model is varied based on the data requirements. An experienced model user is capable to choose the most suitable model in accordance with the location, the demands of the risk assessment, and the available data.

There are two methods to run the hydraulic models based on the model application and the form of the input design discharge. In case the design discharge is a peak discharge estimate, a steady flow mode should be set up for the models. The steady flow mode is the least time-consuming mode from a simulation standpoint. However, this mode may not capture the complicated flow dynamics in complex surface such as urban floodplains. When the design discharge is a complete hydrograph, an unsteady mode should be selected for running the models. In this case, the discharge rates and water level throughout the model area can change over time. However, simulation in unsteady mode requires high computational resources, especially when 2D or 3D are applied.

2.8 Previous studies of urban flood and summary

Urban flooding becomes the major risk to many cities around the world. Many studies agree that the problem caused by urban floods is projected to increase in the future (Hammond et al., 2015). In the last decades, urban floods brought significant disruption to the city services and wider negative effects on population. This can be seen in the case of flooding in January 2011 in Brisbane, the state capital of Queensland, 23 people were killed in the Lockyer Valley and one in Brisbane, and an estimated 18,000 properties were inundated (van den Honert and McAneney, 2011). Another example is a massive flood in Thailand that inundated Bangkok during the 2011 monsoon season. This flood caused tremendous damage, including 813 dead nationwide, seven industrial estates, and 804 companies with inundation damage, and total losses estimated at 1.36 trillion baht (Komori et al., 2012). A similar case in Beijing in July 2012, a flash flooding caused by one of the heaviest rainfall in the past 60 years killed 79 people and caused US $2 billion in direct economic losses, destroying at least 8,200 homes in the city and affecting more than 1.6 million people (Huang et al., 2013). By the reason of the worst effect of urban floods, numerous studies were conducted to assess urban flood risk which is crucial for improving disaster mitigation options and economical optimizations of possible measures.

Arrighi et al. (2013) carried out a research of urban micro-scale flood risk estimation in the city of Florence, Italy, by using parsimonious hydraulic modeling and census data. The flood hazard assessment was conducted by hydrological analysis and hydraulic model composed by two parts: 1D unsteady flow model (HEC-RAS) for the river and a quasi-2D storage cell model for the urban flood prone area. In the study, the Digital Surface Model (DSM) was derived by lidar data with kriging and it is characterized by a horizontal resolution of 1 m x 1 m and a vertical accuracy of 0.15 m. Meanwhile, the flood damage estimated on structures, household contents and commercial contents, was calculated through stage-damage curve method.

Singh et al. (2018) conducted a research to assess potential impact of flooding on urban road in Bangalore capital of the state of Karnataka, India. The flood hazard map produced in terms of flood depth and flood velocity, was obtained by using 2D

hydrodynamic model MIKE 21 while flood vulnerability of the urban road network was estimated by applying safety speed to flood water depth curve. The vulnerability curve of safety speed to flood water depth here means that the speed of vehicles will reduce due to increase in flood water depth and the amount of reduction is based on safety factor derived from experimental data and expert judgement accordingly for Indian context. This study gave a narrative where tangible and intangible losses can be quantified with limited data.

According to JICA (2011), to learn of inundation situation of the project for flood protection and drainage improvement for Phase III, interview survey with the Sangkat (commune) chiefs and households in the project study (the Trabek Basin and the adjacent areas of Wat Phnom Basin, Central Market, and the Royal Palace and National Museum) was carried out. The result of survey could provide information of flood hazard and sanitary condition across study area. Later, simulation model under scenarios with and without retention pond was set up to analyze inundation situation in the same project area of Phase III (JICA, 2016). Then, the flood hazard map of flood water level was obtained. The result showed that flood condition was worse especially at the south of the Olympic Stadium. Even though 3 projects of JICA's work have been completely done, serious floods in some areas still occur. Therefore, the Project for Flood Protection and Drainage Improvement in Phnom Penh (Phase IV) is implemented. In this project case, JICA (2017) used coupling model of MOUSE and MIKE 21 to simultaneously compute flow in sewer, drainage system and surface flow. It is noted that hyetograph of design rainfall intensity used as input in the model is based on IDF curves created by JICA since 1997.

Based on literature of urban flood simulation in Phnom Penh, JICA has produced hazard maps according to each project areas. However, only hazard maps as the function of flood depth were produced, there is no a methodology developed for flood hazard maps as the function of two combination of two parameters: flood depth and flood duration yet. In the view of the gap, the assessment of flood hazard as the function of flood depth and flood duration is carried out in this study. The design rainfall adopted in this study is created with new IDF developed by rainfall ratio method.

CHAPTER 3
STUDY AREA

This chapter describes the characteristics of the selected study area, the drainage system in Phnom Penh, pump stations, channel, and ground surface characteristics in the study area.

3.1 Study area

The capital city of Cambodia, Phnom Penh, covers an area of 678 km^2 and is home of population of 2.2 million (NIS, 2017). It is spread out over a flat alluvial floodplain where an intersection of the Mekong River, Tonle Sap River and Bassac River crosses each other. This intersection is called "Four Faces or Chaktomuk". The gradient feature of Phnom Penh is slightly inclined from north to south and from west to east. The overall elevation difference of the city is around 10 m where the high land area with elevation of 14 m is situated at Pochentong Airport and the low land with elevation 4 m is at Tumpun area. Phnom Penh capital city is governed by tropical monsoon climate. The annual average rainfall from 1985 to 2013 is around 1,414 mm. The difference in annual rainfall is high where the maximum was 2,150 mm in 2000 and the minimum was 1,100 mm in 2006. Figure 3-1 presents the annual rainfall from 1985 to 2013 and 5-year moving average, suggests a slight increasing trend of annual rainfall in Phnom Penh city.
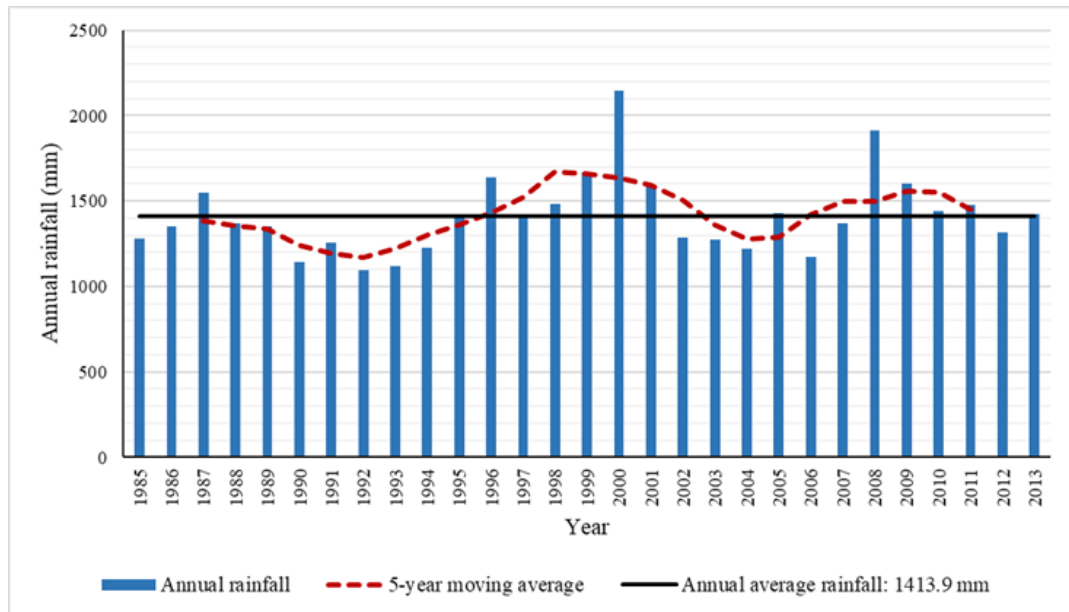
Figure 3-1: Annual rainfall of Pochentong station (1985-2013) and 5-year moving average

An independent catchment in Phnom Penh city covering an area of 12.5 km^2 as shown in Figure 3-2 is selected for this study. This area consists of residences, commercial companies, roads and many municipal administrations such as Royal Palace, Olympic Stadium and embassies and it is adjacent to the Tonle Sap River at the east. The land use for the study area is divided into road, building, and open spaces. As described earlier, water is drained from the north to south to the Beoung Trabek Station, P1, and from west to east. Since the elevation at the outfall is higher, water is pumped out by four pumping stations located as shown in Figure 3-2.

Flood simulation in this study is carried out based on the polder system concept by assuming that the inflow to the study area is from the accumulation of rainfall within the study area only. A polder is known as a lowland area prevented the inflow from outside by dikes or embankments, that forms an artificial hydrological system (Segeren, 1983). Thus, the selected area is considered as polder system since it is protected from overflow from rivers by natural levees along the Mekong/Sap River at eastern part and Tumpun Dike at southern part. The boundary at northern part and western part are Russian Federation Boulevard and Yothapol Khmarak Phoumin Boulevard,

accordingly. The elevation of the boulevards is relatively high preventing the inflow from neighboring areas.
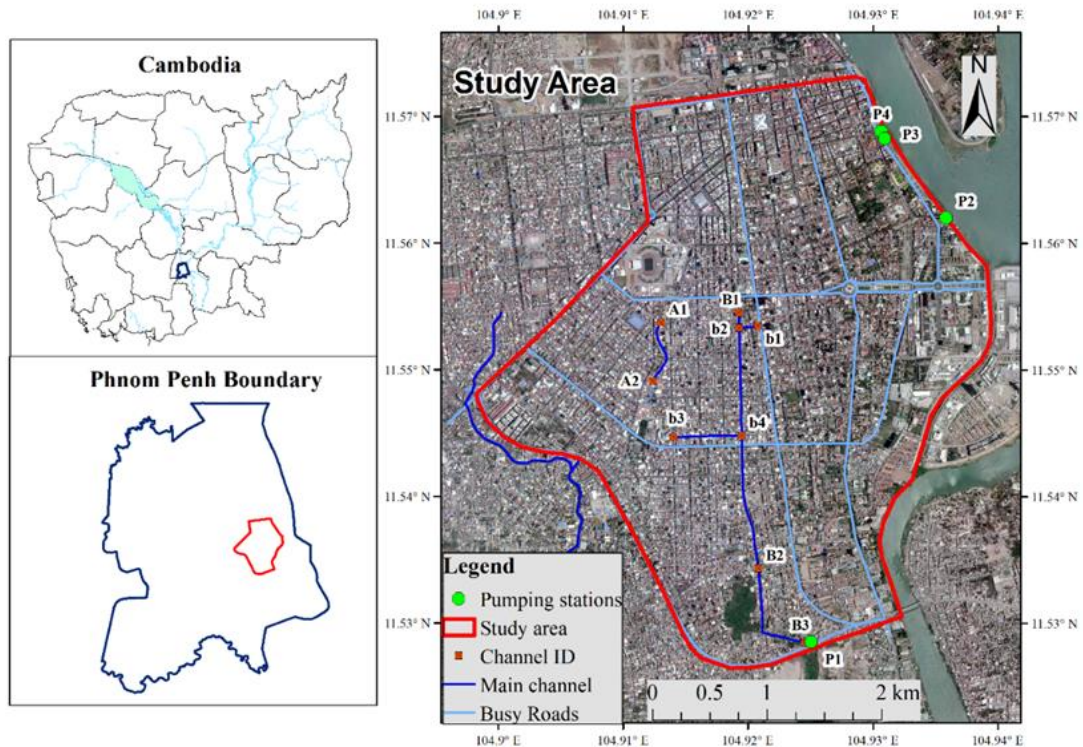
Figure 3-2: Map of study area

3.2 Drainage system in Phnom Penh

Urban drainage facilities in Phnom Penh have been built, operated and maintained by Ministry of Public Works and Transport (DPWT) and local authorities, Khan and Sangkat. DPWT is in charge of maintenance and operation work of drainage main pipe network with diameter of 600 mm or more while local authorities control the drainage pipe network with diameter smaller than 600 mm (JICA, 2016). According to JICA (1999) on the study on drainage and sewerage improvement project in Phnom Penh, the sewage network mainly consists of circle-shape concrete pipe with longitudinal gradient ranging from 1/500 to 1/2000. The total length of drainage pipes and number of manholes are gradually increasing (JICA, 2016). At the end of 2013, total length of pipes is about 478 kilometers and number of manholes is about 34,000. The total length of drainage pipe and number of manholes constructed in 2006-2013,

are shown in Table 3-1. Total length of drainage canals is around 55 kilometers and the amount of pumping stations is 12. Details of drainage canals and pumping stations managed by DPWT as of September 2014, are shown in Table 3-2 and Table 3-3 respectively.

The urban drainage facilities were constructed since the early 1900's with the combined functions of draining storm water and domestic wastewater. During a period of Pol Pot regime from 1970 to 1975, civil war began and all infrastructures including drainage system were deteriorated due to superannuated age and poor maintenance. Consequently, Phnom Penh is being frequently affected by floods and poor environmental conditions during the rainy season. With this regard, a study team of the Japan International Cooperation Agency (JICA) carried out a master plan called "The Study on Drainage Improvement and Flood Control in the Municipality of Phnom Penh" from March 1998 to August 1999. Based on this master plan, three projects for flood protection and drainage improvement had been completely implemented under the Japan's Grant Aid scheme. Outline of three Grant Aid Projects in the past are summarized in Table 3-4 (JICA, 2017). The area of each project is shown in Figure 3-3.

Table 3-1: Total length of drainage pipe and number of manholes from 2006 to 2013

Drainage pipe (m)								
Pipe size	2006	2007	2008	2009	2010	2011	2012	2013
Ø200 cm								
Ø180 cm					301	301	301	301
Ø160 cm	85	85	85	85	85	85	85	85
Ø150 cm	8,331	9,631	10,847	13,918	17,966	17,966	18,752	19,782
Ø120 cm	775	17,820	17,820	17,820	18,187	18,187	18,187	18,187
Ø100 cm	42,837	57,962	65,620	81,250	82,110	82,417	84,325	87,876
Ø80 cm	26,675	41,712	46,317	50,601	50,939	51,452	51,452	52,125
Ø60 cm	124,106	142,125	147,297	157,628	158,068	160,173	160,545	162,049
Ø50 cm	51,753	59,873	64,488	64,488	66,237	66,237	66,237	66,237
Ø40 cm	13,815	18,942	22,049	22,049	22,105	22,105	22,105	22,105
Ø30 cm	33,883	42,902	46,115	46,755	46,755	47,173	47,536	48,412
U-drain					320	320	320	320
Total (m)	302,260	391,052	420,638	454,594	463,073	466,416	469,845	477,479
Length of pipe installed in a year		88,792	29,586	33,956	8,479	3,343	3,429	7,634
Manholes								
Size	2006	2007	2008	2009	2010	2011	2012	2013
$Rg_{200x130}$					45	45	61	127
$Rg_{130x130}$	1,993	3,420	3,701	4,510	4,530	4,558	4,617	4,785
$Rg_{110x110}$	1,395	1,669	1,823	2,025	2,025	2,025	2,025	2,052
Rg_{90x90}	5,171	8,080	8,545	9,120	9,142	9,233	9,266	9,354
Rg_{70x70}	6,629	9,103	9,334	16,662	16,682	16,822	16,895	17,104
Total	15,188	22,272	23,403	32,317	32,424	32,683	32,864	33,422
Manholes installed in a year		7,084	1,131	8,914	107	259	181	558

Table 3-2: Total length of drainage canals managed by DPWT

No	Name	Total length (m)	Improved length (m)	Canal Type
1	Beoung Trabek Upper Canal	2,410	2,410	Reinforced Concrete Canal
2	Beoung Trabek Downstream Canal	850	0	Earth Canal
3	Beoung Tumpun Canal	3,710	3,710	Improved Earth Canal
4	Stoung Mean Chey Canal	1,900	0	Earth Canal
5	East & West Tuol Sen Canals	1,118	1,118	Improved to Reinforced Concrete Canal
6	Beoung Salang canal	1,260	887	Improved Earth Canal (887 m)
7	Canal Baraing	3,700		Earth Canal
8	Canal Lou Pram	1,700		Earth Canal
9	Tuol Poung Ror Canal	7,500		Earth Canal
10	Prey Speu Canal	7,000		Earth Canal
11	O Akuch Canal	4,200		Earth Canal
12	598 Canal	1,850		Earth Canal
13	Tuol Sampoeuv Canal	5,000		Earth Canal
14	Kop Srov Canal	4,700		Earth Canal
15	Bak Touk Canal	3,800		Earth Canal
16	O Veng Canal	4,150		Earth Canal
	Total	54,848	8,125	
Improved to Reinforced Concrete Canal		3,528		
Improved in Earth Canal		4,597		
Normal Earth Canal		46,723		

Table 3-3: List of pumping stations managed by DPWT

Station Name		Electrical Engine Driven				Diesel Engine Driven				Total Discharge Capacity (m³/sec)	Observation (Date of Equipment)
		Nos	Pump type	Power /Unit (kW)	Capacity/ Unit (m³/sec)	Nos	Pump type	Power/ Unit (HP)	Capacity /Unit (m³/sec)		
1	Boeng Trabek	8	Horizontal	132	1.00	1 unit of Backup Generator, 1000KVA				8.00	Operation since 2003 (ADB Loan)
2	Boeng Tumpun	5	Submergible Pump	280	3.00	2 units of Backup Generator, 700 KVA each				15.00	Operation since 2004 (Japan's Grant Aid)
3	Tuol Kork I	2	Vertical shaft	45	0.47	2	Vertical shaft	145	0.69	2.32	Constructed in 1970's
4	Tuol Kork II	1	Vertical shaft	45	0.47	2	Vertical shaft	145	0.69	1.85	Constructed in 1970's
5	Chak Tomuk	2	Pump gate	45	0.70	1 unit of Backup Generator, 200 KVA				1.40	Operation since 2010 (Japan's Grant Aid)
6	Preah Kumlung 1	1	Pump gate		0.20	-				0.20	Operation since 2004 (Joint Reseach with Kubota)
7	Preah Kumlung 2	2	Pump gate	22	0.35	-				0.70	Operation since 2010 (Japan's Grant Aid)
8	Phsar Kandal	2	Pump gate	45	0.70	1 unit of Backup Generator, 200 KVA				1.40	Operation since 2010 (Japan's Grant Aid)
9	Phsar Chaas	2	Pump gate	45	0.70	1 unit of Backup Generator, 200 KVA				1.40	Operation since 2010 (Japan's Grant Aid)
10	Svay Pak Kun No.9	4	Submergible Pump	75	0.13	3	Vertical shaft	190	0.38	1.66	Operation since 2006
11	Kop Srov	5	Vertical shaft	400	2.80	-				14.00	Operation since 2010
12	Tuol Sampeo	3	Submergible Pump		0.66	-				1.98	Operation since 2014

Table 3-4: Completed Projects under Japan's Grant Aid (JICA, 2017)

Project	Project Period	Target Area	Project Components
Phase I	2001 - 2004	Southwest area of the city (Tompun watershed)	• Construction: Dike Reinforcement, Drainage Channel, Pumping Station, Sluiceway, Bridge, Road
Phase II	2006 - 2010	City center and northeast area of the city (Central Market Area, Royal Palace & National Museum Area, Wat Phnom Basin)	• Construction: Revetment, Drainage Pipe, Underground reservoir, Pumping Station
Phase III	2010 - 2015	Trabek Area (Southeast of the city) (Catchment area of Trabek Pumping Station)	• Construction: Sediment Chamber, Drainage Pipe (21km) • Procurement: Cleaning Equipment of Drainage pipe (8 units) • Operation training

Although drainage conditions in the most part of city center have greatly improved by Phase I, Phase II and Phase III, areas in the northern part of city center such as the Tuol Kork Basin and Wat Phnom North (Figure 3-3) are still experiencing serious flooding in the rainy season. Therefore, the RGC requested implementation of Japan's Grant Aid "the Project for Flood Protection and Drainage Improvement in Phnom Penh (Phase IV)" to improve drainage condition in those areas as shown in Figure 3-3. As a result, the GOJ accepted to carry out a Preparatory Survey on the Project through JICA and this work is ongoing.
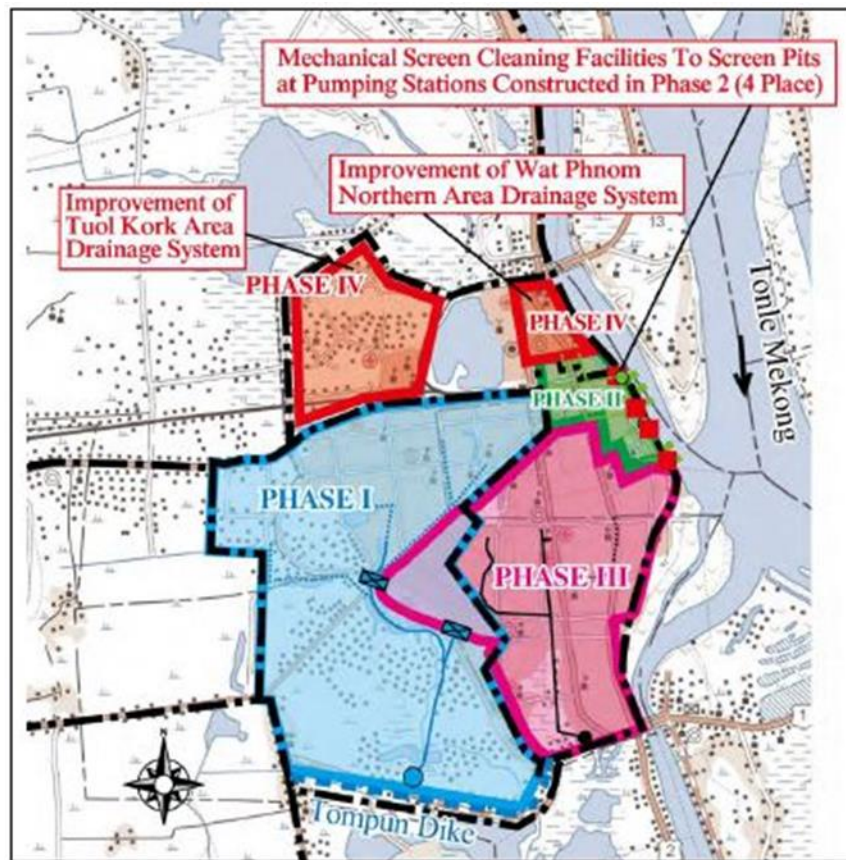
Figure 3-3: Area of the project under the Japan's Grant Aid scheme from March 1998 to August 1999 (JICA, 2017)

3.3 Flood protection

The construction of outer ring dikes for the protection of Phnom Penh City from flooding of neighboring rivers, lakes and swamps had started in the 1960's. Phnom Penh is defended against flooding coming from overflow of the Mekong and Tonle Sap rivers by Kop Srov Dike at northern part, natural levees along the Mekong/Sap rivers, and Tumpun Dike at southern part, as shown in Figure 3-4. When the Master Plan of 1999 was carried out, Kop Srov Dike built a part of the northwest administrative boundary of the Municipality of Phnom Penh, linking National Road 4 with National Road 5. Due to urbanization of the Phnom Penh administrative area, the function of Kop Srov Dike has turned into a dike which does not just protect the city from river overflow flooding, but also works as a ring road to bypass the city downtown. In the

same way, Tumpun dike has two roles: acts as a dike and a ring road. The crests of these two dikes are made from concrete or asphalt.
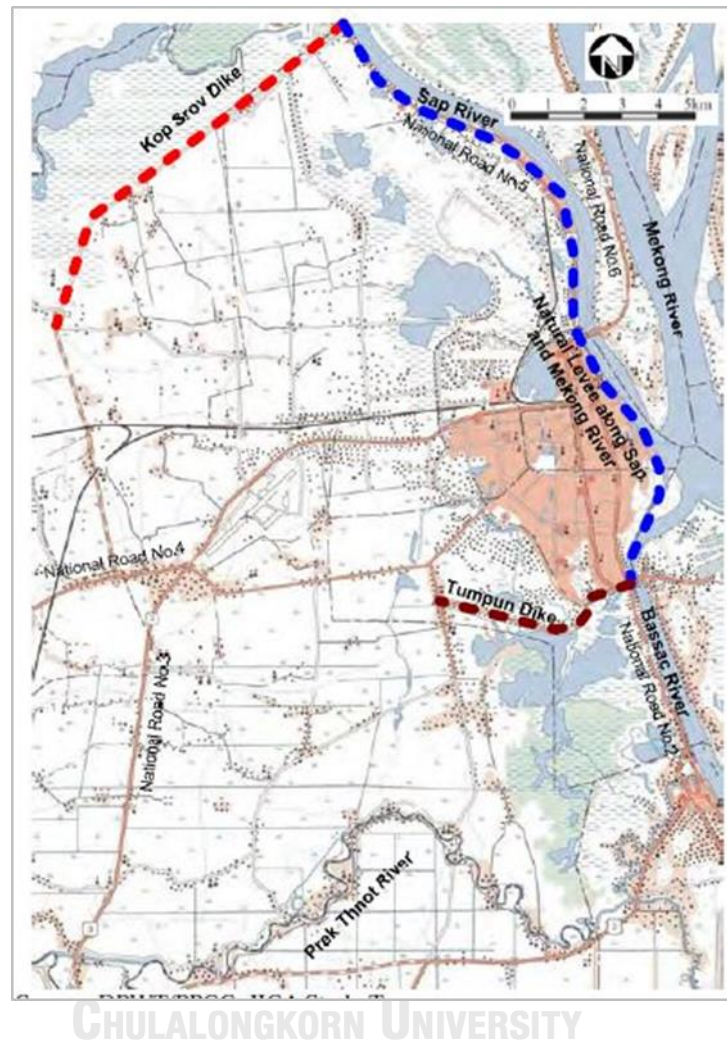
Figure 3-4: Map of dikes in and around Phnom Penh City (JICA, 2016)

3.4 Pump stations

In the selected study area, there are 4 pumping stations as shown in Figure 3-2. The Beoung Trabek pumping station (P1) located at the south of the study area where is the outlet of the whole pipeline network. It has the total capacity of 8 m^3/s. The information of all 4 pumping stations in the study area are list in Table 3-5. For the pumps (P2, P3, and P4), there are underground reservoirs which store the flooded water before draining out from the study area. To control the operation of these pumps, the pump rating tables were created by setting up to start operating if the headwater depth

is 0.5 m above the elevation of the bottom of the storage reservoir. It is noted that, rating tables set up in the model for this study were based on the interview with the pumping operators. The rating tables are listed in Figure 3-5, Figure 3-6, and Figure 3-7 for pumps P2, P3, and P4 respectively. For pump P1, it is installed at the end of channel and operated to pump the water out from the study area directly without underground reservoir. Likewise, rating table shown in Figure 3-8 is created at the inlet of the pump P1 to control pumping operation.

Table 3-5: Information of pumping station in study area

Pumping station ID	Pump unit	Capacity/unit m³/s	Total capacity m³/s
P1	8	1.00	8.00
P2	2	0.70	1.40
P3	2	0.35	0.70
P4	2	0.70	1.40
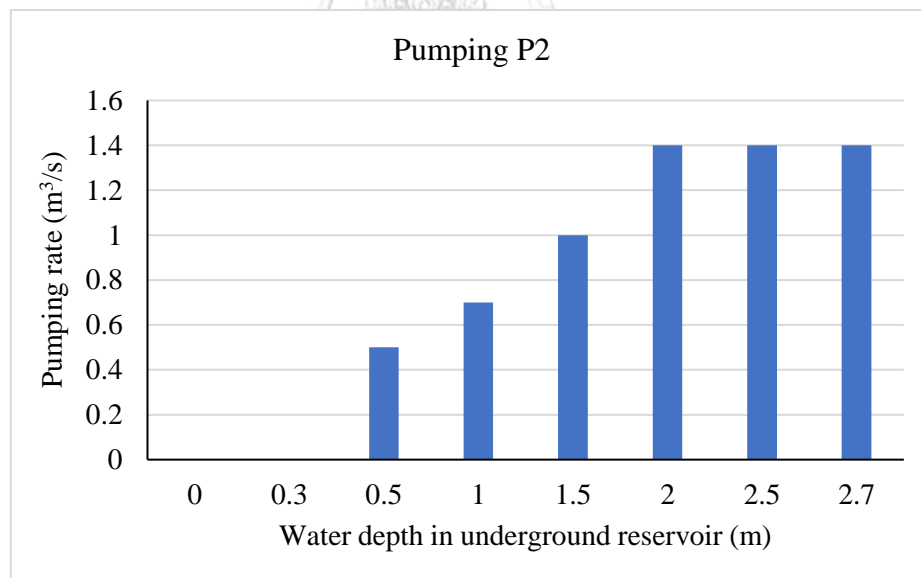
Figure 3-5: Pumping rating table for pump P2
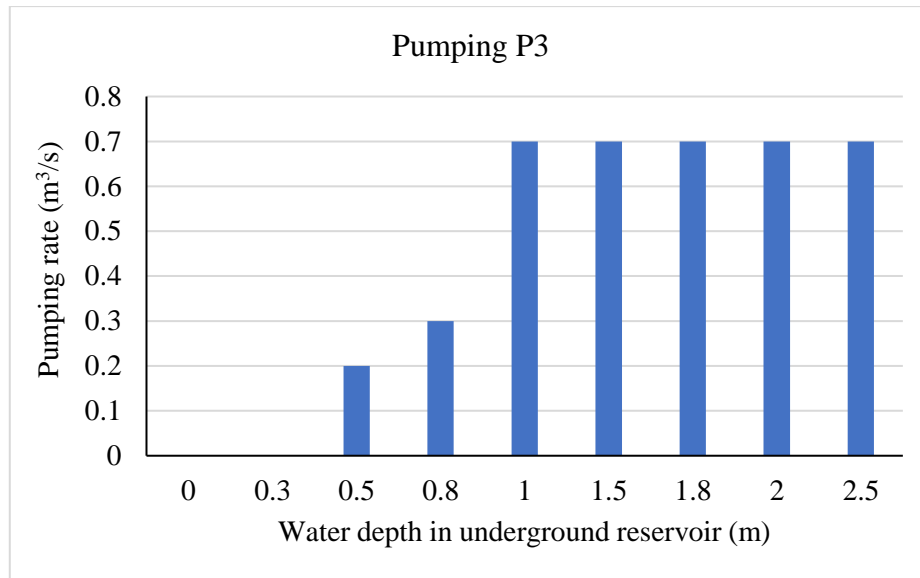
Figure 3-6: Pumping rating table for pump P3
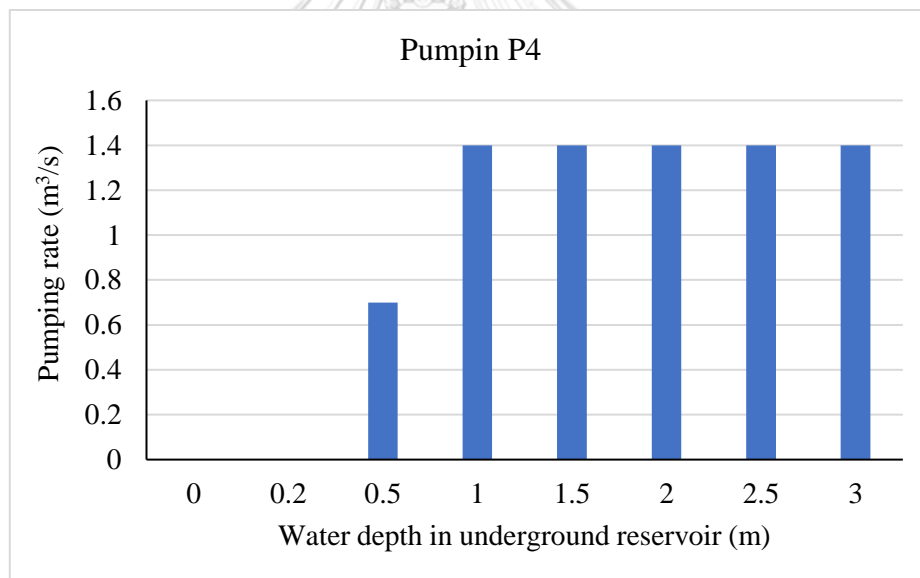
Figure 3-7: Pumping rating table for pump P4
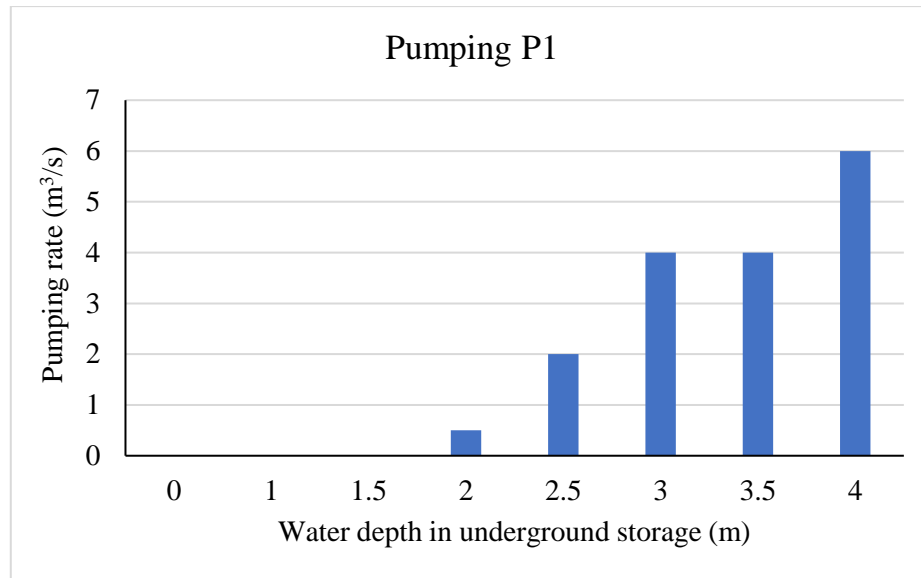
Figure 3-8: Pumping rating table for pump P1

3.5 Drainage channels

There are several of main drainage channels in the study area as shown in Figure 3-2 and summarized in Table 3-6. For the total channel length, 70 percent are made from concrete, and 30 percent are made from earth. Initial values of roughness coefficient of each channel are determined based on their material as recommended by Chow (1959). However, these values are recommended only for channel with good maintenance. Thus, the roughness coefficient of each channel in this case is expected to increase since the channels were constructed long time ago with poor maintenance. The Beoung Trabek open channel (B1 to B2) has a role as the outlet of storm drain while another channel (A1 to A2) works as a connection between two storm drains.

Due to lack of cross-section data, creating channels and their slopes in the model was based on the elevation of the grid elements. It is noted that the elevation of the grid elements belonging to the channels from upstream to downstream do not constantly decrease. Thus, the elevation of channel bed slopes has been adjusted to be constant based on the upstream and downstream elevation of the grid element. As the results, the adjusted slopes of each channel were in the range between 0.00092 and 0.00179.

Table 3-6: Information of open channels in study area

ID		Channel type	Length (m)	Height (m)	Width (m)	Manning coefficient n
Start	End					
A1	A2	Concrete	585.3	3.0	4.0	0.014
B1	B2	Concrete	970.5	3.0	8.0	0.014
b1	b2	Concrete	594.7	3.0	3.0	0.014
b3	b4	Concrete	162.7	3.0	4.0	0.014
B2	B3	Earth	970.5	3.0	15.0	0.025

3.6 Surface characteristics

The depth of the overland flow is relatively varied with topography and roughness of the surface layers. In this study, Phnom Penh raster image with 2 m resolution is used to categorize the characteristics of the land use. Four land use types were classified such as building, street, dense turf, and average grass cover with the roughness coefficient of 0.03, 0.02, 0.30, and 0.20 respectively. The roughness values in Table 3-7 selected for land use types are based on FLO-2D reference manual (O'Brien and Garcia, 2009). The Manning's coefficient set to each grid in GDS is shown in Figure 3-9.

Table 3-7: Overland flow Manning's n roughness values (O'Brien and Garcia, 2009)

Surface	n-value
Dense turf	0.17 - 0.80
Average grass cover	0.20 - 0.40
Open ground with debris	0.10 - 0.20
Open ground, no debris	0.04 - 0.10
Asphalt or concrete	0.016 - 0.05
Building roof	0.03
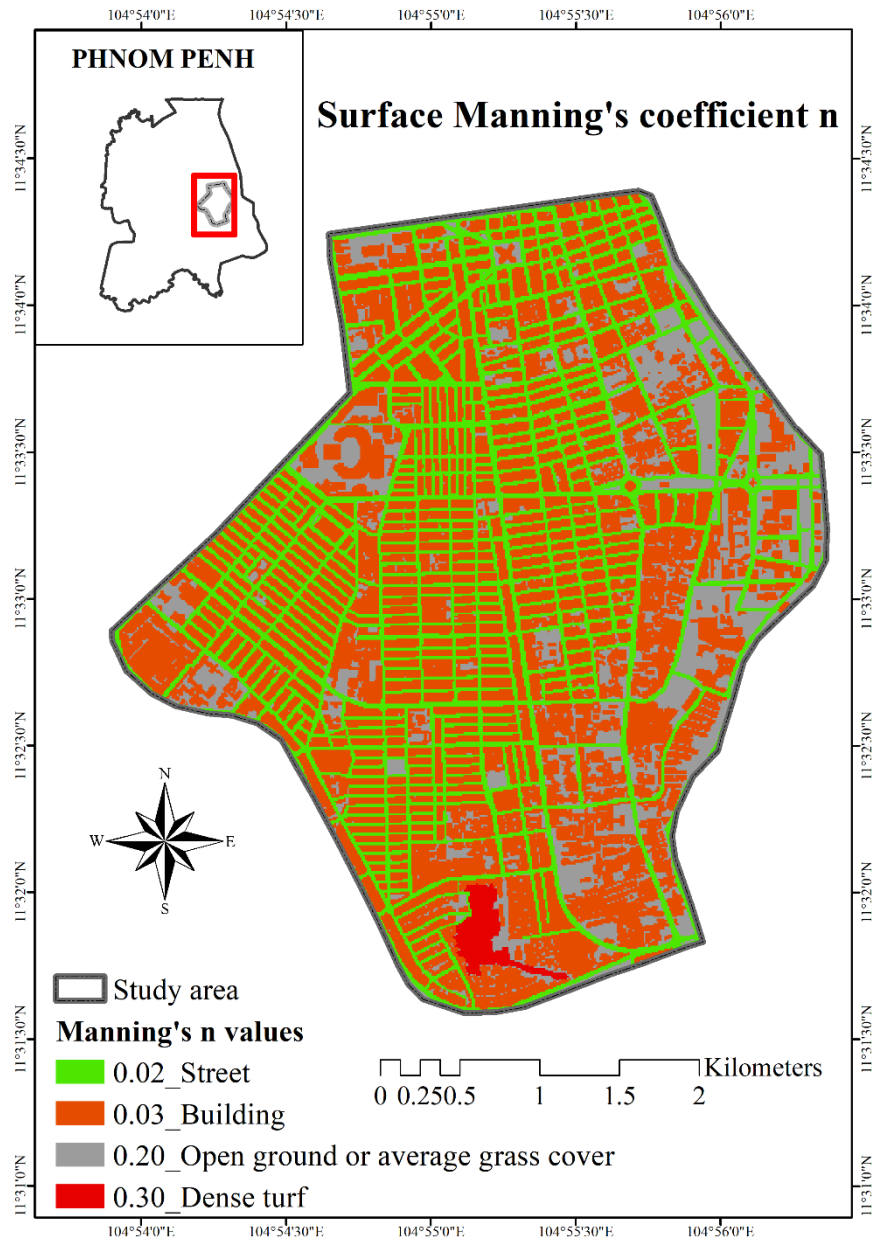
Figure 3-9: Manning's coefficient n assigned to the land use surface

CHAPTER 4
METHODOLOGY

The methodology applied in this thesis is demonstrated through a case study of an urban area in Phnom Penh, Cambodia. This chapter describes the conceptual of the FLO-2D model, model set up and the method to develop flood hazard maps in the study area. The overall framework is developed and the explanation to reach the objectives are provided in this chapter.

4.1 Hydrodynamic modeling FLO-2D

4.1.1 Overview of FLO-2D

As briefly described above, FLO-2D is a grid-based physical process model used to delineate flood hazard. Several previous studies suggest that FLO-2D is efficient for flood hazard simulation. It uses the dynamic wave approximation to the momentum equation to simulate rainfall-runoff and flood hydrographs over unconfined flow surfaces or in channels. The computation of flow flood discharge and flow depth in the grid elements relied on a small time-step and spatial resolution of the grid elements. The grid element size between 8 m x 8 m and 130 m x 130 m is recommended and the number of grid elements is unlimited (O'Brien and Garcia, 2009).

4.1.2 Grid Developer System (GDS)

The Grid Developer System (GDS) is a pre-processor tool used to create and edit the FLO-2D grid system. It arranges all necessary input data by superimposing the grid system on the DTM set of points, interpolates, and assigns elevations. Then, it will establish geographical boundaries, import shape file image and generate required data files to run the FLO-2D model.

4.1.3 Mapper++ of FLO-2D

FLO-2D Mapper++ is the post-processor program that creates maps and other plots of the FLO-2D model results including hydraulic variables, water surface elevations, duration of inundation, impact force, static pressure, specific energy,

sediment scour or deposition, and others. Mapper++ can also generate time series of flow depth and velocity at user selected locations, flow depth profiles along user defined cross sections, and hazard maps.

4.1.4 Rainfall-runoff

To calculate runoff volume in FLO-2D, rainfall can be assigned as uniform or spatially variable over the grid system. The excess rainfall generating direct runoff is simulated by considering the initial abstraction of infiltration process. In FLO-2D, losing through infiltration is estimated by employing either the Green-Ampt infiltration model, the SCS curve number method, or the Horton model. In this study, Green-Ampt infiltration method is applied to compute infiltration over the study area. However, it is noted that infiltration value is zero for the street, building, and impervious surface in the grid elements.

The Green and Ampt (1911) equation was developed based on an approximate physical theory of infiltration process which is sensitive to rainfall intensity, i.e. runoff is produced when the rainfall intensity is higher than the potential infiltration rate. Even though rainfall has stopped, infiltration continues until all the available water has drained or has been infiltrated. The cumulation infiltration F and the infiltration rate f of Green-Ampt equations are presented as Eq. 4-1 and Eq. 4-2 respectively.

$$F(t) = Kt + \psi \Delta\theta \ln\left(1 + \frac{F(t)}{\psi \Delta\theta}\right) \qquad \text{(Eq. 4-1)}$$

$$f(t) = K\left(\frac{\psi \Delta\theta}{F(t)} + 1\right) \qquad \text{(Eq. 4-2)}$$

where: ψ = the wetting front soil suction head

   K = the hydraulic conductivity

   $\Delta\theta = \eta - \theta_i$

   η = the soil porosity; θ_i = the initial soil moisture

To apply the Green-Ampt model, it is required to specify its parameters such as hydraulic conductivity, soil suction, volumetric moisture deficiency, porosity, soil storage depth and the percent impervious area.

4.1.5 Channel flow routing

Channel flow is simulated as one-dimensional (1D represents water surface elevation across channel) in the downstream direction. In FLO-2D, channels can be simulated with either rectangular or trapezoidal or natural-shaped cross sections. The governing equations are continuity and momentum equation as explained in section 2.4.2. The method used for flow routing is the dynamic wave momentum equation. This method is applied because slopes of the channels in the study area are mild. Therefore, both inertial and pressure forces are important and backwater effects cannot be negligible.

4.1.6 Overland flow

Overland flow on the floodplain is the simplest FLO-2D model. The model computes overland flow in eight directions, the four compass directions (north, east, south, and west) and the four diagonal directions (northeast, southeast, northwest and southwest). The eight flow directions associated with numbers recognized by the model are shown in Figure 4-1. In FLO-2D model, the buildings or other obstacles are represented by the Area Reduction Factor (ARFs) used to simulate the reduced storage volume of a grid element. Thus, the grid element surface storage area can be adjusted using ARFs. The variables affecting the variation of overland flow depth and flow velocities are topography and the grid element roughness.
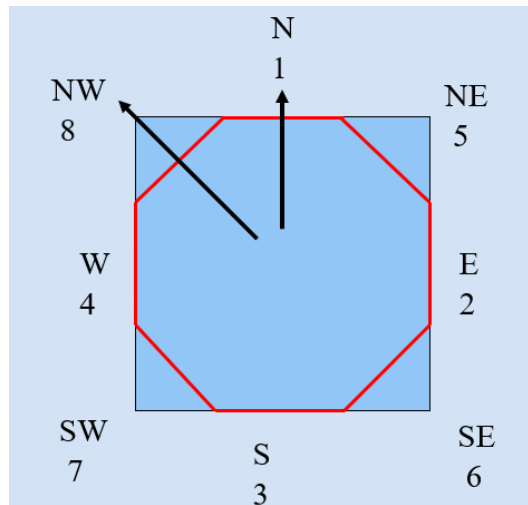
Figure 4-1: Overland flow in eight directions in a grid element in GDS (O'Brien and Garcia, 2009)

4.1.7 Storm drain modeling

FLO-2D Storm Drain Model is an SWMM integrated software tool which allows FLO-2D model to simulate the volume exchange between the surface water and storm drain system as shown in Figure 4-2.
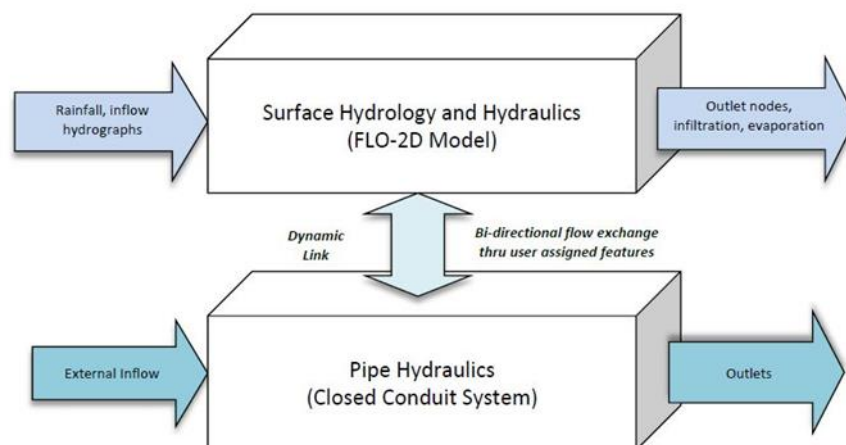
Figure 4-2: Volume exchange of surface water and closed pipe system

The continuity equation (Eq. 4-3) and momentum equation for x-direction (Eq. 4-4) are used as the governing equations in solving the unsteady water flow through a closed conduit network (Rossman, 2006).

$$\frac{\partial A}{\partial t} + \frac{\partial Q}{\partial x} = 0 \qquad \text{(Eq. 4-3)}$$

$$\frac{\partial Q}{\partial t} + \frac{\partial \left(\frac{Q^2}{A}\right)}{\partial x} + gA\frac{\partial H}{\partial x} + gAS_f + gAh_L = 0 \qquad \text{(Eq. 4-4)}$$

where: x = distance along the conduit

t = computational timestep

A = cross sectional area of the pipe

Q = pipe discharge

H = hydraulic head of water in the conduit

S_f = friction slope or head loss per unit length of pipe

h_L = local energy loss per unit length of pipe

g = gravitational acceleration

Before the simulation, it is required to input the initial conditions for the discharge Q and head H in each pipe at time t = 0 and set the boundary conditions at the inlet of pipe x = 0 and end of the pipe x = L for all timesteps. Then, two equations above will be applied to compute unsteady flow along the pipe network and solved for the discharge Q and head H.

Pipeline network consists of the junction nodes (Figure 4-3) that connect two or more conduits together. Hence, there is another necessary equation expressed as Eq. 4-5 to study the change in hydraulic head H.

$$\frac{\partial H}{\partial t} = \frac{\sum Q}{A_{store} + \sum As} \qquad \text{(Eq. 4-5)}$$

where: H = flow depth (difference between the node head and the pipe invert elevation)

A_{store} = node surface area

$\sum As$ = surface area contributed by the conduits connected to the node.

$\sum Q$ = net flow at Node J contributed by all connected conduits plus external inflows
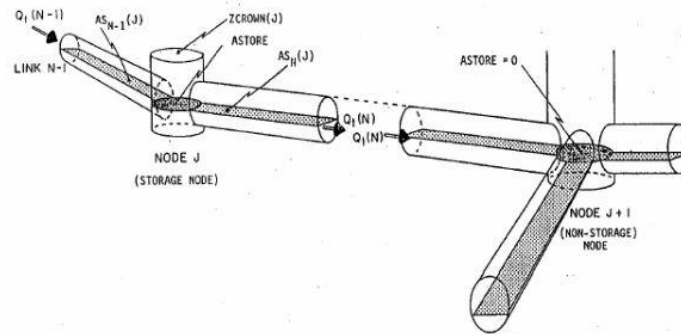
Figure 4-3: Node-Link Representation of a Drainage System (Rossman, 2006)

At the inlet where surface runoff discharge flows into the pipeline system, weir and orifice equations are applied to compute the inflow discharge under inlet control as expressed in Eq. 4-6 and Eq. 4-7 respectively. Note that, orifice equation is automatically applied when the inlet is completely submerged.

$$Q_w = CLH^m \qquad \text{(Eq. 4-6)}$$

where: Q_w = weir discharge

C = weir coefficient

L = crest length

H = FLO-2D grid element water depth that contains the inlet structure

m = 1.5 for a broad crested weir

$$Q_0 = C_d A \sqrt{2gH} \qquad \text{(Eq. 4-7)}$$

where: Q_0 = orifice flow rate at depth H

C_d = discharge coefficient hardcoded to 0.67

A = L x h; cross-sectional orifice area, computed from inlet opening length (L) and height (h)

g = gravitational acceleration

H = FLO-2D grid element water depth that contains the inlet structure

4.2 Method

To obtain the objective, it is necessary to understand clearly the problem and the basic principles of the study, data requirement, a technique of data collection, and relevant information which can be analyzed as described in the following sections. An overall flowchart of the methodology in this study is briefly described in Figure 4-4.
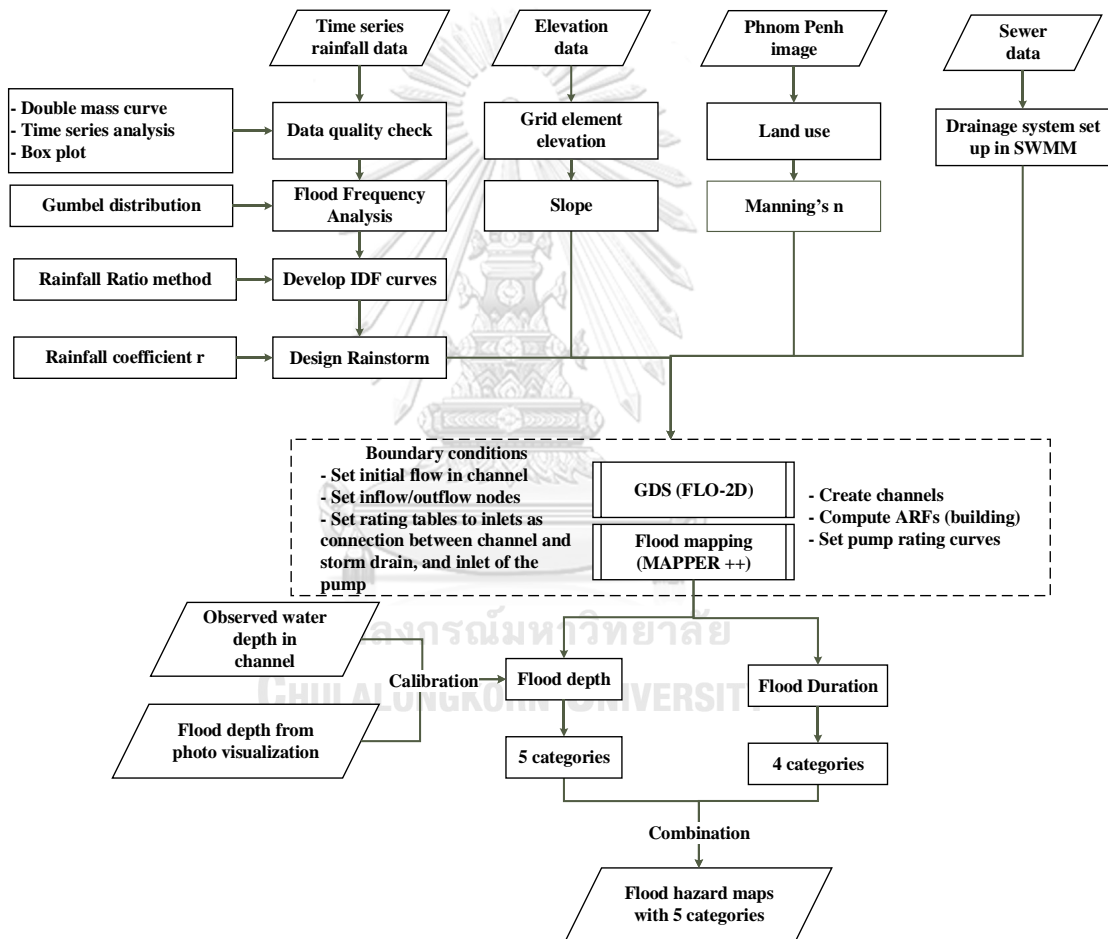
Figure 4-4: Overall framework flowchart

4.3 Data collection

The computer modeling is commonly comprised of three main components: input, model, and output. To reduce uncertainty and increase reliability of the output,

quality check of the input data is required. For instance, the important available data of FLO-2D which are required to check in order to generate flood maps in this study are summarized in Table 4-1.

Table 4-1: Available data for flood hazard assessment

No	Data	Period	Resolution	Source	Purpose
1	Rainfall	2010-2016	5 min	ITC station	Compute storm advancement coefficient r
		1985-2013	Daily	Pochentong station	Perform flood frequency analysis and apply it for rainfall ratio method
2	IDF curve	-	-	JICA	Compare with new IDF curve developed by rainfall ratio method
3	DEM	2016	2 m x 2m	MRC	Assign elevation to grid elements in the study area
4	Drainage system	2010 and 2015	-	Phnom Penh Capital Hall	Set up drainage system in SWMM as database for GDS
5	Phnom Penh Image	2016	2 m x 2 m	MRC	Categorize the characteristics of the land use
6	Historical flood depth	2015 and 2018	-	ITC	Calibrate model

4.3.1 Rainfall data check

Based on literature, rainfall is the main driving element attributing to urban floods. Thus, time series rainfall data analysis is an important procedure in order to select the extreme event for inundation mapping. In this study, daily rainfall dataset of Pochentong station from 1985 to 2013 is used for the analysis of rainfall pattern. However, to have reliable model results, quality check of rainfall data is needed before preforming frequency analysis.

Once, rainfall data has been checked and analyzed, those annual maximum daily rainfall data between 1985 and 2013, are used to apply in rainfall ratio method to develop IDF curve for Phnom Penh. Then, design rainfall hyetographs as input of FLO-2D model are produced based on obtained IDF curve.

Daily rainfall data of Pochentong station is used to represent the rainfall in study area while other two stations namely: Phnom Penh Ville and Chruy Chongvar (Figure 4-5) are not used for this purpose because the period of available data of those stations are shorter than Pochentong station. More importantly, rainfall data of Pochentong station is more reliable since all the projects of JICA of improving drainage system in Phnom Penh employ only data recorded from this station to analyze and design sewer system (JICA, 2001, JICA, 2011, JICA, 2016, JICA, 2017). Even though the statement above suggests good quality of rainfall data at Pochentong station, data quality check for this station is performed to confirm its reliability over the period selected for this study. The analysis of double mass curve, pattern and trend and box plot is performed for assessing data quality.

Double mass curve is used to check the consistency of rainfall data by comparing data of single station to that of a set of neighboring stations. In this study, consistency of rainfall data of Pochentong is checked against rainfall dataset of two other stations in Phnom Penh city namely Phnom Penh Ville and Chruy Changvar station from 1985 to 2008 which are the period where data from all stations are available. It is noted that only two surrounding rainfall stations used for the test might not give sufficiently robust result to ensure the consistency of the record at the test station. However, this contributes more or less to data quality check.
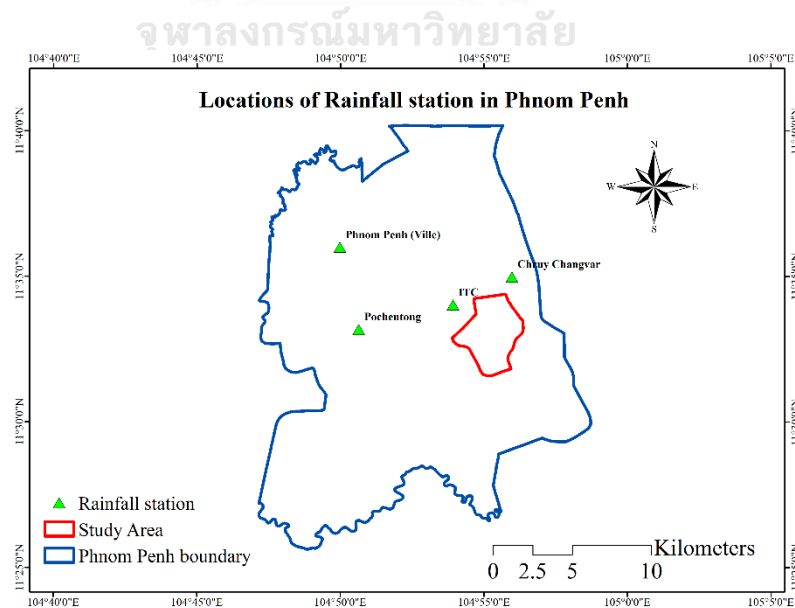
Figure 4-5: Locations of rainfall station in Phnom Penh

4.3.2 Rainfall frequency analysis

Probability analysis of rainfall of Pochentong station is carried out using maximum daily rainfall. The probability distribution models often used to fit extreme values are Exponential Distribution, Gumbel Distribution, Extreme Value Distribution, Log-Pearson Type III Distribution, and Log-Normal Distribution and so forth. In this study, the Gumbel distribution was employed to perform the probability analysis of rainfall. The function of Gumbel distribution shown in Eq. 4-8 is given as follows:

$$F(x) = \exp\left(-\exp\left(-\frac{(x-\mu)}{\alpha}\right)\right) \qquad \text{(Eq. 4-8)}$$

where: μ = the location parameter

α = the scale parameter

The random variable X_T associated with a given return period, T is show as following expression:

$$X_T = \overline{X} + K_T S \qquad \text{(Eq. 4-9)}$$

where: $\overline{x}$ = the mean of annual maximum daily rainfall

S = the standard deviation of the annual maximum daily rainfall

K_T = the frequency factor associated with return period T

The frequency factor associated with return period, T is presented by following equation:

$$K_T = -\frac{\sqrt{6}}{\pi}\left[0.5772 + \ln\left(\ln\left(\frac{T}{T-1}\right)\right)\right] \qquad \text{(Eq. 4-10)}$$

The result of probability analysis of annual maximum daily rainfall fitted with Gumbel distribution is shown in Chapter 5. In order to prove that Gumbel distributions can be applied to fit the maximum daily rainfall, Chi-Square test of goodness of fit is carried out. The formula of Chi-Square test is as follows:

$$\chi^2_{\;0} = \sum_{i=1}^{k} \frac{(O_i - E_i)^2}{E_i}$$ (Eq. 4-11)

where: O_i = the observed frequency in the ith class interval

E_i = the expected frequency in the ith class interval

A hypothesized distribution fits with observed data when the null hypothesis is true. In contrast, the null hypothesis is rejected when

$$\chi^2_{\;0} > \chi^2_{\;k-p-1,\alpha}$$ (Eq. 4-12)

where: k = the number of bins or class intervals

p = the number of parameters of the hypothesized distribution

The probability density function (PDF) of the Gumbel distribution used to compute expected probability is expressed in Eq. 4-13

$$f(x, \mu, \alpha) = \frac{1}{\beta} \exp\left[-\left(z + \exp(-z)\right)\right]$$ (Eq. 4-13)

where: $z = \dfrac{x - \mu}{\alpha}$

4.3.3 Drainage system set up

Prior to importing drainage system data to GDS of FLO-2D, the drainage system data file must be set up in SWMM model. This task was done by Heng et al. (2017). The information and procedure of setting up the drainage system in SWMM is described herein. The existing drainage system data in study area consist of pipeline, manholes, pumping stations, and invert elevation. The location of pipeline and manhole extracted from CAD file was set up in the model SWMM. Based on available pipe data from JICA's project, the diameter of pipe ranges between 0.8 m to 2 m. The position of the manhole from CAD file is placed from one to another with the distance as the multiple of 10 m since the grid cell size created in FLO-2D model is 10 m x 10 m. The slope of the pipeline was calculated from the invert elevation of the manhole. The process flowchart to get storm drain system in SWMM5.0 as database in GDS is shown

in Figure 4-6. The result of storm drainage system processed in SWMM5.0 is presented in APPENDIX A.

The overflow runoff discharge of floodplain surface typically passes into pipeline system by the manhole. In FLO-2D model, there are 5 types of manhole inlets shown in APPENDIX B which are available to set up to exchange the flow between floodplain surface and pipelines. Type 1 and type 4 inlet were used to control and divert the flow. Type 1 inlet, the Curb Opening Inlet at Grade (Figure 4-7) of the manhole was used for most inlets in the study area while Type 4 inlet was used to connect the flow from the channel outlet to storm drain and used as inlets for pumping station P1, which diverts water from the Beoung Trabek channel.

The input parameters for a Type 1 inlet shown in Eq. 4-6 and Eq. 4-7 are weir coefficient (C), curb opening length (L), and curb opening height (h). Type 4 inlet in FLO-2D is a kind of inlet that has an inflow discharge represented by a rating table (stage-discharge data). In this study, the input parameters (stage-discharge table) for Type 4 inlets is based on Manning's equation shown in Eq. 4-14.
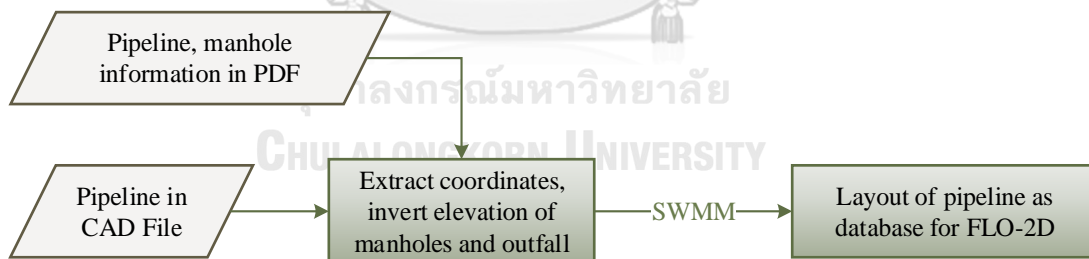
Figure 4-6: Flowchart of producing storm drain system

Figure 4-7: Manhole components and detail of Curb Opening Inlet at Grade of the manhole

$$Q = \frac{1}{n} A R^{2/3} S_0^{1/2}$$
(Eq. 4-14)

where: Q = the flow discharge (m³/s)

A = the wetted area (m²)

R = the hydraulic radius (m)

S_0 = the channel bottom slope

An example of designing stage-discharge data for inlet type 4 in this study is detail described herein. A rectangular channel (segment A1-A2 in Figure 3-2) has following parameters: the bottom width is 4 m, the channel height is 3 m, the bottom slope is 0.000116, and the Manning's coefficient for concrete material is set up to 0.035 which is the obtained value after calibration. Based on Eq. 4-14, the stage-discharge table can be computed as following:

- If the normal flow stage is y = 0, the discharge is Q = 0 m³/s

- If the normal flow stage is y = 1 m, the discharge is

$$Q = \frac{1}{0.035}(1 \times 4)\left(\frac{1 \times 4}{(2 \times 1) + 4}\right)^{2/3}(0.00116)^{1/2} = 2.97 \text{ m}^3/\text{s}$$

- If the normal flow stage is y = 2 m, the discharge is

$$Q = \frac{1}{0.035}(2 \times 4)\left(\frac{2 \times 4}{(2 \times 2) + 4}\right)^{2/3}(0.00116)^{1/2} = 7.78\,\text{m}^3/\text{s}$$

- Then, change the value of normal flow stage in the channel ranging from 0 m to 3 m to obtain discharge Q value. Finally, stage-discharge table can be created for the Type 4 inlet.

4.4 Storm design

Flood hazard assessment depend on meteorological and hydrological data availability in order to provide reliable results. However, rainfall in this study is very limited in which only daily rainfall data are available for analysis. Therefore, the procedure shown in Figure 4-8 is applied to develop IDF curve based on daily rainfall, then create the design rainstorms of different return periods.
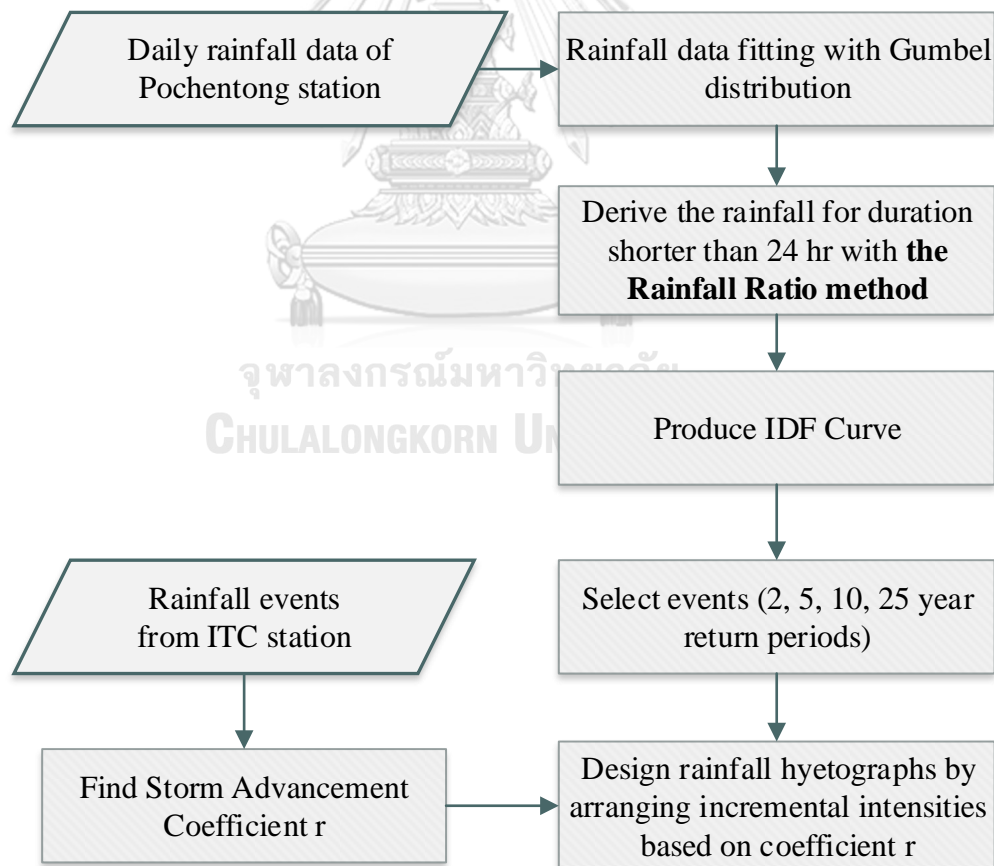
Figure 4-8: Overall flowchart of rainstorm design

The following steps are detailed to determine rainfall hyetographs:

a. Develop intensity-duration-frequency (IDF) curves for different return periods of 2 to 100 years, for duration of 10 minutes to 24 hours. In this case, daily rainfall of Pochentong Station between 1985 and 2013 are used to derive short time interval intensities. Various equations can be applied to express rainfall intensity and its corresponding duration. In this study, Horner Type which its constants applied in rainfall ratio method is used to express the relation between probable rainfall intensity and its duration as following equation:

$$I = \frac{a}{(b+D)^n} \qquad \text{(Eq. 4-15)}$$

where: I = the rainfall intensity (mm/hr)

D = the rainfall duration (hr)

a, b, n = the constants

b. In order to obtain the rainfall for durations less than 24 hours, the rainfall ratio method is applied. The rainfall of duration D for any return period is derived from the 24 hours Extreme rainfall based on Eq. 4-16 (Watkins and Fiddes, 1984):

$$RR = \frac{D}{24}\left(\frac{b+24}{b+D}\right)^n \qquad \text{(Eq. 4-16)}$$

where: RR = rainfall ratio for conversion of 24 hr rainfall into D hr rainfall

D = rainfall duration (hours)

b, n = the constants of Horner equation

b = 0.2 and n = 0.9 the constant values for Phnom Penh recommended by Ministry of Public Works and Transport, Cambodia (CR-PRIP Team, 2015).

It is noted that in case there is enough data of higher-time resolution of rainfall, the rainfall ratio can be calculated, and the constants b and n can be determined. In this study the rainfall data in ITC station between 2010 and 2016 is 5-minutes time resolution that can be adopted to compute the rainfall ratio and determine the constants b and n. However, prior to using rainfall data of ITC station for determining the rainfall ratio, it is required to check the correlation of rainfall data between these two stations first. Since the correlation between both stations is very low, the values of constants b and n recommended by Ministry of Public Works and Transport (CR-PRIP Team, 2015) are adopted in this study.

Another significant aspect of applying the rainfall ratio method is that the historical annual maximum daily rainfall is recommended to be fitted to Extreme Value Type 1 (Gumbel) or Generalized Extreme Value (GEV) distribution (MRC, 2010, CR-PRIP Team, 2015). As indicated previously, it is clear that Gumbel distribution is fitted to annual maximum daily rainfall data of Pochentong station used to represent rainfall distribution in the study area. Therefore, the rainfall ratio can be applied for this study.

c. In this case, the rainfall data is single point rainfall. Therefore, it is required to be adjusted for spatial distribution over the study area. This can be carried out by applying an Areal Reduction Factor (ARF). According to MRC (2010), in the case of convective rainfall in Cambodia for durations less than or more than 8 hours, the ARF can be determined as Eq. 4-17 and Eq. 4-18:

For D ≤ 8 hrs:
$$ARF = 1 - 0.04 D^{-0.33} A^{0.50}$$
(Eq. 4-17)

For D > 8 hrs:
$$ARF = 1 - 0.02 A^{0.50}$$
(Eq. 4-18)

d. The design rainstorms for particular return periods can be obtained by the incremental intensity (Eq. 4-19) of the rainfall totals of the calculated durations up to the time of concentration:

$$I_j = \frac{R_{A,D_j} - R_{A,D_{j-1}}}{D_j - D_{j-1}} \left(\frac{mm}{hr} \right) \text{ for } D_j > D_{j-1} \qquad \text{(Eq. 4-19)}$$

where: I_j = jth incremental intensity (mm/hr)

$R_{A,D}$ = areal rainfall for duration D (mm)

e. The incremental intensities can then be arranged around the highest intensity (peak value). The graphical location of the peak is determined by the storm advancement coefficient r which is the ratio of the time to peak relative to the total duration of the design storm.

The successive subsections will describe in detail the calculation starting from IDF curve development up to rainfall hyetograph design.

4.4.1 IDF curve development

First, the Rainfall Ratio equation (Eq. 4-16) is applied to calculate the rainfall ratio and mean maximum rainfall of Pochentong station for duration less than 24 hours (from 10-minutes to 24-hours duration). Then, the standard deviation for each new mean rainfall can be computed as Eq. 4-20. The results of rainfall ratio, new mean maximum rainfall and new standard deviation are shown in Table 4-2.

$$SD_{NEW} = P_m \times \left(\frac{SD}{Mean} \right) \qquad \text{(Eq. 4-20)}$$

where: SD_{NEW} = the standard deviation for each new mean rainfall (mm)

SD = the standard deviation of annual maximum daily rainfall (mm)

Mean = the mean of annual maximum daily rainfall (mm)

P_m = the new mean maximum rainfall for duration less than 24 hour (mm)

Table 4-2: The results of rainfall ratio, new mean maximum rainfall and new standard deviation

Duration	Rainfall ratio, RR	Mean max. rainfall, P_m	SD_{NEW}
10 min	0.30	29.55	7.59
15 min	0.38	36.87	9.46
20 min	0.43	42.19	10.83
30 min	0.51	49.54	12.72
1 hr	0.62	61.00	15.66
2 hr	0.72	70.71	18.15
3 hr	0.77	75.70	19.43
6 hr	0.85	83.48	21.43
12 hr	0.93	90.79	23.30
18 hr	0.97	95.02	24.39
24 hr	1.00	98.03	25.16

As explained earlier, Gumbel distribution can be fitted to the extreme annual maximum daily rainfall of Pochentong station. Hence, the Gumbel distribution is applied to derive rainfall depth or intensity for each duration according to Eq. 4-21.

$$P_T = P_m + K_T \times SD_{NEW}$$ (Eq. 4-21)

where: P_T = the rainfall for the return period T (mm)

K_T = the Gumbel factor for different return period

By applying Eq. 4-10, the values of K_T for a range of return periods can be determined as in Table 4-3.

Table 4-3: The factors for Gumbel distribution for different return period (T)

Return period (T)	K_T
2	-0.16
5	0.72
10	1.30
25	2.04
50	2.59
100	3.14

4.4.2 Selection of design rainfall events

The simulation of runoff can apply for either historical rainfall events, or design rainfall. Normally, historical rainfall event is adopted for model calibration prior to design rainfall commonly used for infrastructure design.

In this study, four different design events 2, 5, 10 and 25-year return period are used to assess for flood analysis due to following reasons:

– Rainfall event of 2-year return period was used for the design of secondary drainage infrastructure such as pipe network system in Phnom Penh.

– Rainfall event of 5-year return period was used for the design of primary drainage infrastructure such pump stations, and drainage canals.

– Rainfall event of 10-year return period was used for design of important infrastructures to protect the city such as dikes.

– Rainfall event of 25-year return period is assessed to analyze serious flooding hazard in the selected study area.

4.4.3 Rainfall hyetograph design

According to JICA (1999) and rainfall events recorded in ITC station and other stations from 2010 to 2018, the rainfall patterns are characterized by the fact that all rainfall events terminate within 6 hours. Therefore, the rainfall duration design of this assessment is 6 hours and the incremental intensities are arranged around the peak intensity which the location of peak is estimated by the storm advancement coefficient r.

4.4.3.1 *Storm advancement coefficient r*

The storm advancement coefficient is determined by analyzing historical storm hyetographs. Various durations of the heavy rainfall events are analyzed in the vicinity of the peak of the storm and computing the mean value of the storm advancement coefficient.

The procedure to determine the storm advancement coefficient is explained as follows:

– Collect historical data of rainfall events and classify them into groups of same durations such as 30 min, 60 min, 120 min.

– Divide storm duration into same time intervals such as every 10 min, every 15 min.

– Specify the period of time interval and rank in each storm event of the same duration. Rank the periods = n. The highest rainfall period has the rank = 1. The lowest rainfall period has the rank = n.

– Select the period number having the rank = 1 in each storm event.

– Determine the mean (average) of period of time interval having the rank = 1 for all storm events.

– Determine the storm advancement coefficient by Eq. 4-22.

$$r = \frac{m_{mean} - 0.5}{n} \qquad \text{(Eq. 4-22)}$$

where: r = the storm advancement coefficient

m_{mean} = mean period number having minimum mean rank

n = number of periods in storm duration

An example of the calculation of the storm advancement coefficient of the events of 2-hour duration are given as following tables (Table 4-4 and Table 4-5):

Table 4-4: Rainfall depth distribution of 2-hour events

Event	Date	Rainfall (mm)	Rank	Rainfall depth in each period (mm)								Rank of each period's rainfall							
				1	2	3	4	5	6	7	8	1	2	3	4	5	6	7	8
1	4/23/2011	103.4	1	10.4	10.4	38.4	29.0	11.6	1.6	0.2	1.8	4.5	4.5	1	2	3	7	8	6
2	10/8/2015	72.6	2	4.2	13.0	25.4	13.6	14.4	1.4	0.4	0.2	5	4	1	3	2	6	7	8
3	9/10/2013	67.4	3	0.6	0.4	11.6	26.2	12.8	8.4	5.4	2.0	7	8	3	1	2	4	5	6
4	11/13/2016	66.4	4	10.0	0.8	15.0	9.8	19.4	8.8	0.6	0.2	3	6	2	4	1	5	7	8
5	5/22/2014	64.8	5	9.6	10.8	18.2	21.8	2.2	1.6	0.4	0.2	4	3	2	1	5	6	7	8
6	10/8/2013	63.6	6	6.8	5.0	12.6	22.8	13.4	2.4	0.4	0.2	4	5	3	1	2	6	7	8
7	5/29/2011	58.2	7	0.4	12.2	15.0	17.2	5.8	6.6	0.4	0.2	6.5	3	2	1	5	4	6.5	8
8	11/8/2014	58	8	4.0	4.6	13.0	18.8	5.4	8.0	4.0	0.2	6.5	5	2	1	4	3	6.5	8

Table 4-5: Period of the events with minimum rank

Event	Period with minimum rank
1	3
2	3
3	4
4	5
5	4
6	4
7	4
8	4
Mean	3.875

Therefore, $r = \dfrac{3.875 - 0.5}{8} = 0.42$

Repeat the same calculation steps for duration of 3-hour and 6-hour rainfall events. The storm advancement coefficient of 3-hour and 6-hour duration are 0.22 and 0.13 respectively. Since the rainfall hyetographs are designed with 6-hour duration, the storm advancement coefficient r = 0.13 is applied.

4.5 Flood simulation

4.5.1 Development of Grid Based System in FLO-2D

The developed grid element size should match to the topographic data resolution and result in an acceptable number of total grid elements. There should be equitable between the grid element size, resolution of the desired FLO-2D result and the model

computer runtime. Therefore, the grid system was created with the cell size of 10 m (square grid) in this study and a Phnom Penh image with a resolution of 2 m x 2 m was also employed to visualize the computational domain. The grid elevation was obtained from the surveyed interpolation DTM data (point) in this study area. The ground surface elevation of the study area produced by GDS is shown in APPEXDIX C.

4.5.2 Simulation of flood depth

Square grids of 10 m x 10 m are assigned to the floodplain of the study area. The depth of flooding of each grid is computed and grouped into five depth categories: Very Low, Low, Medium, High and Very High on the basis of four critical flood depths 0.10 m, 0.30 m, 0.60 m and 1.2 m. The basis of the selected critical depth is in reference to the data analysis from questionnaire surveys of public perceptions on the urban flood in Phnom Penh conduced in 2016 (Heng et al., 2016). It was reported that when the water level was less than 0.30 m, it is very common for citizens. Hence, the damage was estimated to be minor since citizens can adapt to this condition. In case the flood depth varied between 0.30 m and 0.60 m, the damage is considered moderate which would contribute to negative effects on business, traveling, and health. Besides, such damage will be huge as the flood depth increases between 0.60 m and 1.2 m. If the flood depth increases above 1.2 m, it would probably cause death. Once the depth of flooding in each grid is computed, the area of flooding of each category can be calculated by multiplying the grid cell size (100 m^2) and the number of grids. The area under each category is expressed as percentage with respect to the total floodplain area excluding the building area.

4.5.3 Simulation of flood duration

Many researchers agreed that the duration of flooding is an important factor for the hazard assessment; however, there is very limited literature to quantify this parameter. Keokhumcheng et al. (2012) determined the duration of flooding by using three inundation maps of flood depth. Those three maps are rising flood, peak flood, and receding flood from the model simulation. Using the same method, the duration of flooding in this study is determined by overlapping the three inundation maps of rising

flood, peak flood, and receding flood. Map of rising flood is the map produced when the flood is starting to occur on the floodplain. Map of peak flood is the map produced during the peak water level on the floodplain area. The last map is receding flood, which is the map produced after 6 hours of rainfall event.

To determine flood duration, the flood depths of three maps are categorized into flood-effected area when the flood depth is higher than impending depth of 0.10 m. The duration of flooding of flood-effected area is classified under three categories: short, medium, and long. Figure 4-9 shows how the flood duration was classified based on superimposing three maps of flood depth. The grids with blue color represent the flood depth which are higher than 0.1 m while empty grids represent flood depth lower than 0.1 m. The areas demonstrated as flooded in all three maps (grid No. 4 in Figure 4-9) are considered to have a long duration of flooding since the floods start occurring since the beginning of rainfall and cannot be drained within 6 hours after rainfall. The areas seen as having floods in any two of three maps are considered to have a medium duration of flooding (grid No. 3 in Figure 4-9). The areas which are flooded in one of three maps are considered to have a short duration of flooding (grid No. 2 in Figure 4-9). The areas which are not shown as having floods in any flood maps, but it is vulnerable to flooding are categorized to have a very short duration (grid No. 1 in Figure 4-9).

The area of flooding under each category is computed by counting the number of grids belonging to that category and expressed as percentages with respect to the total floodplain area excluding the building.
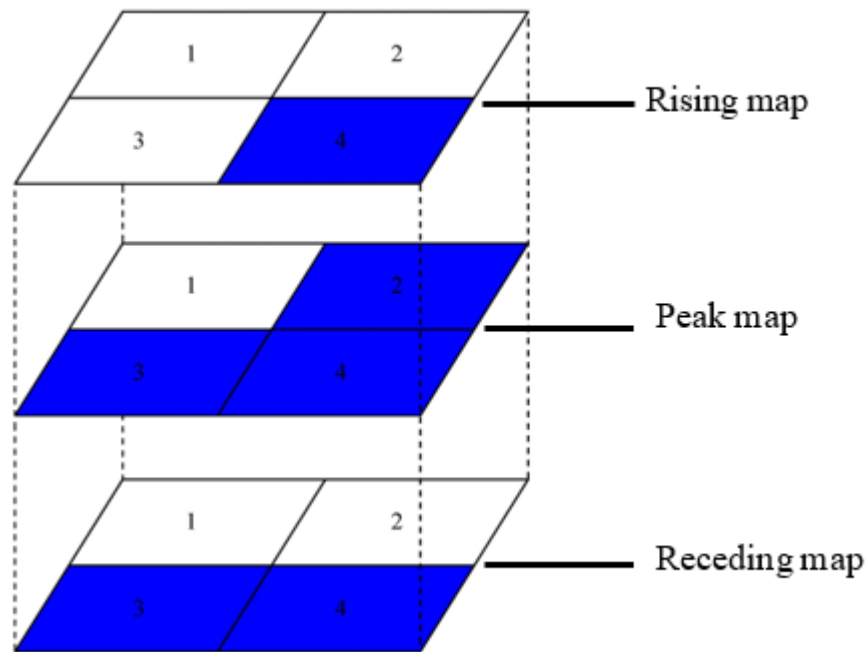
Figure 4-9: Overlapping of three flood depth maps to define flood duration

4.6 Hazard assessment

4.6.1 Hazard parameters

Through the hydrodynamic modeling, floods of various exceedance probabilities are transformed into a spatial domain in terms of depth, flow velocity and duration of flooding. According to United Nations (1991), the flood hazard assessment depends on many parameters such as depth of flooding, duration of flooding, flood wave velocity, and rate of arising water level. Many parameters can be taken into consideration in the hazard assessment according to characteristics of study area and floods types. Keokhumcheng et al. (2012) considered the depth and duration of flooding for hazard assessment since the feature of study area is a floodplain with flat topography. With similar characteristics to the study conducted by Keokhumcheng et al. (2012), two major parameters of flood depth and flood duration are also considered in this study.

4.6.2 Hazard indices for flood depth and duration

From flow simulation results, two parameters of flood depth and flood duration estimated for each grid and maps of each individual parameter have been prepared. In this study, hazard index (HI) is used to represent the severity or the degree of flood hazard. Ranges of hazard index scales are tested to determine appropriate scale of each hazard category that closely reflects actual flood hazard situation. The hazard index, HI_d is used as flood depth hazard index while HI_t represents as flood duration hazard index.

The idea of setting the value of HI_d is that a smaller value of HI_d is set for a lower flood depth, while a greater value of HI_d refers to higher flood depth. The options of HI_d value for different categories of flood depth hazard are shown in Table 4-6. According to Keokhumcheng et al. (2012), the flood duration is linearly proportional to the flood depth. Hence, the values of HI_t assigned for different categories of flood duration hazard are similar to that of HI_d. The options of HI_t value for different categories of flood duration hazard are shown in Table 4-7.

Table 4-6: Hazard index options for depth of flooding

Depth (D) of flooding (m)	Flood depth category	Hazard index
$0 \leq D \leq 0.1$	Very low	0
$0.1 < D \leq 0.3$	Low	1
$0.3 < D \leq 0.6$	Medium	2
$0.6 < D \leq 1.2$	High	3
$D > 1.2$	Very high	4

Table 4-7: Hazard index options for duration of flooding

Duration of flooding	Flood duration category	Hazard index
Area not flooded in any inundation maps	Very short	0
Areas flooded in one of three inundation maps	Short	1
Areas flooded in two maps of three inundation maps	Medium	2
Areas flooded in three inundation maps	Long	3

4.6.3 Flood hazard index for combination of two parameters

The combined effect of two parameters, namely the depth of flooding and duration of flooding has been considered while classifying the hazard at the grid point. In this study, flood hazard index (HI) is used to represent the combination of those two parameters. The HI for each grid can be computed by the following equation (Eq. 4-23).

$$HI = \mu HI_d + \beta HI_t \qquad\qquad \text{(Eq. 4-23)}$$

where μ and β is the weighting factor for HI_d and HI_t, respectively and $\mu+\beta=1$

According to Keokhumcheng et al. (2012), the weighting factor is found to be $\mu=0.5$ and $\beta=0.5$ equally since these weighting factor values provide the maximum variation of HI. More importantly, $\mu=0.5$ and $\beta=0.5$ represent equally the influence of flood depth and flood duration for combination of those two parameters. Based on the possible combinations of HI_d and HI_t, 13 groups of HI can be classified as shown in Table 4-8. It is noted that the maximum of HI is converted to 100 for convenience. The other values of HI are converted proportionally. The new HI is categorized into five equal intervals to represent flood hazard areas. They are: $0 \leq HI = 20$ representing very low flood hazard, $20 < HI \leq 40$ representing low flood hazard, $40 < HI \leq 60$ representing medium flood hazard, $60 < HI \leq 80$ representing high flood hazard, and $80 < HI \leq 100$ representing very high flood hazard.

Table 4-8: Hazard index for combination of two parameters

No. Scenario	Function of flood depth and duration	Hazard index	Hazard category
1	Very low and very short	0	Very low
2	Low and short	28.6	Low
3	Low and medium	42.9	Medium
4	Low and long	57.1	Medium
5	Medium and short	42.9	Medium
6	Medium and medium	57.1	Medium
7	Medium and long	71.4	High
8	High and short	57.1	Medium
9	High and medium	62.5	High
10	High and long	85.7.4	Very high
11	Very high and short	71.4	High
12	Very high and medium	85.7	Very high
13	Very high and long	100	Very high

4.7 Model calibration

In this study, the calibration of FLO-2D model was done using two approaches according to two different forms of observed data. The first approach used to calibrate the model involved the time series data. However, the time series data is not robust enough to judge the model performance since it is such a short duration of a rainfall event. Therefore, the second approach was attempted using flood extent map developing from questionnaire survey and flood photo visualization. The second approach was previously used by Luo et al. (2018) to evaluate FLO-2D model due to lack of historical observed water level.

4.7.1 Time series data

On 1st December 2018, a water level station was installed to measure the water level in the Beoung Trabek channel. The station is located with the GPS coordinates of 11°32'12.7"N and 104°55'15.1"E. To calibrate the model, 3-hour period water level data recorded during a rainfall event of total depth 45 mm on 27th December 2018 was extracted to compare with the simulated data. This 3-hour period water level was extracted because its associated given rainfall depth was the highest one among all data recorded.

4.7.2 Flood extent and photo visualization

According to Heng et al. (2016), 100 respondents in four districts including Tuol Kouk, 7 Makara, Daun Penh, and Chankarmon were interviewed. The spatial distribution of the 100 samples is presented in Figure 4-10. The interviewed sample is equivalent to 3.45 sample/km². The questionnaire was designed to measure the public perception on urban flood in Phnom Penh in terms of flood characteristics, the causes and the impact of urban flood. Flood extent map was produced based on this questionnaire survey. However, the result of flood extent did not correspond to a specific rainfall event. It shows the overall or memorable experience of the citizens with the flood in front of their houses or shops. This result was used to identify and compare with the spatial distribution of flood area from the simulated flood extent.

In order to verify the flood depth, eight points of water depth were used to compare with the simulated water depth with specific events. Six points of water depth were judged by the flood photo visualization. Six photos were collected through the social media, Facebook, which were posted during two flood events on 1st August 2015 and 3rd September 2015 with the total depth of 103 mm and 86.5 mm respectively. Once, the photos were collected, the photo's locations were identified using experiences of local research team or asking directly to the person posting the photos. For the flood depth (D_{photo}), it was estimated through referenced physical objects in the photos. The technique used to estimate the water depth based on the photos is presented in Figure 4-11. The referenced inundation photos collected from the social media, Facebook are shown in APPENDIX D. The last two points were the water level in channel measured directly during a rainfall event on 14th September 2018 with the total rainfall depth of 45 mm.
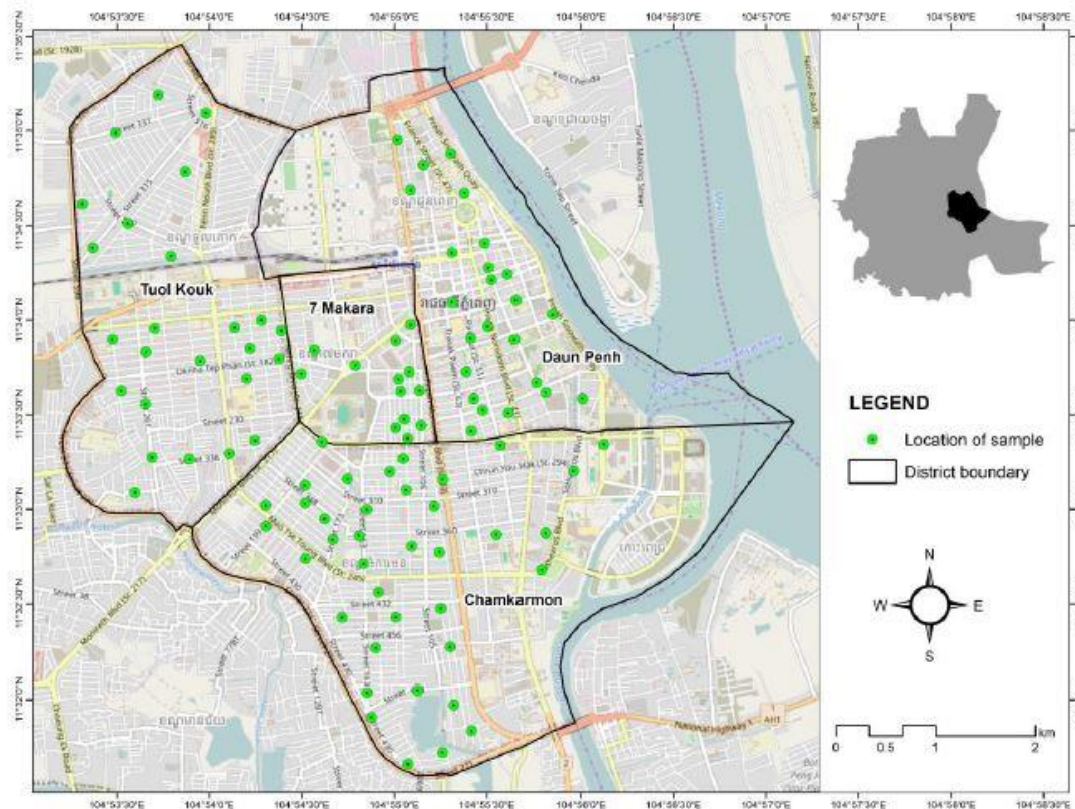
Figure 4-10: Spatial distribution of the 100 samples (Heng et al., 2016)
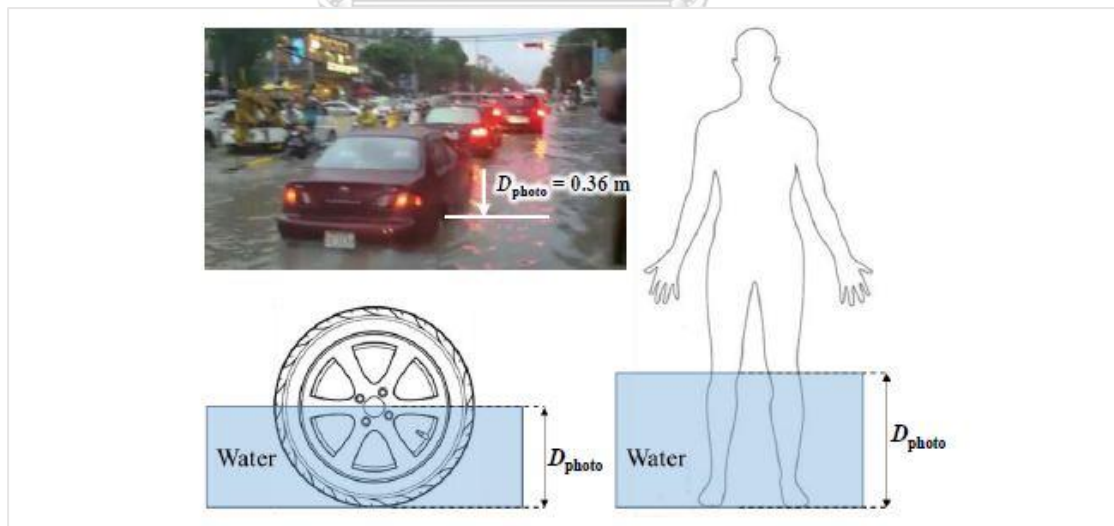
Figure 4-11: Graphical illustration of flood depth observation via photo visualization

The statistical indicators used to evaluate the agreement between observed and simulated data of time series are Nash-Sutcliff Efficiency (NSE), Root Mean Square

Error (RMSE), and coefficient of determination (R^2) which are given as following equations respectively:

$$NSE = 1 - \left[\frac{\sum_{i=1}^{n}\left(Y_i^{obs} - Y_i^{sim}\right)^2}{\sum_{i=1}^{n}\left(Y_i^{obs} - Y^{mean}\right)^2} \right] \qquad \text{(Eq. 4-24)}$$

where: Y^{obs} = the observed water depth (m)

Y^{sim} = the simulated water depth (m)

Y^{mean} = the mean of observed water depth (m)

$$RMSE = \sqrt{\frac{\sum_{i=1}^{n}\left(Y_i^{obs} - Y_i^{sim}\right)^2}{n}} \qquad \text{(Eq. 4-25)}$$

where: n = number of samples

$$R^2 = \frac{SSR}{SST} \qquad \text{(Eq. 4-26)}$$

where: $SSR = \sum_{i=1}^{n}\left(Y_i^{sim} - Y^{mean}\right)^2$ = explained variation

$SST = SSR + SSE = \sum_{i=1}^{n}\left(Y_i^{obs} - Y^{mean}\right)^2$ = total variation

$SSE = \sum_{i=1}^{n}\left(Y_i^{obs} - Y_i^{sim}\right)^2$ = unexplained variation

4.8 Summary

This section has described the detail overview of FLO-2D model, and the methods to develop flood hazard maps.

The framework of this study is shown in Figure 4-4. FLO-2D model is used to simulate urban flood in the study area. Some available data such as drainage system in SWMM model and initial values of manning's coefficient are obtained from previous work of Heng et al. (2017). In this study, detail of rainfall probability frequency analysis, develop IDF curves based on rainfall ratio method, rainfall hyetograph design, model performance evaluation, and methodology to develop flood hazard as the function of flood depth and flood duration have been added as new contributions.

CHAPTER 5
RESULTS AND DISCUSSIONS

This chapter presents and discusses the results associated with the method explained in CHAPTER 4.

5.1 Rainfall quality check

5.1.1 Double mass curve

Based on Figure 5-1 showing annual rainfall cumulation of Pochentong station plotted against the average cumulation of two other stations, it does not have a break in the slope of the double mass curve. Thus, it indicates that the rainfall record of Pochentong station was consistent. According to this test, rainfall data of Pochentong station can be used for further analysis
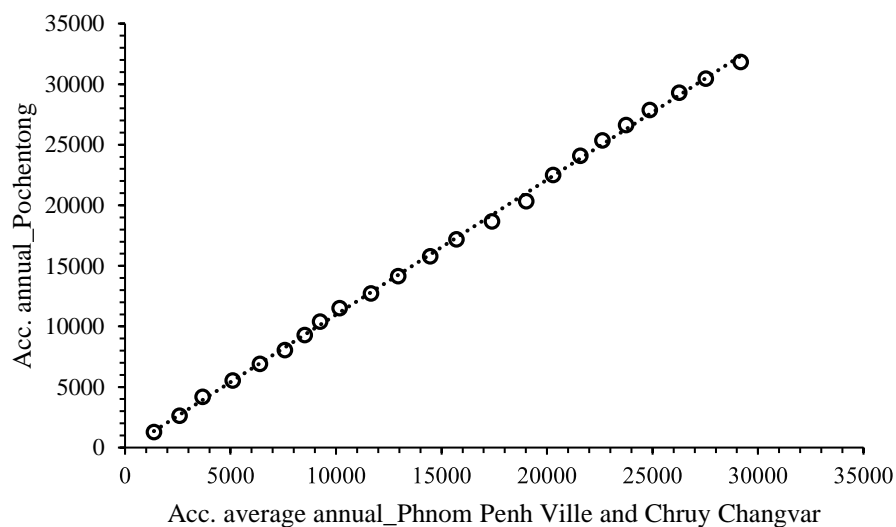
Figure 5-1: Consistency test by double mass curve

5.1.2 Rainfall pattern and trend

Figure 5-2 shows daily rainfall of 3 stations in Phnom Penh from 1985 to 2008. It is noted that Phnom Penh Ville station recorded higher rainfall followed by Pochentong station and Chruy Chongvar station, respectively. According to Figure 5-2, Phnom Penh Ville station recorded the highest rainfall depth of 257.0 mm occurred in

May 1996. This rainfall depth is extreme comparing to other stations. This value is therefore considered suspicious. Regarding to Chruy Chongvar station, the recorded rainfall data were much lower compared to that of Pochentong station. Due to particularly high rainfall value at Phnom Penh Ville station and too low rainfall value at Chruy Chongvar station, respectively, the recorded data of these two rainfall stations were not selected to represent the flood condition in this study. Another reason, these two stations has shorter records than the records at Pochentong station. The rainfall data of Pochentong station is likely to be more reliable and better represent the average rainfall with longer recorded data from 1985 to 2013. Therefore, this study is conducted using the rainfall data in Pochentong station.
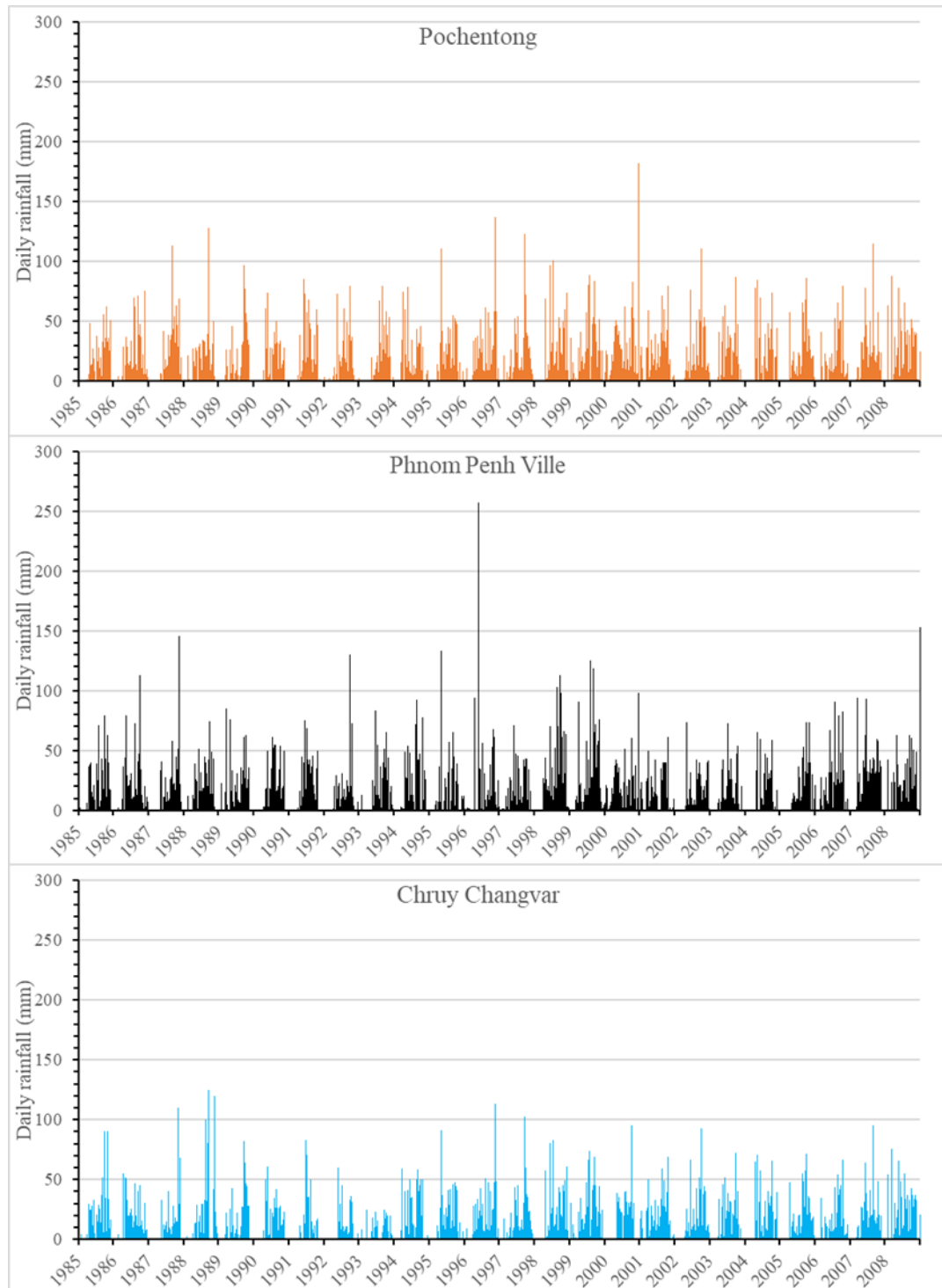
Figure 5-2: Daily rainfall of Pochentong, Phnom Penh Ville and Chruy Changvar

Figure 5-3 shows monthly average rainfall between 1985 to 2008. It demonstrates that 6 months of dry seasons (from November to April), monthly average rainfall was less than that of other 6 months of rainy season, evidently it is true. More

importantly, the highest monthly average rainfall belonged to September while the lowest amount occurred in February. The variation of the average rainfall amount of each month comparing those 3 stations, it was such a small difference. There were no any unusual average values occurred.
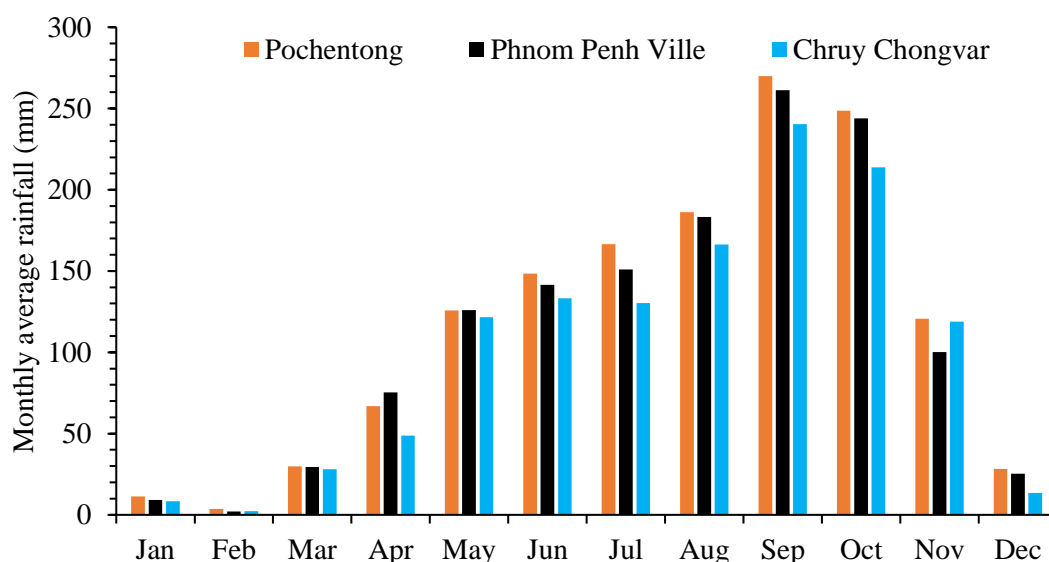
Figure 5-3: Monthly average rainfall of 3 stations in Phnom Penh

Based on Figure 5-4, the graph of annual rainfall of 3 stations, it is noticed that there was no distinct difference of rainfall amount of 3 stations except annual rainfall amount in 2000. The annual rainfall of Pochentong station in 2000 was around 2,200 mm which is greatly higher than two other stations where the rainfall amount for Phnom Penh Ville and Chruy Chongvar were only around 1,300 mm and 1,200 mm respectively. Thus, the rainfall amount of Pochentong in 2000 is particularly high. However, it is true that the extreme value existed in Phnom Penh in 2000 according to the analysis report of Cambodia Disaster Loss and Damage Information System by National Committee for Disaster Management and United Nations Department Programme (2013).
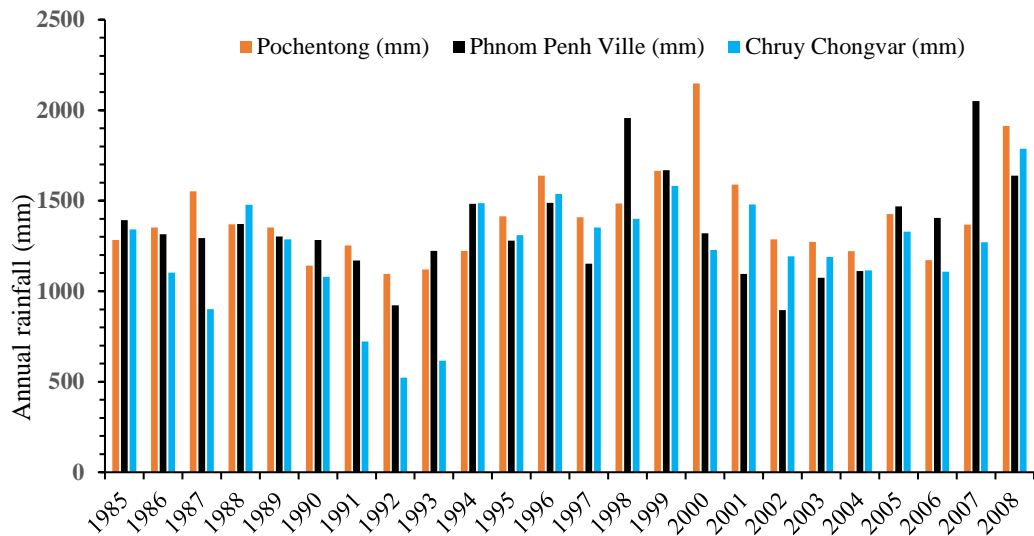
Figure 5-4: Annual rainfall of 3 stations in Phnom Penh

Moving averages of rainfall is a technique used to indicate the rainfall trend. Based on the 5-year moving averages of 3 rainfall stations in Phnom Penh shown in Figure 5-5, it is observed that the trend of rainfall recorded in 3 stations are similar. From 1987 to 1991, the trend of rainfall of 3 stations descent altogether and it started going up from 1991 to 1998 where same trend is clearly identified. The rainfall dataset of Pochentong station has similar trend as two other stations.

However, between 2000 and 2006, the trend of rainfall of Pochentong station is higher than the other two stations. This higher trend is caused by the extreme events existed in Phnom Penh in 2000 as mentioned earlier. Therefore, having the higher trend and longer recorded data covering the flood events from the year of 2000 are suitable for developing the IDF curve to represent current flood condition in this study area.
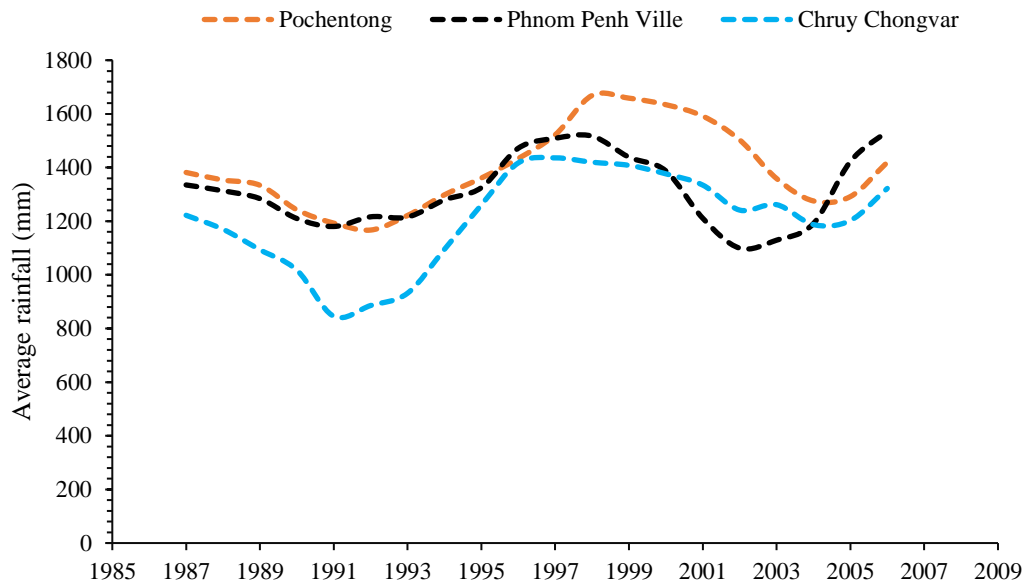
Figure 5-5: 5-year moving averages of rainfall of 3 stations in Phnom Penh

5.1.3 Box plot

Figure 5-6 shows the magnitude in maximum daily rainfall between datasets of 3 stations in Phnom Penh. It displays the mean is 97.9 mm and 100.8 mm for Pochentong and Phnom Penh station except the mean of Chruy Chongvar station which is around 80.2 mm, less than two other stations. Referring to the same figure, it demonstrates that there are three outliers of rainfall data. Two among them are high extreme values of 182.5 mm and 257.0 mm for Pochentong and Phnom Penh Ville stations respectively and another one belonging to Chruy Chongvar station is low extreme value of 25.0 mm.

The high extreme rainfall value of 182.5 mm in Pochentong station occurred in 2000 can be confirmed by the information as mentioned earlier that many provinces including Phnom Penh capital were seriously flooded in that year. Another extreme rainfall value of 257.0 mm in Phnom Penh Ville which occurred in May 1996 is still considered suspicious as mentioned above since there is no any evident have been found to confirm the possibility of this high extreme value. Turning to the last outlier value which is the low extreme rainfall in Chruy Chongvar station. This low extreme value occurred between 1993 and 1994 (Figure 5-2). Likewise, two other stations also had

low rainfall during those two years because the extreme drought occurred in that period (Chhinh and Millington, 2015).
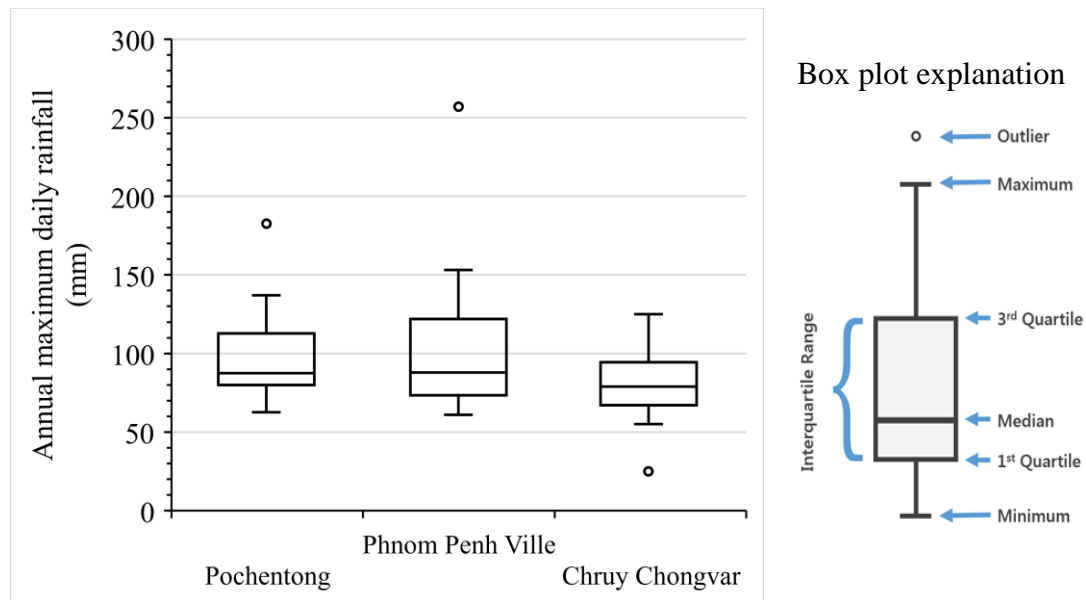
Figure 5-6: The box plot of annual maximum daily rainfall of 3 stations in Phnom Penh

5.2 Rainfall frequency analysis

By using Eq. 4-8 to Eq. 4-10, the result of probability analysis of annual maximum daily rainfall fitted with Gumbel distribution is shown in Figure 5-7. Based on graphical visualization, the maximum daily rainfall is fitted with this distribution. However, to prove that Gumbel distributions can be applied to fit the maximum daily rainfall, Chi-Square test of goodness of fit is carried out using Eq. 4-11 and Eq. 4-12.

To test goodness of fit, the null (H_0) and alternative (H_1) hypothesizes are defined as below:

H_0: Rainfall data follows Gumbel distribution

H_1: Rainfall data do not follow Gumbel distribution
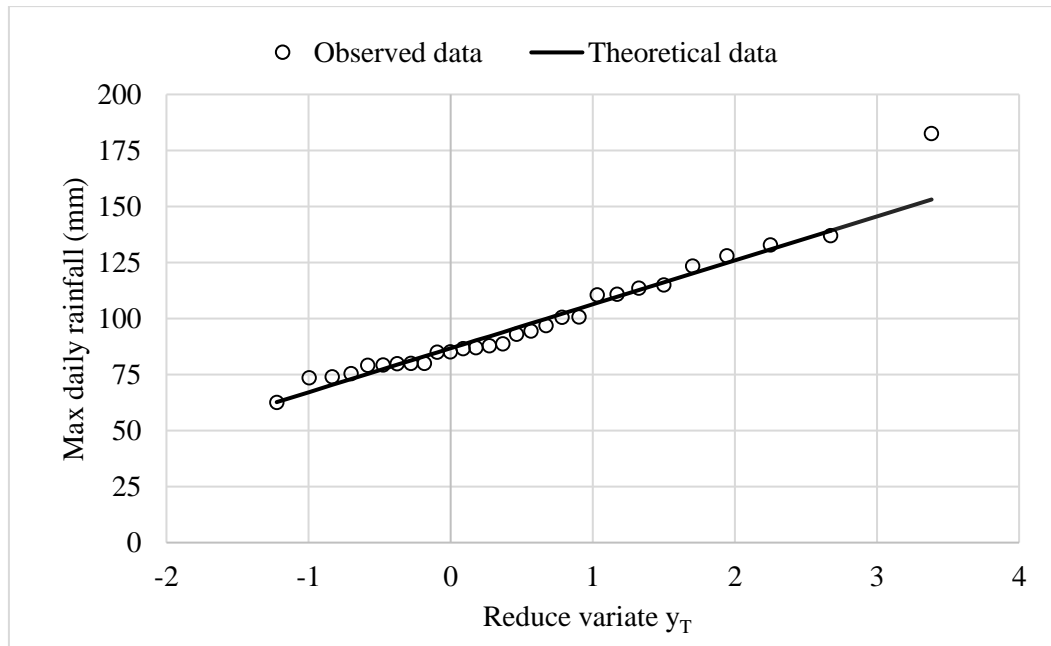
Figure 5-7: Result of Gumbel extreme value distribution of maximum daily rainfall

The observed rainfall data is classified into 15 bins with the observed frequency as shown Table 5-1.

Table 5-1: Observed rainfall bin and frequency

Rainfall (mm)	Observed frequency (O_i)
< 60	0
60 - 70	1
70 - 80	8
80 - 90	6
90 - 100	3
100 - 110	2
110 - 120	4
120 - 130	2
130 - 140	2
140 - 150	0
150 - 160	0
160 - 170	0
170 - 180	0
180 -190	1
> 190	0

Supposed that rainfall data: $X \sim$ Gumbel (μ_x, α_x)

Based on observed rainfall data of n = 29 years, the Gumbel distribution parameters: $\mu_x = 86.71$ and $\alpha_x = 19.62$. By using Eq. 4-13, the probability and frequency of expected rainfall could be determined as shown in the Table 5-2.

Table 5-2: Calculation of expected frequency

Rainfall (mm)	Probability (p_i)	Expected frequency ($E_i = np_i$)	$(O_i - E_i)^2/E_i$
< 60	0.020	0.59	0.586
60 - 70	0.076	2.20	0.652
70 - 80	0.149	4.31	3.153
80 - 90	0.185	5.35	0.078
90 - 100	0.172	5.00	0.800
100 - 110	0.135	3.92	0.943
110 - 120	0.095	2.77	0.547
120 - 130	0.063	1.83	0.015
130 - 140	0.040	1.17	0.594
140 - 150	0.025	0.73	0.726
150 - 160	0.015	0.45	0.446
160 - 170	0.009	0.27	0.271
170 - 180	0.006	0.16	0.164
180 -190	0.003	0.10	8.198
> 190	0.005	0.15	0.150

The Chi-square value can be calculated:

$$\chi^2_0 = \sum_{i=1}^{k} \frac{(O_i - E_i)^2}{E_i} = 0.586 + 0.652 + ... + 0.150 = 17.324$$

Based on the Chi-square distribution table in APPENDIX E, the critical value of Chi-square with the significance (α) equal to 0.05 is

$$\chi^2_{15-2-1,0.05} = \chi^2_{13,0.05} = 22.362$$

It is seen that $\chi^2_0 < \chi^2_{k-p-1,\alpha}$, which implies that the null hypothesis (H_0) cannot be rejected. Thus, it indicates that the maximum daily rainfall of Pochentong is fitted

with Gumbel distribution. Based on Eq. 4-9 and Eq. 4-10, daily maximum rainfall followed Gumbel distribution can be calculated as shown in Table 5-3.

Based on observed daily maximum rainfall, the mean value is $\bar{x} = 98.0$ mm and the standard deviation $S = 25.2$. Then, the maximum daily rainfall X_T associated with a given return period, $T = 2$-year return period can be determined:

$$K_T = -\frac{\sqrt{6}}{\pi}\left[0.5772 + \ln\left(\ln\left(\frac{T}{T-1}\right)\right)\right] = -\frac{\sqrt{6}}{\pi}\left[0.5772 + \ln\left(\ln\left(\frac{2}{2-1}\right)\right)\right] = -0.164$$

$$X_{T=2} = \overline{X} + K_T S = 98.0 - 0.164 \times 25.17 = 93.9 mm$$

Table 5-3: Computed rainfall and return period as the result of Gumbel distribution

Return period T (year)	Daily maximum rainfall (mm)
2	93.9
5	116.1
10	130.9
25	153.1
50	163.3
100	177.0

5.3 IDF curve development

Based on the annual maximum daily rainfall of Pochentong station between 1985 and 201, the mean and standard deviation are 98.03 mm and 25.16 mm respectively. Applying Eq. 4-16 and Eq. 4-20, the rainfall ratio, new mean and standard deviation of maximum rainfall is shown in Table 5-4.

Table 5-4: The results of rainfall ratio, new mean maximum rainfall and new standard deviation

Duration	Rainfall ratio, RR	Mean max. rainfall, P_m	SD_{NEW}
10 min	0.30	29.55	7.59
15 min	0.38	36.87	9.46
20 min	0.43	42.19	10.83
30 min	0.51	49.54	12.72
1 hr	0.62	61.00	15.66
2 hr	0.72	70.71	18.15
3 hr	0.77	75.70	19.43
6 hr	0.85	83.48	21.43
12 hr	0.93	90.79	23.30
18 hr	0.97	95.02	24.39
24 hr	1.00	98.03	25.16

Then, the Gumbel distribution is applied to derive rainfall depth or intensity for each duration and frequency using Eq. 4-21 with the values of Gumbel factor in Table 4-3. The results of rainfall depth and rainfall intensity are presented in Table 5-5, and Table 5-6, accordingly. Then, Intensity-Duration-Frequency curves as shown in Figure 5-8 can be plotted using the data from Table 5-6.

Table 5-5: The rainfall depth for each duration and frequency

Duration	Rainfall depth (mm)					
	2 yr	5 yr	10 yr	25 yr	50 yr	100 yr
10 min	28.31	35.01	39.45	45.06	49.22	53.35
15 min	35.31	43.68	49.21	56.21	61.40	66.55
20 min	40.41	49.98	56.31	64.32	70.26	76.15
30 min	47.45	58.69	66.13	75.53	82.51	89.43
1 hr	58.43	72.27	81.43	93.00	101.59	110.11
2 hr	67.72	83.76	94.38	107.79	117.75	127.63
3 hr	72.51	89.68	101.04	115.41	126.06	136.64
6 hr	79.96	98.90	111.44	127.28	139.03	150.69
12 hr	86.97	107.56	121.19	138.42	151.20	163.89
18 hr	91.01	112.56	126.83	144.86	158.24	171.51
24 hr	93.90	116.14	130.86	149.46	163.26	176.96

Table 5-6: The rainfall intensity for each duration and frequency

| Duration	Rainfall intensity (mm/hr)					
	2 yr	5 yr	10 yr	25 yr	50 yr	100 yr
10 min	169.84	210.06	236.69	270.34	295.29	320.07
15 min	141.25	174.70	196.85	224.83	245.59	266.19
20 min	121.23	149.93	168.94	192.95	210.77	228.45
30 min	94.91	117.38	132.26	151.06	165.01	178.86
1 hr	58.43	72.27	81.43	93.00	101.59	110.11
3 hr	24.17	29.89	33.68	38.47	42.02	45.55
6 hr	13.33	16.48	18.57	21.21	23.17	25.12
12 hr	7.25	8.96	10.10	11.54	12.60	13.66
18 hr	5.06	6.25	7.05	8.05	8.79	9.53
24 hr	3.91	4.84	5.45	6.23	6.80	7.37
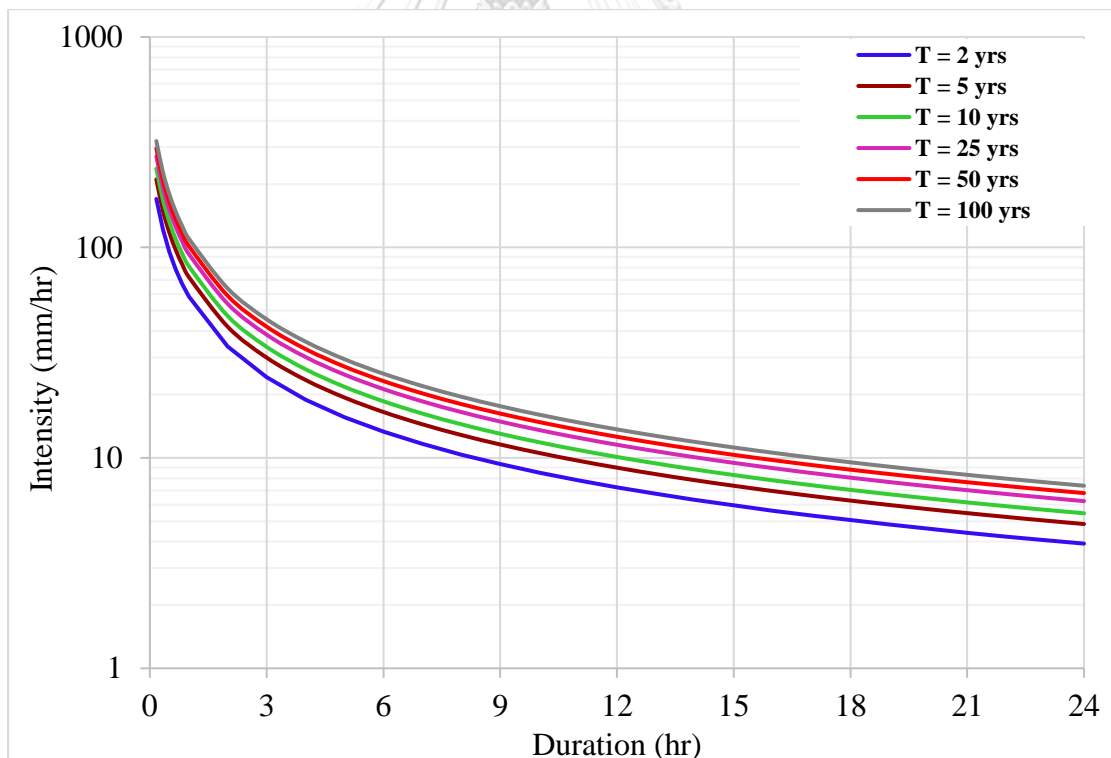
Figure 5-8: Intensity-Duration-Frequency curves

When the equation of Horner Type shown in Eq. 4-15 is applied to different return periods to express IDF curves, the equations can be listed below.

For T = 2 -year return period

$$I = \frac{68.865}{(0.2+D)^{0.9}}$$

For T = 5-year return period

$$I = \frac{85.310}{\left(0.2+D\right)^{0.9}}$$

For T = 10-year return period

$$I = \frac{95.940}{\left(0.2+D\right)^{0.9}}$$

For T = 25-year return period

$$I = \frac{109.648}{\left(0.2+D\right)^{0.9}}$$

For T = 50-year return period

$$I = \frac{119.674}{\left(0.2+D\right)^{0.9}}$$

For T = 100-year return period

$$I = \frac{129.718}{\left(0.2+D\right)^{0.9}}$$

5.4 Comparison of IDF curve

By comparing the IDF curves developed by JICA and IDF curves using the rainfall ratio method (Figure 5-9 to Figure 5-11), it is found a significant difference of rainfall intensity, especially in the short duration. For 2, 5, and 10-year return periods, the rainfall intensity developed by rainfall ratio is higher than that of JICA estimation. This is because JICA created IDF curves based on short sub-daily rainfall since 1980-1997 which did not cover the extreme events in 2000, 2010, and 2012. Another reason could be the effect of climate change which leads to higher rainfall intensity with short duration. This is the reason why IDF curve developed by JICA is lower than current IDF curve using Rainfall Ratio method produced in this study. The graphs showing the difference between IDF curves produced by JICA and by rainfall ratio method are illustrated in Figure 5-9, Figure 5-10, and Figure 5-11.
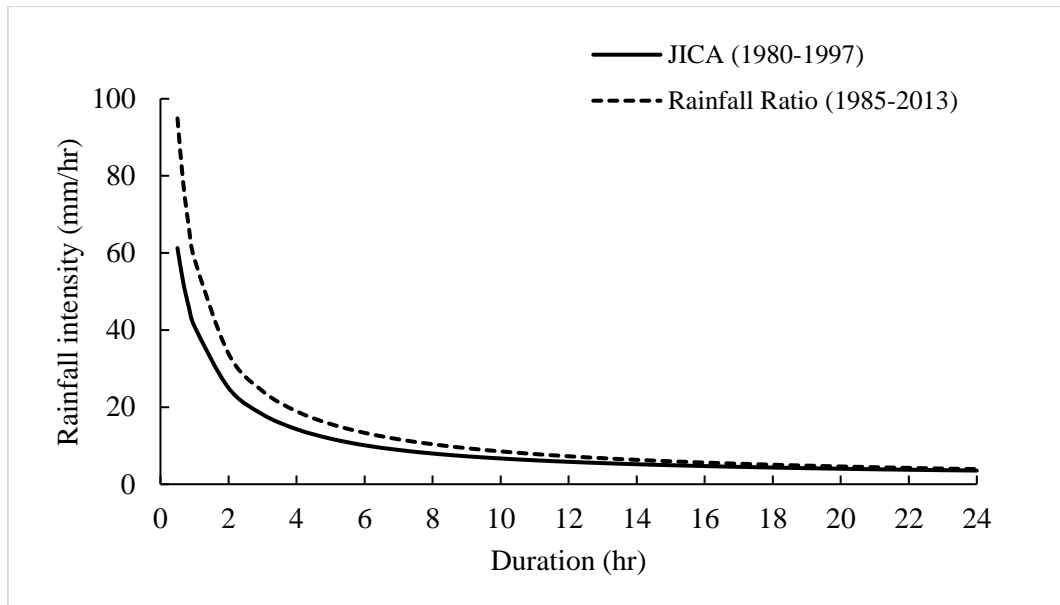
Figure 5-9: Phnom Penh IDF curves for 2-year return period
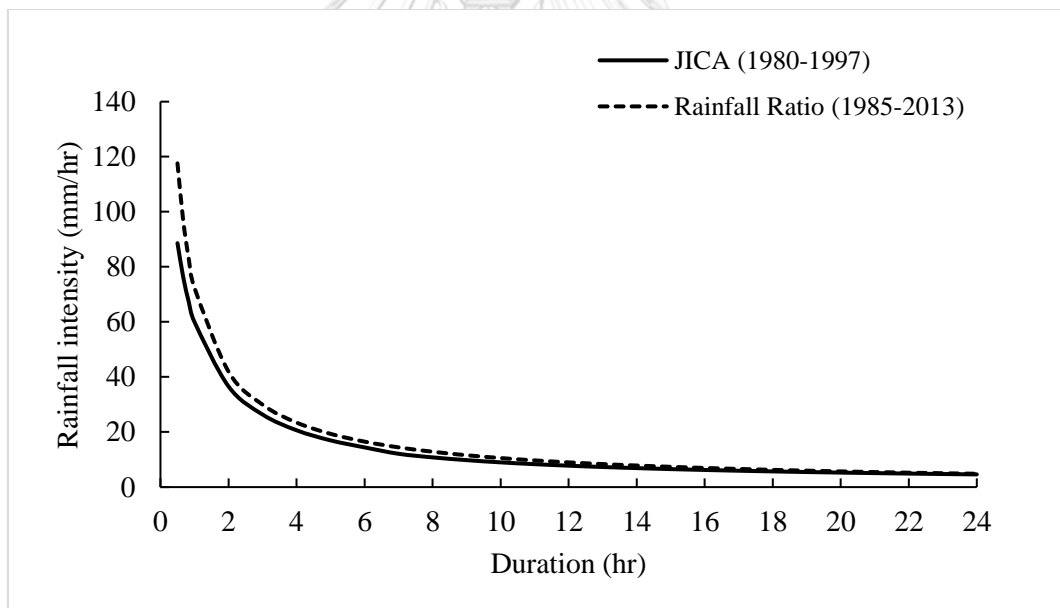
Figure 5-10: Phnom Penh IDF curves for 5-year return period
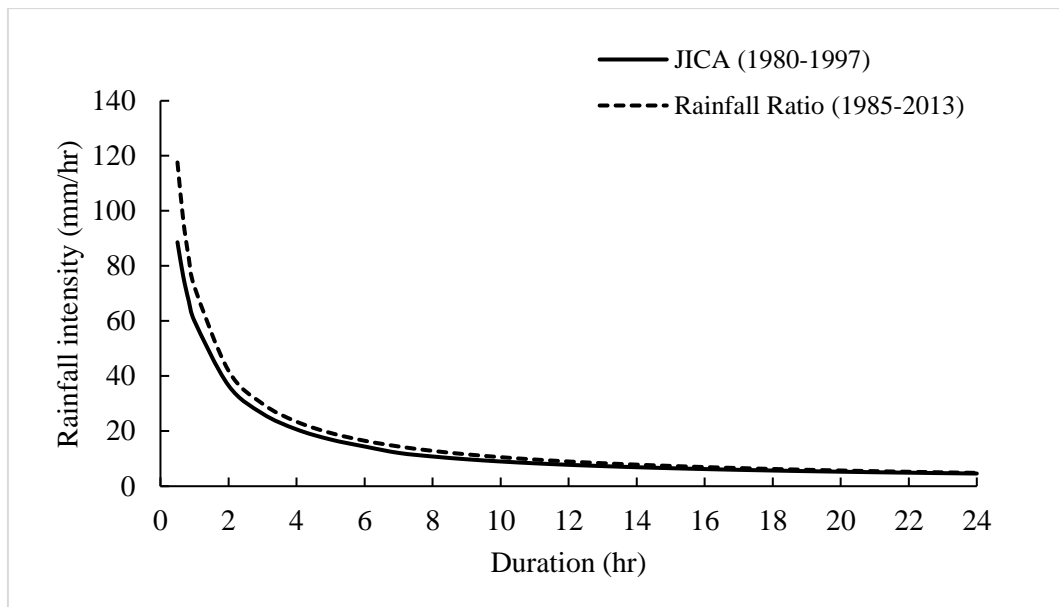
Figure 5-11: Phnom Penh IDF curves for 10-year return period

5.5 Rainfall hyetograph design

In the case of single point rainfall, Eq. 4-17 is applied to adjust rainfall for spatial distribution over the study area while Eq. 4-19 is used to compute incremental intensity of the rainfall totals of the calculated duration up to the time of concentration. The computation of design rainfall for 2, 5, 10 and 25-year return period are presented in Table 5-7, Table 5-8, Table 5-9, and Table 5-10, respectively.

Table 5-7: Computation of design rainfall for T = 2-year return period

Time (hrs)	0.25	0.5	1	2	3	6
Point rainfall (mm)	35.3	47.5	58.4	67.7	72.5	80.0
ARF	0.78	0.82	0.86	0.89	0.90	0.92
Areal Rainfall (mm)	27.4	39.0	50.2	60.1	65.4	73.7
Incremental intensity (mm/hr)	109.7	46.4	22.3	9.9	5.3	2.8
No of 15 min increments	1	1	2	4	4	12

Table 5-8: Computation of design rainfall for T = 5-year return period

Time (hrs)	0.25	0.5	1	2	3	6
Point rainfall (mm)	43.7	58.7	72.3	83.8	89.7	98.9
ARF	0.78	0.82	0.86	0.89	0.90	0.92
Areal Rainfall (mm)	33.9	48.3	62.0	74.3	80.9	91.2
Incremental intensity (mm/hr)	135.7	57.4	27.6	12.3	6.5	3.4
No of 15 min increments	1	1	2	4	4	12

Table 5-9: Computation of design rainfall for T = 10-year return period

Time (hrs)	0.25	0.5	1	2	3	6
Point rainfall (mm)	49.2	66.1	81.4	94.4	101.0	111.4
ARF	0.78	0.82	0.86	0.89	0.90	0.92
Areal Rainfall (mm)	38.2	54.4	69.9	83.8	91.1	102.7
Incremental intensity (mm/hr)	152.9	64.6	31.1	13.9	7.3	3.9
No of 15 min increments	1	1	2	4	4	12

Table 5-10: Computation of design rainfall for T = 25-year return period

Time (hrs)	0.25	0.5	1	2	3	6
Point rainfall (mm)	56.2	75.5	93.0	107.8	115.4	127.3
ARF	0.78	0.82	0.86	0.89	0.90	0.92
Areal Rainfall (mm)	43.6	62.1	79.8	95.7	104.0	117.3
Incremental intensity (mm/hr)	174.6	73.8	35.5	15.8	8.4	4.4
No of 15 min increments	1	1	2	4	4	12

The design rainfall hyetographs of 2, 5, 10, and 25-year return period using r = 0.13 are illustrated as shown in Figure 5-12, Figure 5-13, Figure 5-14, and Figure 5-15. Moreover, the comparison between design rainfall and actual rainfall are also done. However, the comparison can be done for only 2-year (Figure 5-12) and 5-year return period (Figure 5-13) due to the availability of actual data. For 2-year return period, the increase in design rainfall intensity is more rapid than that of the actual rainfall. The design rainfall intensity better captures the decreased intensity. However, the design rainfall overestimates the actual intensity when rainfall proceeds in time at about 3.5 hrs. For 5-year return period, the time of concentration of the design rainfall is delayed

from that of the actual rainfall but the patterns of the design and actual rainfall intensity are similar.

Figure 5-12: 6-hour design rainfall hyetograph for T = 2-year return period

Figure 5-13: 6-hour design rainfall hyetograph for T = 5-year return period
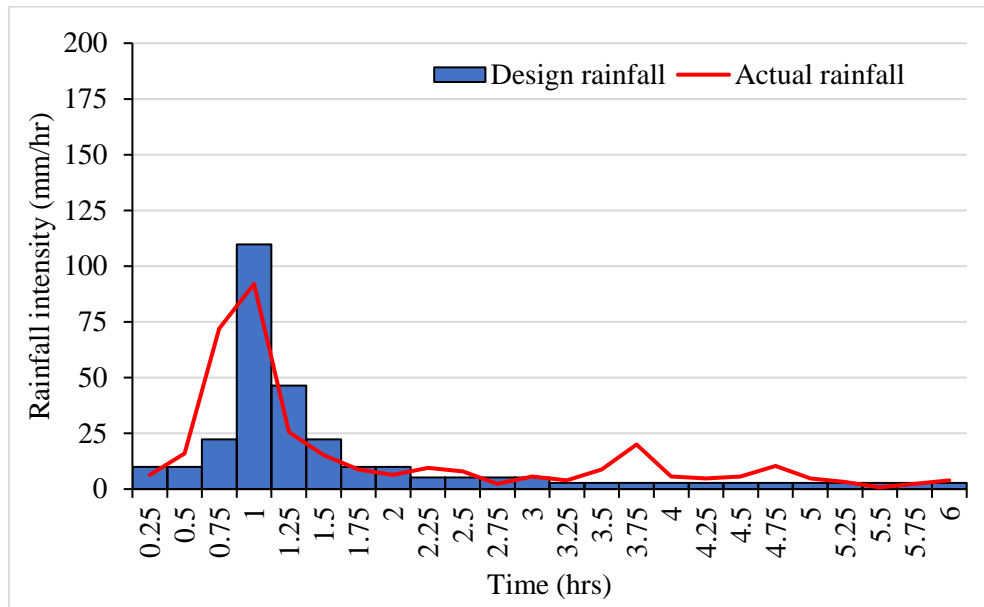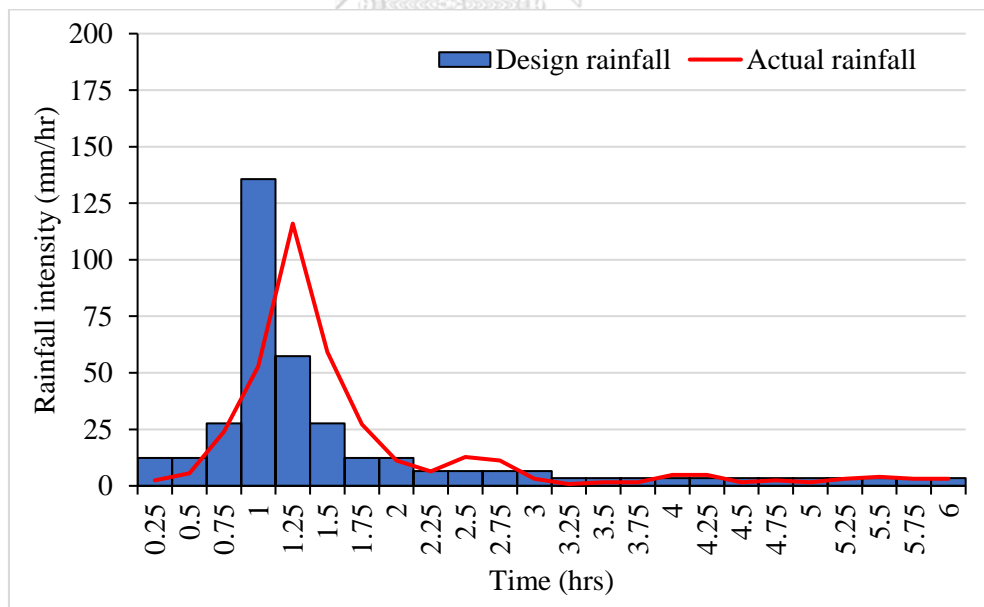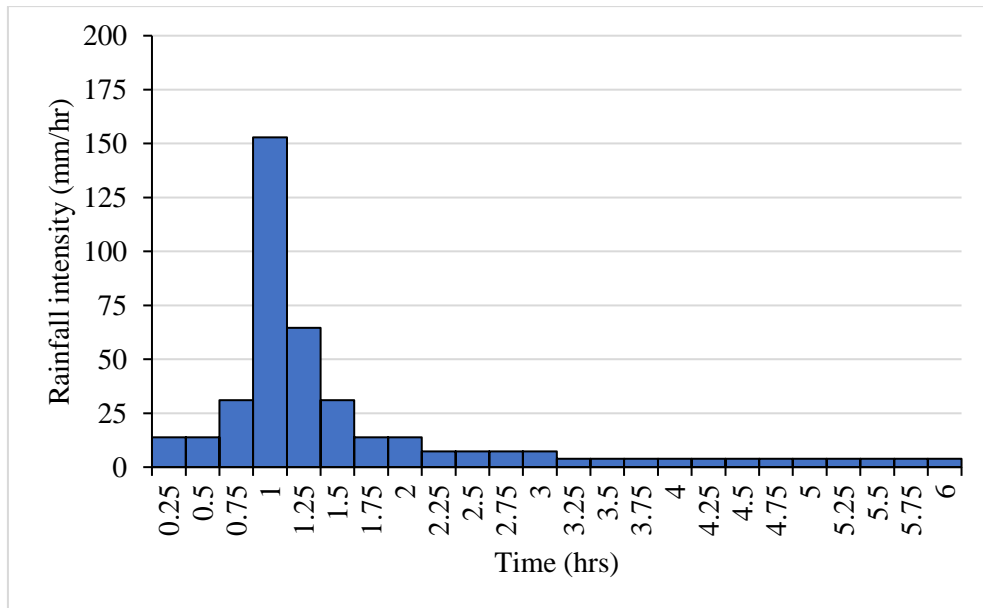
Figure 5-14: 6-hour design rainfall hyetograph for T = 10-year return period

Figure 5-15: 6-hour design rainfall hyetograph for T = 25-year return period
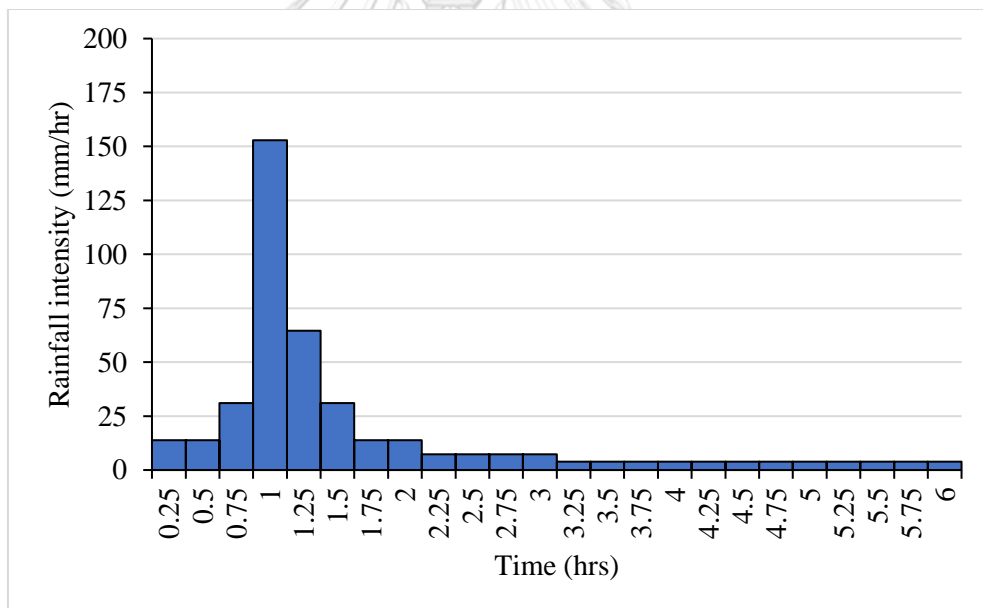
5.6 Model calibration

5.6.1 Sensitive parameters

Determination of flood flow through the study area is performed by FLO-2D model. The hydrodynamic model was first calibrated with the data of time series of

water depth in the channel. During the calibration, the weir coefficient of drainage inlets, pump operating curve, initial flow in the channels and the Manning's n of floodplain, channels were adjusted by trial and error to get good agreement between the observed and simulated water level.

Initial flow is an uncertain and crucial parameter because drainage system in Phnom Penh is a combined system draining both wastewater and stormwater. Figure 5-16 shows observed water level recorded from 8th December 2018 to 3rd March 2019 which is the dry period with little rainfall, the existing flow in the channel ranges between 1.14 m and 1.85 m. The existing flow values ranging between 1.14 m and 1.85 m was therefore used as initial flow in the model to represent the uncertainty of household wastewater flow into the channels. The way to fill the existing flow depth in the channel is setting up hydrograph in the channel which is suggested by Karen O'Brien (Manager at FLO-2D Software, Inc).
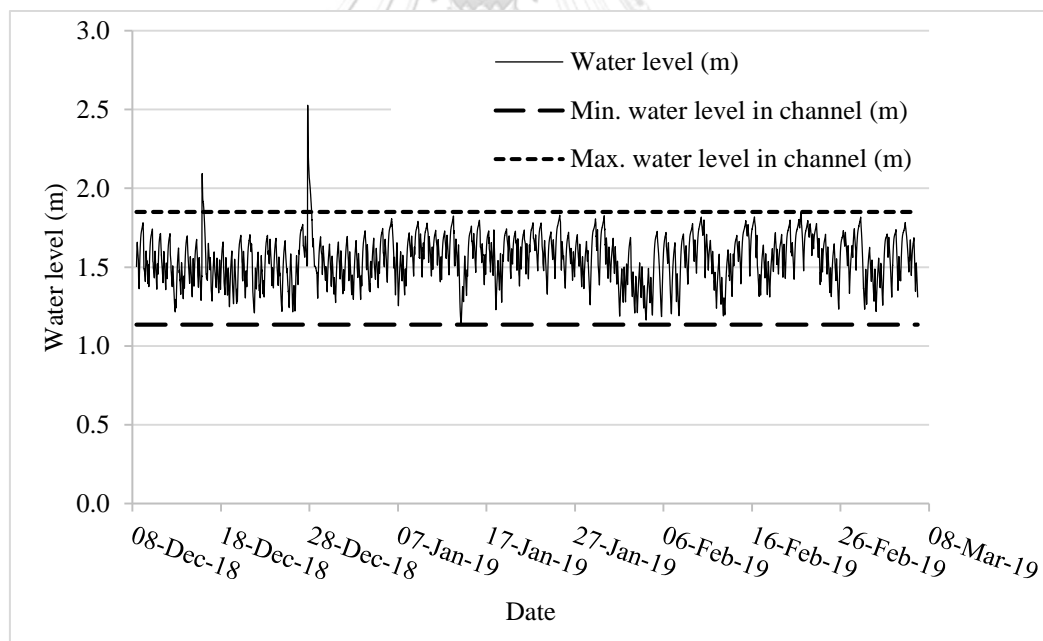
Figure 5-16: Observed water level in channel from 08 December 2018 to 3 March 2019

Setting up the initial flow (hydrograph) in the channel, agreement between observed and simulated water level in channel is expected to have a better fit. However, the results indicate that the simulated water level was less than the observed one. Then,

the initial flow hydrograph was adjusted by adopting the existing maximum water level (1.85 m) as input to the model with an aim to increase the simulated water level in the channel. The new result showed that the simulated water level was still lower than the observed water level. Therefore, Manning's n of the channels which was found to be a sensitive parameter to water level in channel, was adjusted. Two parameters: initial flow and Manning's n were considered as sensitive parameters since they made a large variation of water level in the channels. The scenarios of sensitivity analysis of initial flow (hydrograph variation) and the Manning's n of the channels were carried out and presented in Figure 5-17 and Figure 5-18.
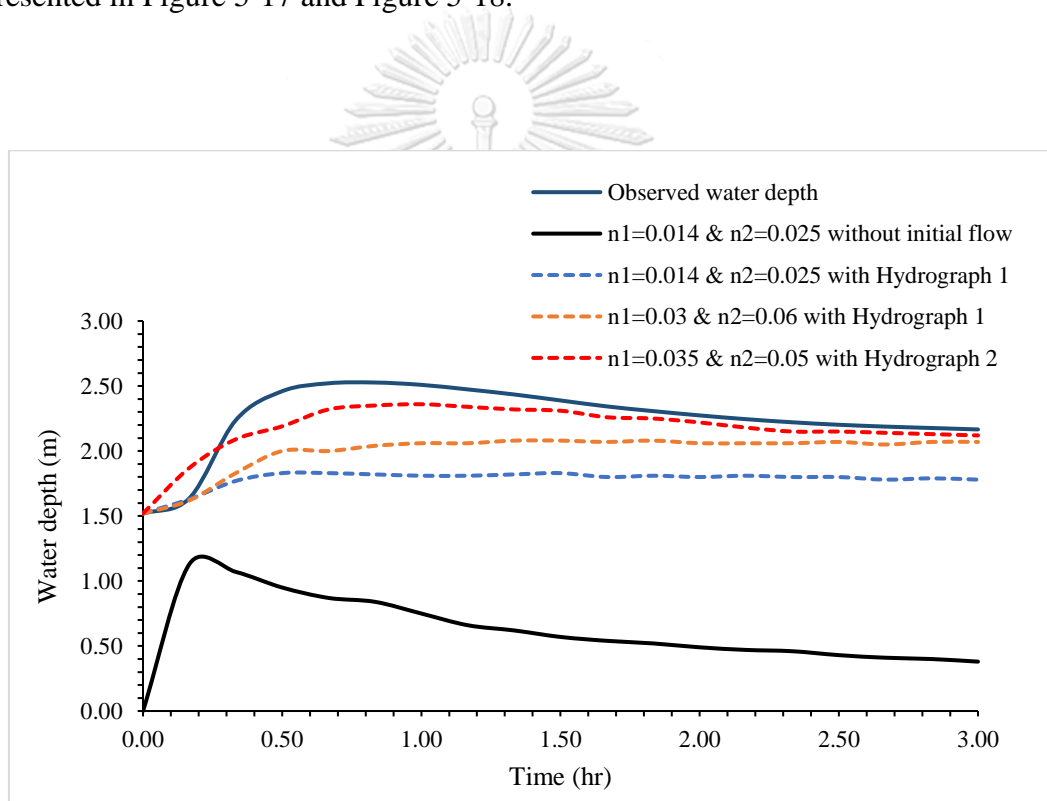
Figure 5-17: The simulated and observed water depth in the channel
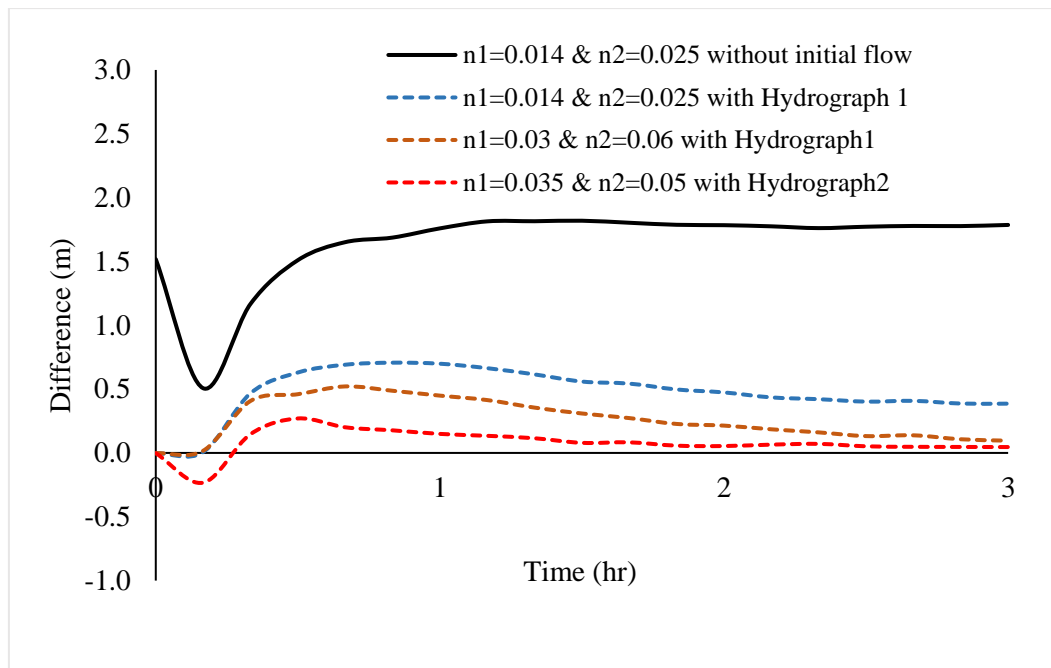
Figure 5-18: Difference between observed and simulated results in case Manning's n of channel variation

According to serval previous flood studies such as Muleta and Nicklow (2005), Ritter and Muñoz-Carpena (2013) RMSE is an indicator used in order to define the fitness of simulated data with observed data. The lowest value of RMSE indicates the best agreement between simulated data and observed data. Figure 5-17 shows the simulated water depth of all scenarios and the observed water depth while Figure 5-18 shows the difference between observed and simulated water depth.

There is no absolute way to calibrate flood models. Having good understanding of the processes and modeling experience reduce burdensome calibration task and contribute to reasonably good results. Major steps of calibration performed in this study are explained as below

The first simulation scenario was that the Manning's coefficient of concrete n1 = 0.014 and Manning's coefficient of earth n2 = 0.025 were assigned to the channels. These coefficients were based on Chow (1959). The initial flow was not set up in the model for the first simulation. The result of this scenario showed that the simulated

water depth ranging from 0.5 m to 1.90 m which was much lower than that of observed one. The value of RMSE was equal to 1.67 m.

Then, the scenario 2 was created by just adding the hydrograph 1 (constant discharge 14.5 m^3/s) into the scenario 1. The result indicated that the difference was reduced with the RMSE value of 0.51 m. However, the simulated water depth was still lower than observed water depth.

Hence, in order to make an attempt for better result, the scenario 3 was developed by adjusting the Manning's n1 equals to 0.03 and n2 equals to 0.06. The result of this scenario was better with the RMSE value of 0.31 m. Once, these two parameters were identified as sensitive parameters for water depth in the channel, the initial flow (hydrograph) and Manning's coefficient n were adjusted at the same time for better fit. Based on trial and error, the scenario 4 was finally set up. The parameters for this scenario were adjusted to be n1 equals to 0.035 and n2 equals to 0.05 with the hydrograph 2 as presented in Table 5-11. The RMSE value of this scenario was 0.13.

Since the value of RMSE of scenario 4 was the lowest value among all scenarios set up in the model, the parameter set of this scenario was selected to be used for further analysis. Therefore, the calibrated Manning's n of concrete channel was found to be 0.035 (n$_1$) and 0.050 (n$_2$) for earth channel with hydrograph 2 shown in Table 5-11.

The calibrated Manning's n values are higher than that recommended by Chow (1959), which are 0.014 for concrete and 0.025 for earth channel. However, the recommended Manning's n is only for new channel or channel with good maintenance. Thus, higher values of calibrated Manning's n are possibly from the superannuated age of the channels with poor maintenance. Another reason of high values of Manning's n could be caused by the effect of garbage and obstacles in the downstream of the channel shown in APPENDIX F. Other parameters such as the weir coefficient of drainage inlets was found to be 1.62, and Manning's n of floodplain is given in Table 5-12.

Table 5-11: Hydrograph 2 set up in the channel as existing flow depth

Time (hr)	Discharge (m³/s)
0	0
0.01	16
0.02	16
0.1	18
0.5	22
1	20
2	18
3	18

Table 5-12: Manning's n set up for floodplain and its range (O'Brien and Garcia, 2009)

No	Surface	n-value	n-value range
1	Dense turf	0.3	0.17 - 0.80
2	Average grass cover	0.2	0.20 - 0.40
3	Building (ARFs)	0.03	0.03 (recommended)
4	Asphalt or concrete	0.02	0.016 - 0.05
5	Open ground with debris	0.2	0.10 - 0.20

5.6.2 Calibration with time series data

A comparison of the observed and simulated water depth is shown in Figure 5-19. The result shows good agreement between the observed and simulated data on the three parameters namely, NSE, RMSE, and R^2. The values of NSE, RMSE, and R^2 were found to be 0.76, 0.13, and 0.91 respectively.

The NSE value range between 0.0 and 1.0 is considered as acceptable results. Higher value of the NSE indicates good agreement between the observed and simulated results. When compared with the observed flow, simulated flow was found to perform moderately well with NSE of 0.76. This value is considered acceptable as it is similar to the values obtained from previous study such as Vu and Ranzi (2017) and Vozinaki

et al. (2017) with similar NSE values. Meanwhile, the value of RMSE which is widely used to quantify the prediction error in terms of the variable units, is found to be 0.13. This value indicates that the error of the water level prediction is around 0.13 m. The R^2 value of 0.91 is such a very good degree of linear correlation between observed and simulated data. This means that 91% of the proportion of the variance of the observed data can be explained by the model. The scatter plot of simulated and observed water depth is shown in Figure 5-20.

The calibration result visualized in Figure 5-19 indicates that the simulated water depth hydrograph has less steep rising limb than that of observed one. The peak water level of the simulated data is lower than the observed data. This result indicates that the model underestimates flood depth and delays the time of peak. This underestimation result could be caused from the effect of garbage and poor resident constructed as obstacle in the channel while in the model there are no any structures along the channel set up.
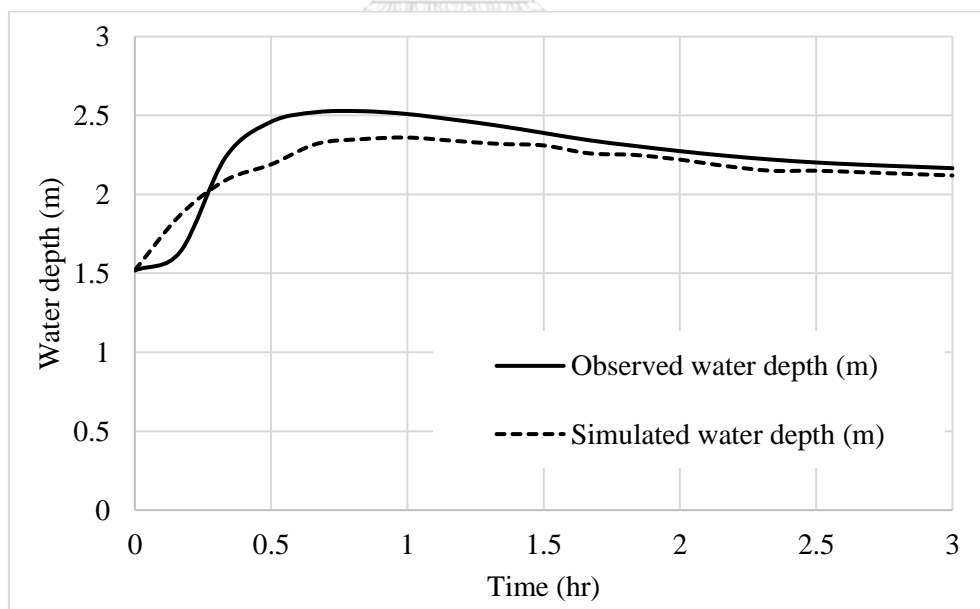

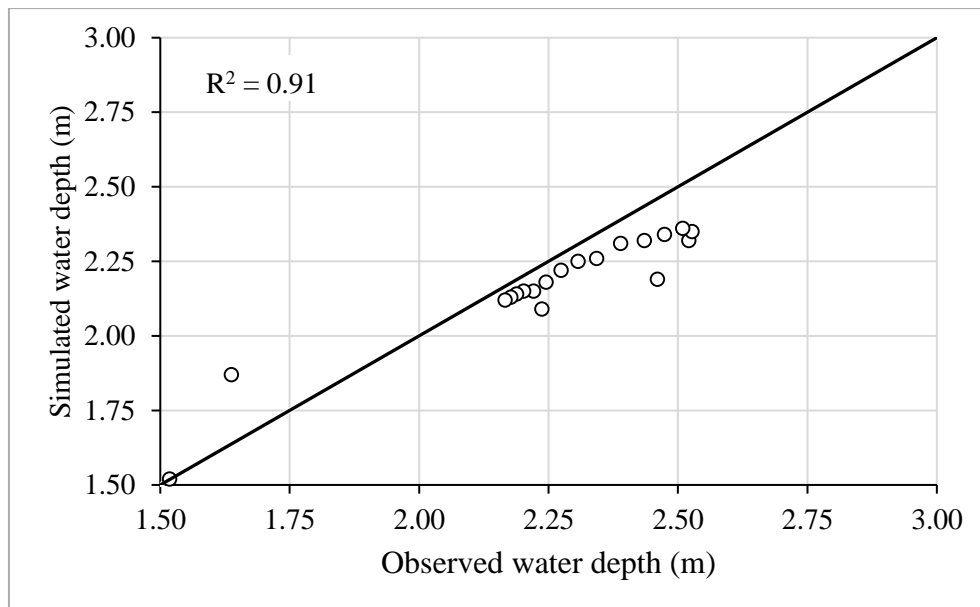Figure 5-19: Result of model calibration with time series data

Figure 5-20: Scatter plot of simulated and observed water depth

Based on the statistical indicator values, it can be concluded that FLO-2D can be used to simulate urban flood in Phnom Penh. However, there are only one point of time series data for calibration which is not robust enough to evaluate model performance. Therefore, FLO-2D is evaluated with the flood extent by questionnaire survey and photo visualization. It is noted that the parameters input in the model for both calibration methods are the same.

5.6.3 Calibration with flood extent and photo visualization

5.6.3.1 *Flood extent*

Since the satellites image of flood extent in the study area is unavailable, flood extent map obtained from questionnaire is used to verify the model accuracy. Figure 5-21 illustrates the flood extent in the study area obtained (a) from questionnaire and (b) from the simulation. As described in section 4.7.2, flood extent obtained from questionnaire did not correspond to any specific rainfall event. Hence, the main purpose of using this flood extent map is only to compare the locations of distinct flood experienced by citizens with the simulation result of an extreme event.

According to Figure 5-21, it is apparent that the flood area produced by the model seems to be well matched with the flood area obtained from the questionnaire. The notable flood area can be seen on the maps in Figure 5-21 by the points A, B, C, D, E, and G, except point F. The areas of points A to E and G were recorded having serious flood by citizen experience. What can be clearly seen in simulated results (Figure 5-21 (b)) is that those areas are flooded which are comparable to that of the actual flood experienced by citizens. The area of point F is suggested by the questionnaire as the area with serious flood, but the model cannot capture flood in this area. It is observed that the distinct flood in the location of point F might be caused by the overflow from the channel. Thus, the inconsistent result could occur because there is no overflow from the channel in the simulation.
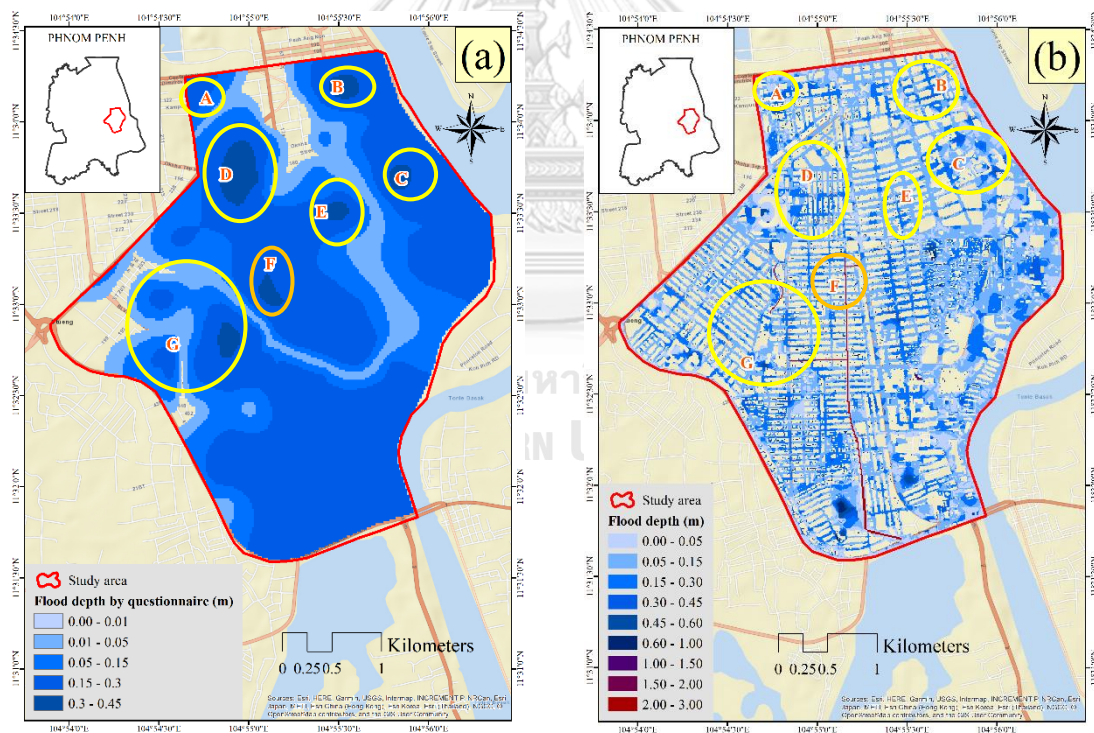

Figure 5-21: Flood extent maps obtained (a) from questionnaire (b) from simulation

5.6.3.2 *Photo visualization*

In the final part of the calibration is comparison of flood depth points from photo visualization and simulated results according to specific events and locations. There are 6 points of flood depth were estimated from the photo visualization during the flood events of 86.5 mm and 103 mm. Other two points are water depth in channel measured directly during the rainfall event of 40.4 mm. These 8 points are used for calibration purposes.

Figure 5-22 shows 8 points of observed flood depth which were estimated by photos visualization while Figure 5-23 shows the simulated flood depth points with specific events (a) event 86.5 mm (b) event 103 mm and (c) event 40.4 mm. For 6 points of the flood depth of rainfall events 86.5 mm and 103 mm (Figure 5-23 (a) and (b)), the model underestimated the flood depth when compared to that of photo visualization (Figure 5-22). This underestimation could be from the assumption that the drainage system is in well function 100% without any blockage of inlets in the model simulation. Without inlet blockage, the flooded water could flow faster into the drainage system and reduces the flood flow on the ground surface area. In actual condition, inlets might be blocked by some garbage or the existing drainage system is deteriorated due to superannuated age.

The last two points are flow depth in Beoung Trabek drainage channel produced by rainfall event 40.4 mm. The simulated flow depth (Figure 5-23 (c)) overestimated the depth of the observed data (Figure 5-22). This overestimation could be caused from setting up high initial flow in channel which is a parameter with high uncertainty.

The flooding depth of simulated results are closed to that caused by rainfall events 103 mm and 40.4 mm. However, the simulated flood depth of event 86.5 mm is much lower than that of photo visualization. The overall regression plot between photo flood depth and simulated flood depth for all 8 points is illustrated in Figure 5-24. The R^2 is found to be 0.93 which implies that photo flood depth and simulated flood depth has high linear correlation. From the Figure 5-24, there are only 4 significant positive correlation between photo and simulated flood depth while the difference of other 4

points are still large. The locations of 4 points with large error are in channel and along the channel. This implies that the main reason of large error is likely to be the overflow of stagnant water from the channel. As discussed earlier, there is no overflow from the channel banks in the simulation while it was reported that channel busts its banks during the rainfall event of total depth 73.5 mm corresponding to 2-year return period (Seangly and Amelia, 2013).
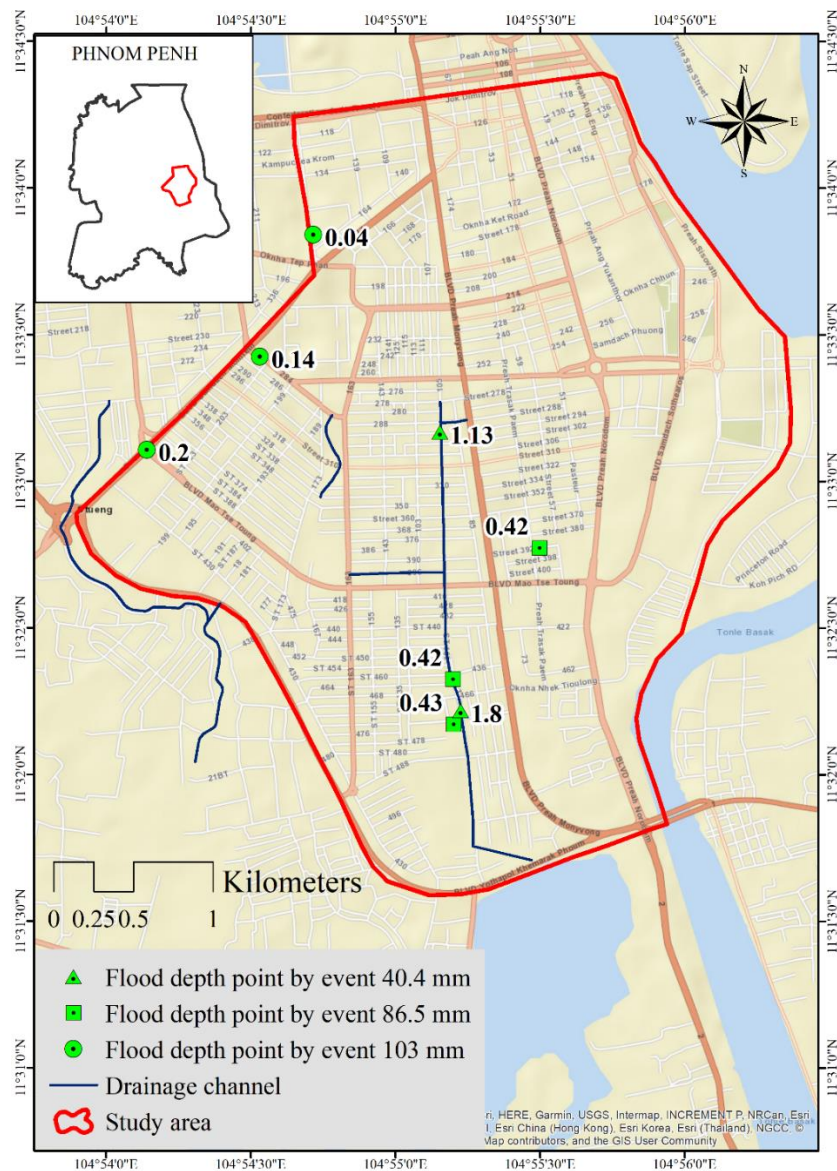

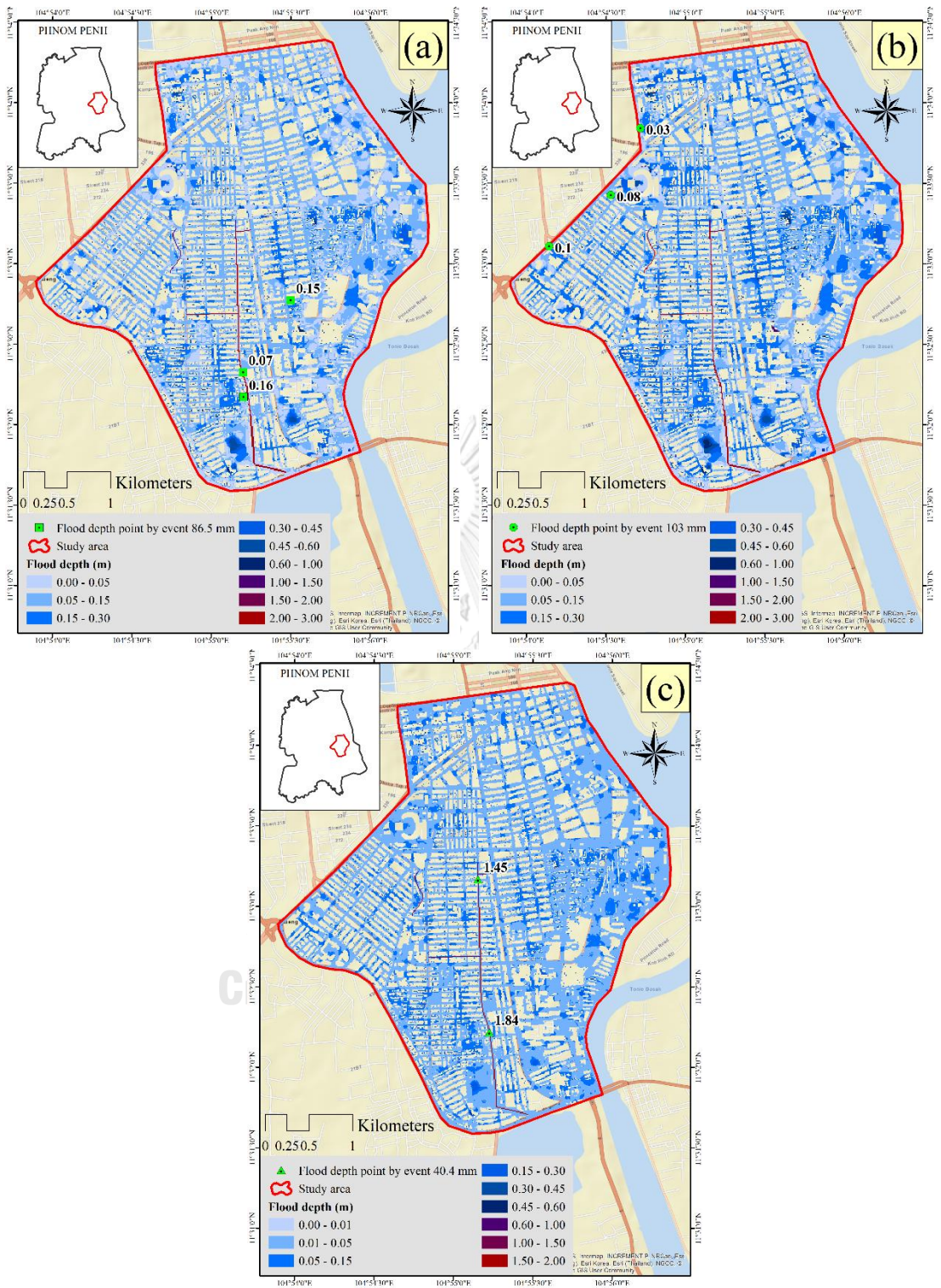Figure 5-22: Flood depth points obtained from photo visualization based on three different events

Figure 5-23: Simulated results of flood extent and flood depth points by

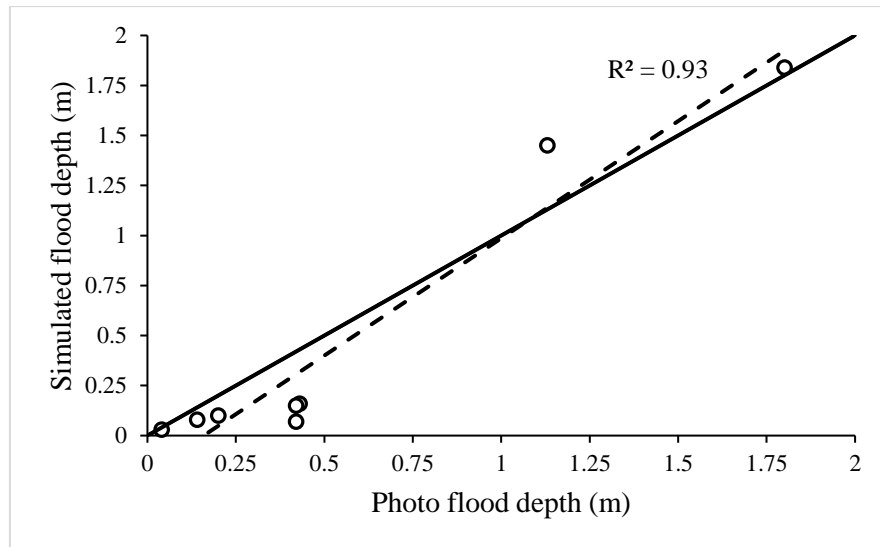(a) event 86.5 mm (b) event 103 mm and (c) event 40.4 mm

Figure 5-24: Regression relationship between Photo flood depth and simulated flood depth for 8 points

In summary, the results of calibration for both methods provide an acceptable agreement between observed and simulated results. Therefore, FLO-2D can be confirmed to be applicable to simulate flood situation in Phnom Penh with different magnitude of extreme rainfall events.

5.7 Computation of flood depth

After the model calibration, FLO-2D model is used to simulate flood inundation for 2, 5, 10, and 25-year return period. The flood inundation for 2-year and 5-year return periods were performed to observe the performance of the drainage system while the simulation of flood inundation for 10-year and 25-year return periods were performed to detect the flood situation when rainfall is extreme than drainage capacity.

The maximum flood depth of simulated results under 4 different magnitudes of rainfall events are illustrated in Figure 5-25. It shows that rainfall event with higher return period lead to higher flood depth. For instance, the area around Beoung Trabek High School (A9) indicates the change of flood depth in terms of the rainfall return periods. It can be seen clearly that the flooding area under medium category of 5-year return period spreads larger than that of 2-year return period. Similarly, the flooding area under medium category of 10-year return period results in spreading wider than

that of 5-year return period. In the case of 25-year return period, some parts of the medium category in 10-year return period is developed to high category.
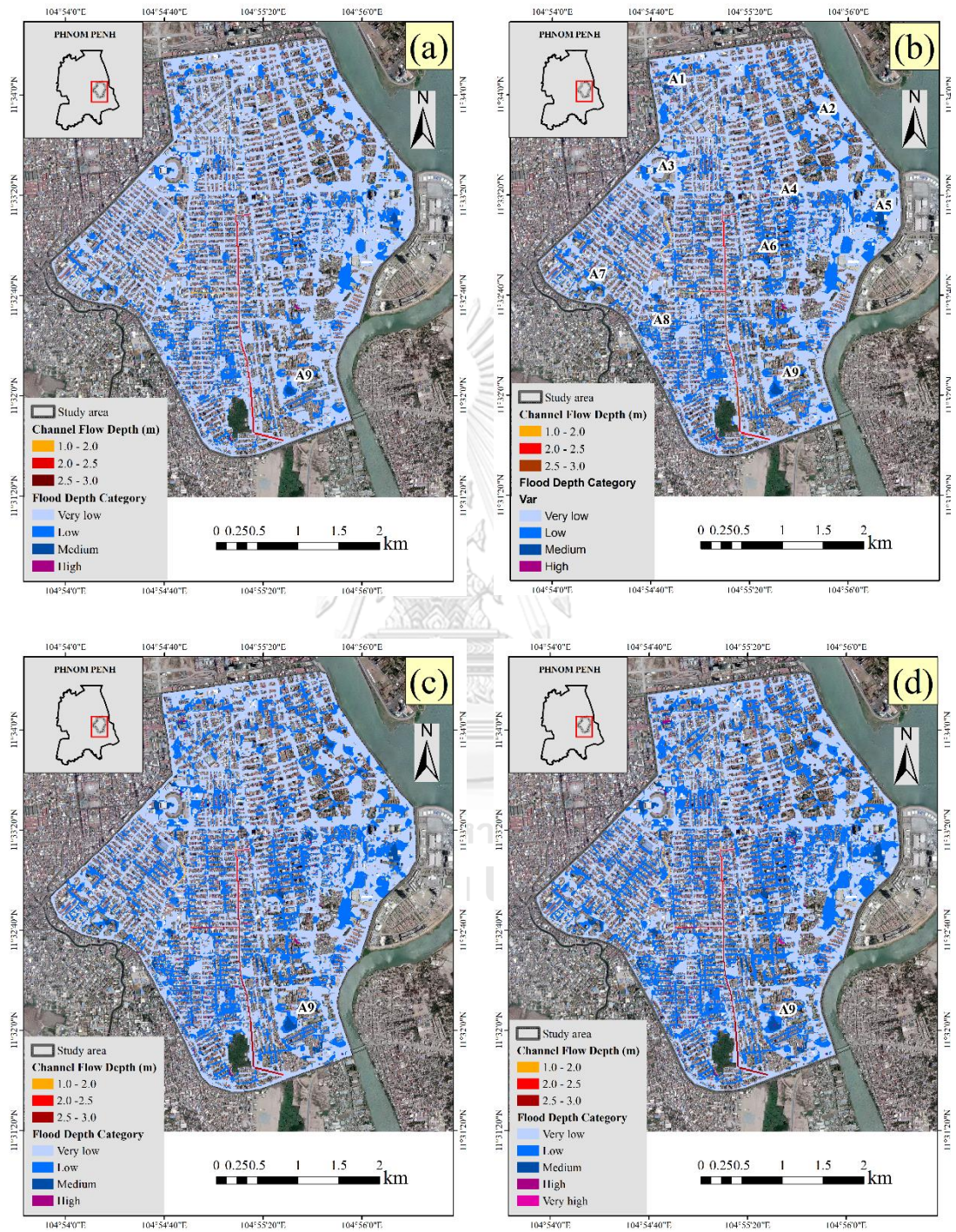

Figure 5-25: Maximum flood depth maps under (a) 2-year (b) 5-year (c) 10-year and (d) 25-year return period

Table 5-13 shows the inundation area of different flood depth categories under 4 different return periods. The inundation areas are 77.1%, 20.5%, 2.0%, and 0.3%, respectively for the depth categories of Very Low, Low, Medium, and High under 2-year return period rainfall event. When rainfall event for 25-year return period is simulated, some parts of the inundation area under Very Low category corresponding to 2-year return period has developed to more severe categories: Low 39.2%, Medium 3.4%, High 1.2% and remains 56.2% as Very Low category.

The results from the model in Table 5-14 show that the spatial distribution of flooding areas tends to moderately increase with higher return periods. Note that, the total study area is 12.5 km^2; however, only flood-prone area of 8.25 km^2 is considered for the determination of the percentage of inundation area. This is because the remaining 4.25 km^2 was set up in the model as Area Reduction Factor (ARFs) where water was completely blocked to those grids.

Table 5-13: Flooding area percentage for flood depth category under different return periods

Flood depth category	Depth (m)	Flooding area percentage (%)			
		2-yrs	5-yrs	10-yrs	25-yrs
Very Low	0.00 - 0.10	77.1	68.1	62.6	56.2
Low	0.10 – 0.30	20.5	28.8	33.6	39.2
Medium	0.30 – 0.60	2.0	2.4	2.8	3.4
High	0.60 – 1.20	0.3	0.7	1.0	1.2
Very high	> 1.20	0.0	0.0	0.0	0.0

Table 5-14: Results of flooding area from the model (the grids are counted as flooding area grids when the water depth is greater than or equal to 0.1 m)

Return period (T)	Flooding area (km^2)
2-year	1.89
5-year	2.63
10-year	3.08
25-year	3.61

From the simulated result of the 2-year and 5-year return period rainfall events (Figure 5-25 (a) and (b)), it was found that the flooding areas are dominantly covered by the flood depth of Very Low and Low category with the depth ranges from 0 m to 0.3 m. According to JICA (2011), it stated that after implementing the project Phase 1 to Phase 3 the flood depth was expected to be around 0.2 m for 2-year and 5-year return period. Note that, the drainage system improvement project implemented by JICA was designed with 2-year return period rainfall event for the pipe networks while 5-year return period was designed for pumping stations and drainage canals. Therefore, the simulated results tend to be reasonable which confirm that the drainage system is capable to cope with hazard of flood depth for 2-year and 5-year return period. Yet, it is observed that there are some noticeable locations representing by points A1 to A9 which are affected from the flood depth ranging from 0.3 m to 0.6 m (medium category) under 5-year return period. Those locations are Kompuchea Krom Boulevard and the street 134 (A1), areas around Royal Palace (A2), areas around Olympic Stadium (A3), areas in Sangkat Boeng Kengkang Ti Mouy (A4 and A6), the National Assembly Street (A5), areas around Khmer Soviet Friendship Hospital (A7), the street 430 and 450 (A8), and area around Beoung Trabek High School (A9). This depth category is starting to disturb the daily life of the citizens and causes the difficulties to vehicle movement. The flood depth is caused by the difference in topographic, and sewer system response of those areas.

From the simulated results of the 10-year and 25-year return period rainfall events, the flood depth of Low category increases while Very Low category decreases.

Based on the Table 5-13, the interesting aspect is Very Low category develops into be more intense categories such as Low, Medium and High. Therefore, it is expected that with higher return periods, the flooding area is expanded and there will be a remarkable increase in flooding areas of the serious categories of flood depth: Medium, High, and Very High.

Another important aspect is the water level in the channel. For all 4 scenarios of rainfall events, the water level in Beoung Trabek channel (Figure 5-26) does not exceed the channel height of 3.0 m. This result implies that there is no overflow from the channel bank to floodplain surface areas. In contrast, according to the news of the Phnom Penh Post (Seangly and Amelia, 2013) published on 10 October 2013, it stated that there was floodwater spilled out from the channel and spread on the street with the water depth around ankle. In addition to the news, the historical rainfall data from Ministry of Water Resources and Meteorology (MOWRAM) indicated that the total rainfall depth for that event is 73.5 mm corresponding to 2-year return period. This implies that the model underestimates the water level in channel. The underestimation of the model might be caused by the following factors:

- The effect of the garbage in the channel: in the model, this factor was not considered for setting up while it was the main factors affecting to the flow characteristics e.g. water depth and velocity. Moreover, the garbage was also the main factor indirectly affected to pumping operation by blocking water at the garbage screen and not allow to be pumped.

- The effect of the hydraulic structures along the channel: in the model, there were no hydraulic structures (culverts, bridges,) set up due to a lack of structure data.
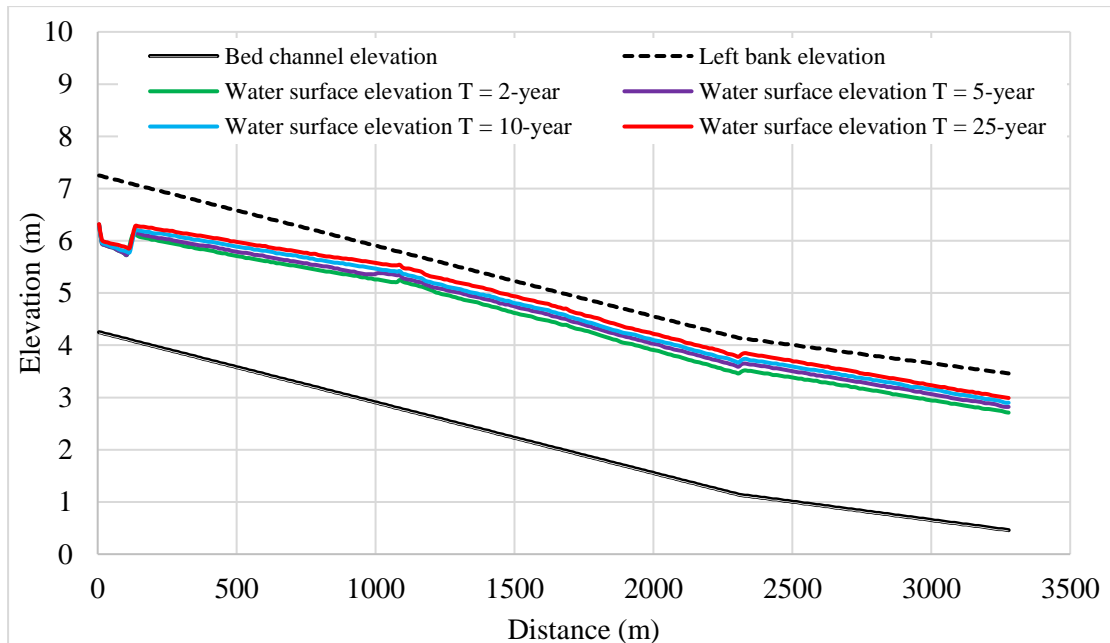
Figure 5-26: Simulated water surface elevation in Beoung Trabek channel for all return period

In summary to the result of flood depth hazard, it indicates that flood extent area is moderately increased with higher return periods of rainfall events. The degree of flood depth is more intense with increasing return period.

5.8 Computation of flood duration

As mentioned in the methodology, the flood duration was determined by overlaying three flood depth maps: rising flood map, peak flood map, and receding flood map. Each map of various return periods is illustrated in APPENDIX G. The duration of the flooding is classified into 4 categories: very short duration, short duration, medium duration, and long duration. The term "very short duration" refers to duration for the area which is insignificant effected by flooding, but this area is confronted with the flooding. The term "short duration" refer to the area where the flood occurs only during peak or high intensity, but the flooding is completely drained within 6 hours after rainfall, while the term "medium duration" refer to the area where the flood starts occurring during the peak and it cannot be drained within 6 hours after rainfall event. The last term is "long duration" which refers to the area that flooding

occur since the beginning of rainfall and it cannot be drained within 6 hours after rainfall.

From the simulated results of flood duration maps for 2-year and 5-year return period (Figure 5-27 (a) and (b)), it is clear that most areas are dominantly covered by the flood duration of very short category followed by short, medium, and long duration respectively. It can be seen from the result in Table 5-15 that the flood prone area corresponding to 2-year return period, 88% (very short and short category) and 5-year return period, 82.6% can be completely drained within 6 hours. It implies that the drainage system in Phnom Penh is capable to drain water for most of the flood prone area in the study area. However, there are few areas which are affected by medium duration for both return period such as: areas around Bak Touk Hight School (B1), Royal Palace (B2), Olympic stadium (B3), National Assembly Street (B4), the corner of Samdach Sothearos Boulevard and Tonle Bassac Park street (B5), Khmer Soviet Friendship Hospital (B6), the street 430 and 450 (B7), and Boeung Trabek areas (B8 and B9). For the simulation of 5-year return period, it is noted that most of the flooding areas having medium duration for 2-year return period become long duration category.

From the simulated results of flood duration maps for 10-year and 25-year return period (Figure 5-27 (c) and (d)), it is apparent that the flooding areas are dominantly covered by the category of very short duration. Results from Table 5-15 shows that rainfall event with higher return period lead to increasing in flooding area under medium duration. This can be seen in the case of flooding area under medium duration for 2-years return period in comparison to that for other return periods. The case of 2-year return, the flooding area under medium duration is 8.5% and it increases to 11.9% for 5-year return period, 16.0% for 10-year return period and 21.6% for 25-year return period. In contrast to flooding area under medium duration, the flooding area under very short duration gradually declines. This can be illustrated briefly in Table 5-15, the flooding area under very short duration decrease from 77.1% for 2-year return period to 56.2% for 25-year return period.
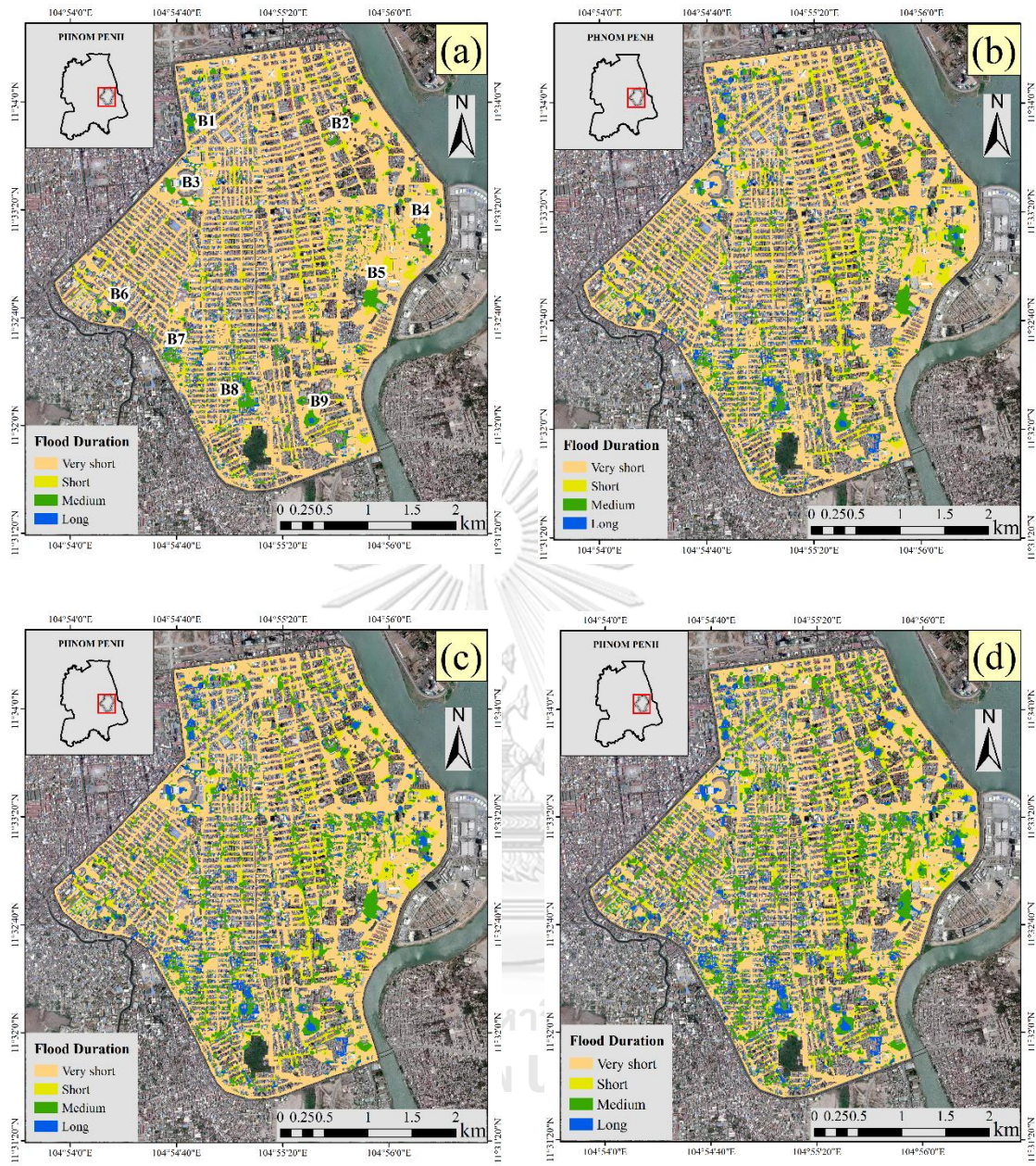
Figure 5-27: Flood duration category maps under (a) 2-year (b) 5-year (c) 10-year and (d) 25-year return period

Table 5-15: Flooding area percentage for flood duration category under different return periods

Flood duration category	Flooding area percentage (%)			
	2-yrs	5-yrs	10-yrs	25-yrs
Very short	77.1	68.1	62.6	56.2
Short	10.9	14.5	14.5	14.3
Medium	8.5	11.9	16.0	21.6
Long	3.5	5.6	6.8	7.9

Turning to flooding areas of very duration category, it has a slight increase from 2-year return period to 25-year return period. When the return period is higher, the flooding areas under very long duration marginally expand. This could be due to low elevation of those area and insufficient capacity of drainage system.

5.9 Development of flood hazard

The severity of flood hazard is divided into five categories such as: very low hazard, low hazard, medium hazard, high hazard, and very high hazard. The flooding areas categorized in very low hazard are considered as areas having insignificant damage and insignificant difficulties for daily lives. For low hazard category, the flooding affects and disturb the citizens for livelihood, however, the damage is minor since the citizens are able to adapt to that hazard category. In medium hazard category, the damage of the properties is moderate, and it is struggling for the transportation on the road. For the high hazard category, the damage is extensive due to high flood depth or long duration of flooding. The last category is very high hazard which the damage is particularly high, and it is likely to harm people lives.

The spatial distribution of each hazard category for 4 different return periods of rainfall is illustrated in Figure 5-28 and the results of flooding area percentage of each hazard category are presented in Table 5-16. It is apparent from results that the floodplain under very low hazard category is constantly the highest one among all categories. For 2-year return period, the hazard categories following very low hazard, are low, medium, and high hazard respectively. For the simulation of other return periods, very low hazard category is followed by medium, low, high and very high

hazard category, accordingly. It is observed that medium hazard category notably increases. The change in flooding area percentage between very low, low hazard category and other categories is conversely different. This can be seen in Table 5-16 that the flooding area in very low hazard category is 77.4% for 2-year return period and it decreases to 56.2% for 25-year return period while the other categories (medium, high, and very high) gradually increase when the return period is higher.
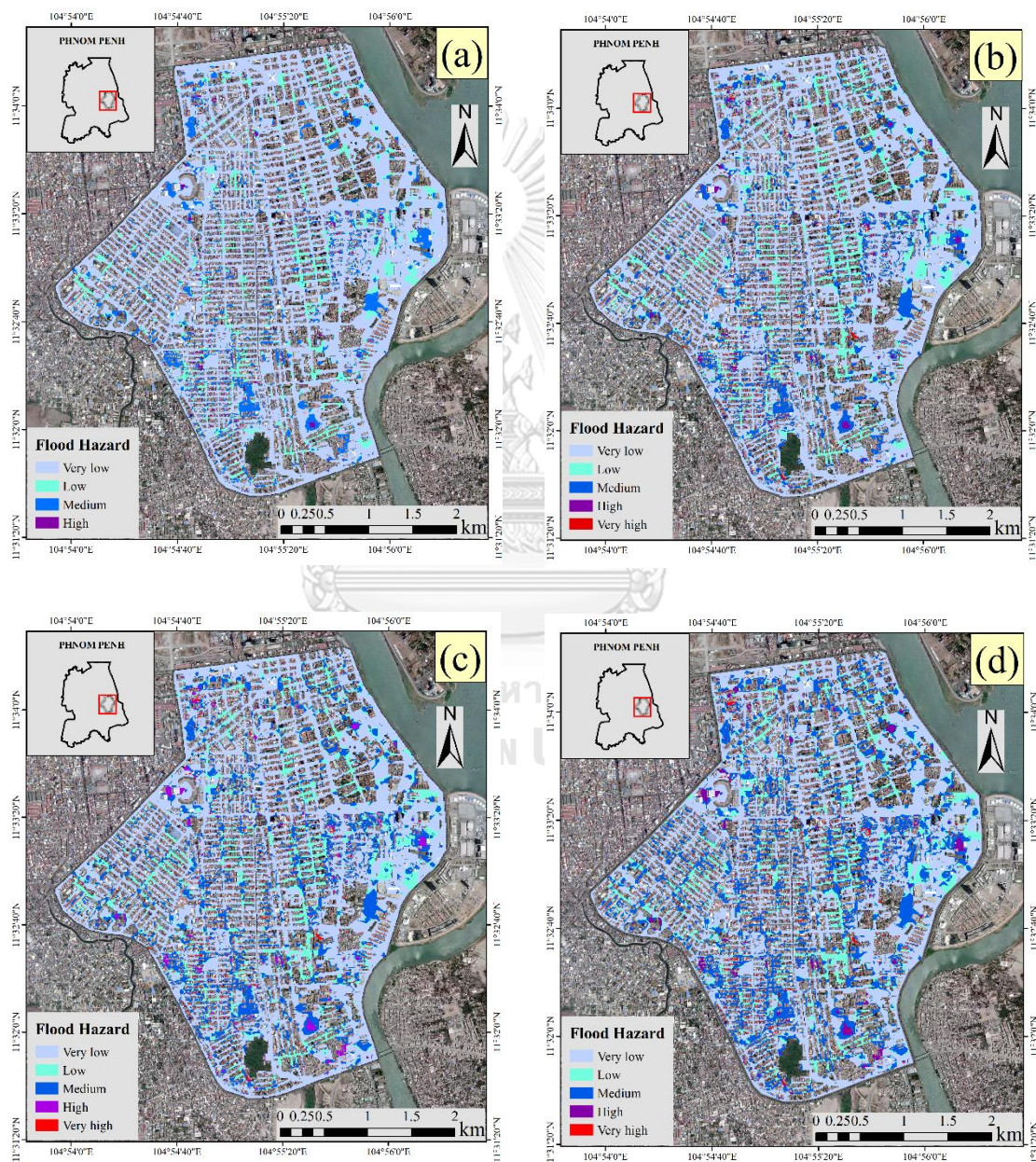

Figure 5-28: Flood hazard category maps under (a) 2-year (b) 5-year (c) 10-year and (d) 25-year return period

Table 5-16: Flooding area percentage of each hazard category under different return periods

Flood hazard category	Flooding area percentage (%)			
	2-yrs	5-yrs	10-yrs	25-yrs
Very low	77.4	68.1	62.6	56.2
Low	10.9	14.5	14.5	14.3
Medium	10.3	15.1	19.9	25.9
High	1.4	1.6	1.9	2.3
Very high	0.0	0.7	1.0	1.2

From the result for 2-year return period, it is noted that the floodplain is vulnerable to hazard ranging from very low to high. Yet, the flooding area under very high hazard category is starting to occur for other return periods (5-, 10-, and 25-year return period) causing harm to human lives.

5.10 Summary

According to results above, it shows that the drainage system implemented by JICA is able to cope with the flood for 2-year return period. For 5-year return period simulation, it is found that the hazard of flood depth is minor. However, some main locations are likely to be affected by flood duration. Starting from 10-year and 25-year return period, the significant flood hazard occurs and harm to the citizens. According to the result, it is beneficial to the policy maker and the urban planner to consider on renewal and maintenance of drainage system in some inundation areas. Moreover, investing in structural measures such as constructing more detention basin or ground storage are possibly able to reduce the water level in the inundation area.

CHAPTER 6
CONCLUSIONS AND RECOMMENDATIONS

6.1 Conclusions

The main goal of this study was to assess the flood hazard based on two parameters: the hazard of flood depth and flood duration in the urban micro-scale flood hazard in Phnom Penh capital. FLO-2D model was selected to simulate the flood inundation in the selected study area for 2-year, 5-year, 10-year, and 25-year return periods. FLO-2D model was successfully calibrated based on two methods: with time series data, and flood extent and flood photo visualization. With the flood hazard methodology developed using the combination of flood depth and flood duration, quantifying of flood hazard in the study area was conducted and conclusions could be made as follows:

1. The result of flood simulation corresponding to 2-year return period indicates that there is not significant hazard for both parameters: flood depth and flood duration in the selected study area. For most area, the flood depth ranges from 0.0 m to 0.30 m and it is completely drained within 6 hours after rainfall event. Thus, it can be concluded that the drainage system implemented by JICA is capable to cope with flooding of 2-year return period.

2. The result of flood simulation corresponding to 5-year return period shows that some main locations are affected by flood duration. This is because pipeline network designed with 2-year return period rainfall event, takes long time to convey the flood water to sewer channel or underground reservoirs.

3. There is no overflow from sewage channel bursting its banks to the ground surface in case the drainage system works 100% of design flow capacity and pumping stations work normally with full capacity as simulation.

4. It is found that the flooding area moderately increases with higher return periods of rainfall events which causes more serious hazard (higher flood depth and longer flood duration) to the study area.

These findings in this study contribute in several ways to our understanding of the degree of hazard for different locations in study area and provide a basis information how the drainage system responds to the heavy rainfall in terms of flood depth and flood duration.

6.2 Recommendations

After conducting this study, some recommendations in terms of data improvement and future study are suggested as follows:

1. For data improvement

    a. Installing more rainfall gauges with higher time resolution to study the rainfall characteristics in urban area.

    b. The filed survey of the hydraulic structures (culverts, and bridge) and channel-section along the channels should be conducted to verify the flow in channel.

    c. Estimating of wastewater in the drainage system should be done.

2. For future study

    a. Improving model accuracy using higher spatial and temporal rainfall data, adding hydraulic structures, improving means of validation when more data is accessible

    b. Modeling effects of changes, such as climate change, expansion of urban area, on flooding to support the implementation of preventive measures.

    c. Assessing vulnerability by considering urbanization, population density, and land-use types for dealing with floods to offer better prioritization to the areas that are relatively highly vulnerable.

REFERENCES

Arrighi, C., Brugioni, M., Castelli, F., Franceschini, S. & Mazzanti, B. 2013. Urban micro-scale flood risk estimation with parsimonious hydraulic modelling and census data. *Natural Hazards and Earth System Sciences,* Vol. 13, pp. 1375-1391.

Birkmann, J., Garschagen, M., Mucke, P., Schauder, A., Seibert, T., Welle, T., Rhyner, J., Kohler, S., Loster, T. & Reinhard, D. 2014. World risk report 2014. Alliance Development Works,

United Nations University.

Burrel, B. C., Davar, K. & Hughes, R. 2007. A review of flood management considering the impacts of climate change. *Water International,* vol. 32, pp. 342-359.

Butler, D. & Davies, J. 2004. *Urban drainage*, Spon Press.

Capital, P. P. 2012. Urban poor assessment. *A Baseline Survey on the Social and Economic Situations and Capacity of Existing Services in Urban Poor Communities.* Phnom Penh Capital.

Chhinh, N. & Millington, A. 2015. Drought monitoring for rice production in Cambodia. *Climate,* 3, 792-811.

Chow, V. T. 1959. *Open-channel hydraulics*, McGraw-Hill New York.

Commission, E. 2007. Directive 2007/60/EC of the European Parliament and of the Council on the assessment and management of flood risks. European Commission Brussels, Belgium.

CR-PRIP Team, C. R. f. P. R. I. P. 2015. Loan 2839-CAM (SF)/ 8254-CAM and Grant 0278-CAM Project

Climate Resilience for Provincial Road Improvement Project. *In:* TRANSPORT, M. O. P. W. A. (ed.).

DHI 2017a. MIK 21 Flow model, hydrodynamic module user guide. Danish Hydraulics Institute.

DHI 2017b. MIKE 11 - A modelling system for rivers and channels: reference manual. Danish Hydraulics Institute.

DHI 2017c. MIKE FLOOD 1D-2D Modelling, user manual. Danish Hydraulics Institute.

Finn, H., Storm, B., Richaud, B., Klinting, A. & Gasc, A. 2018. Flood Forecasting and Water Management System for Thailand. *Advances in Hydroinformatics.* Springer.

Green, W. H. & Ampt, G. 1911. Studies on Soil Phyics. *The Journal of Agricultural Science,* vol. 4, pp. 1-24.

Hammond, M. J., Chen, A. S., Djordjević, S., Butler, D. & Mark, O. 2015. Urban flood impact assessment: A state-of-the-art review. *Urban Water Journal,* vol. 12, pp. 14-29.

Heng, S., Kheav, K., Chhuon, K., Ly, S. & Tsuyoshi, K. 2017. Urban flood modeling in Phnom Penh using Flo-2D. *Energy connectivity, environment, and development.* Asian Institute of Technology.

Heng, S., Ly, S., Chhem, S. & Kruy, P. 2016. Analysis of public perceptions on urban flood in Phnom Penh, Cambodia. *Water Security and Climate Change: Chanllenges and Opportunities in Asia.* Asian Institute of Technology, Bangkok, Thailand.

Hsu, M. H., Chen, S. H. & Chang, T. J. 2000. Inundation simulation for urban drainage basin with storm sewer system. *Journal of Hydrology,* vol. 234, pp. 21-37.

Huang, Y., Chen, S., Cao, Q., Hong, Y., Wu, B., Huang, M., Qiao, L., Zhang, Z., Li, Z. & Li, W. 2013. Evaluation of version-7 TRMM multi-satellite precipitation analysis product during the Beijing extreme heavy rainfall event of 21 July 2012. *Water,* vol. 6, pp. 32-44.

Huong, H. & Pathirana, A. 2013. Urbanization and climate change impacts on future urban flooding in Can Tho city, Vietnam. *Hydrology and Earth System Sciences,* vol. 17, pp. 379-394.

Ivan, M. 2014. *The Risks of Hazard* [Online]. Intermap. Available: http://www.intermap.com/risks-of-hazard-blog/three-common-types-of-flood-explained [Accessed 31 October 2014].

Jacobson, C. R. 2011. Identification and quantification of the hydrological impacts of imperviousness in urban catchments: A review. *Journal of Environmental Management,* vol. 92, pp. 1438-1448.

JICA 1999. The study on drainage improvement and flood control in the municipality of Phnom Penh. Japan International Cooperation Agency.

JICA 2001. Basic design study report on the flood protection and drainage improvement project in the municipality of Phnom Penh in the Kingdom of Cambodia. Japan International Cooperation Agency.

JICA 2011. Preparatory survey report on the project for flood protection and drainage improvement in the phnom penh capital city (phase iii) in the Kingdom of Cambodia. Japan International Cooperation Agency.

JICA 2016. The study on drainage and sewerage improvement project in Phnom Penh metropolitan area. Japan International Cooperation Agency.

JICA 2017. Preparatory survey report on the project for flood protection and drainage improvement in Phnom Penh (phase iv) in the Kingdom of Cambodia. Japan International Cooperation Agency.

Keokhumcheng, Y., Tingsanchali, T. & Clemente, R. S. 2012. Flood risk assessment in the region surrounding the Bangkok Suvarnabhumi Airport. *Water International,* vol. 37, pp. 201-217.

Kimmarita, L. 2019a. *PP gov't to clean capital's canal* [Online]. The Phnom Penh Post. Available: https://www.phnompenhpost.com/national/pp-govt-clean-capitals-canal [Accessed 01 March 2019].

Kimmarita, L. 2019b. *Youths band together to clean 'filthy' Boeung Trabek canal* [Online]. The Phnom Penh Post. Available: https://www.phnompenhpost.com/national/youths-band-together-clean-filthy-boeung-trabek-canal [Accessed 15 March 2019].

Komori, D., Nakamura, S., Kiguchi, M., Nishijima, A., Yamazaki, D., Suzuki, S., Kawasaki, A., Oki, K. & Oki, T. 2012. Characteristics of the 2011 Chao Phraya River flood in central Thailand. *Hydrological Research Letters,* vol. 6, pp. 41-46.

Kvočka, D., Falconer, R. A. & Bray, M. 2016. Flood hazard assessment for extreme flood events. *Natural Hazards,* vol. 84, pp. 1569-1599.

Lerner, D. N. 2002. Identifying and quantifying urban recharge: a review. *Hydrogeology journal,* vol. 10, pp. 143-152.

Liao, C.-H. & Chang, H.-S. 2011. *Explore urban flood vulnerability based on spatial pattern in Taiwan ecological city viewpoint.*

Loucks, D. P., Van Beek, E., Stedinger, J. R., Dijkman, J. P. & Villars, M. T. 2005. *Water resources systems planning and management: an introduction to methods, models and applications*, Paris: Unesco.

Luo, P., Mu, D., Xue, H., Ngo-Duc, T., Dang-Dinh, K., Takara, K., Nover, D. & Schladow, G. 2018. Flood inundation assessment for the Hanoi Central Area, Vietnam under historical and extreme rainfall conditions. *Scientific Reports,* 8, 12623.

Meg, F. 2014. The Phnom Penh survey. *In:* NORA, L. (ed.) *A Study on Urban Poor Settlements in Phnom Penh.* Sahmakum Teang Tnaut.

Molyvann, V. 2003. *Modern Khmer Cities*, Reyum.

Moriasi, D. N., Arnold, J. G., Van Liew, M. W., Bingner, R. L., Harmel, R. D. & Veith, T. L. 2007. Model evaluation guidelines for systematic quantification of accuracy in watershed simulations. *Transactions of the ASABE,* vol. 50, pp. 885-900.

MRC, M. R. C. 2010. Best practice guidlines for flood risk assessment. Mekong River Commission.

Muleta, M. K. & Nicklow, J. W. 2005. Sensitivity and uncertainty analysis coupled with automatic calibration for a distributed watershed model. *Journal of Hydrology,* 306, 127-145.

National Committee for Disaster Management, N. & United Nations Department Programme, N. 2013. Cambodia disaster loss and damage information system. National Committee for Disaster Management.

Nations United, U. 2010. *Natural hazards, unnatural disasters: the economics of effective prevention*, The World Bank.

Niemczynowicz, J. 1999. Urban hydrology and water management – present and future challenges. *Urban Water,* vol. 1, pp. 1-14.

NIS, N. I. o. S. 2017. Population projection of Cambodia 2013-2023. Ministry of Planning, National Institute of Statistics.

O'Brien, J. 2009. FLO-2D User manual, version 2009. *Nutrioso, Arizona.*

O'Brien, J. & Garcia, R. 2009. FLO-2D Reference manual. *Available from: www. flo-2d. com.*

Ozga-Zielinska, M. 1989. Droughts and floods-their definition and modeling. *New Directions for Surface Water Modelling*, pp. 313-322.

Ragab, R., Rosier, P., Dixon, A., Bromley, J. & Cooper, J. 2003. Experimental study of water fluxes in a residential area: 2. Road infiltration, runoff and evaporation. *Hydrological Processes,* vol. 17, pp. 2423-2437.

Ramier, D., Berthier, E. & Andrieu, H. 2011. The hydrological behaviour of urban streets: long-term observations and modelling of runoff losses and rainfall–runoff transformation. *Hydrological Processes,* vol. 25, pp. 2161-2178.

Ritter, A. & Muñoz-Carpena, R. 2013. Performance evaluation of hydrological models: Statistical significance for reducing subjectivity in goodness-of-fit assessments. *Journal of Hydrology,* vol. 480, pp. 33-45.

Rossman, L. 2015. SWMM 5.1 Storm Water Management Model user's manual. US Environmental Protection Agency.

Rossman, L. A. 2006. *Storm water management model, quality assurance report: dynamic wave flow routing,* US Environmental Protection Agency, Office of Research and Development, National Research Management Research Laboratory.

Salvadore, E., Bronders, J. & Batelaan, O. 2015. Hydrological modelling of urbanized catchments: A review and future directions. *Journal of Hydrology,* vol. 529, pp. 62-81.

Seangly, P. & Amelia, W. 2013. *Sewage canal bursts its banks* [Online]. The Phnom Penh Post. Available: https://www.phnompenhpost.com/national/sewage-canal-bursts-its-banks [Accessed 10 October 2013].

Segeren, W. 1983. Introduction to Polders of the World. *Water International,* 8, 51-54.

Sheebe, V. & Alka, B. 2016. Urban Heat Island: Cause for microclimate variations.

Shelby, D. 2012. Phnom Penh, city of water. *In:* NORA, L. (ed.). Sahmakum Teang Tnaut.

Singh, P., Sinha, V. S. P., Vijhani, A. & Pahuja, N. 2018. Vulnerability assessment of urban road network from urban flood. *International Journal of Disaster Risk Reduction,* vol. 28, pp. 237-250.

Takebayashi, H. & Senoo, M. 2018. Analysis of the relationship between urban size and heat island intensity using WRF model. *Urban Climate,* vol. 24, pp. 287-298.

United Nations, D. R. O. 1991. Mitigating natural disasters: phenomena, effects, and options. *Manual for Policy Makers and Planners*, pp. 34-40.

Van de Ven, F. 1990. Water balances of urban areas. *International Association of Hydrological Science*.

van den Honert, R. C. & McAneney, J. 2011. The 2011 Brisbane floods: causes, impacts and implications. *Water,* vol. 3, p. 1149.

Vozinaki, A.-E. K., Morianou, G. G., Alexakis, D. D. & Tsanis, I. K. 2017. Comparing 1D and combined 1D/2D hydraulic simulations using high-resolution topographic data: a case study of the Koiliaris basin, Greece. *Hydrological Sciences Journal,* 62, 642-656.

Vu, T. T. & Ranzi, R. 2017. Flood risk assessment and coping capacity of floods in central Vietnam. *Journal of Hydro-environment Research,* vol. 14, pp. 44-60.

Watkins, L. H. & Fiddes, D. 1984. Highway and urban hydrology in the tropics. London: Pentech Press.

Wright, D. B. 2015. Methods in flood hazard and risk assessment. The Work Bank.

APPENDIX A: Drainage system set up in the SWMM model
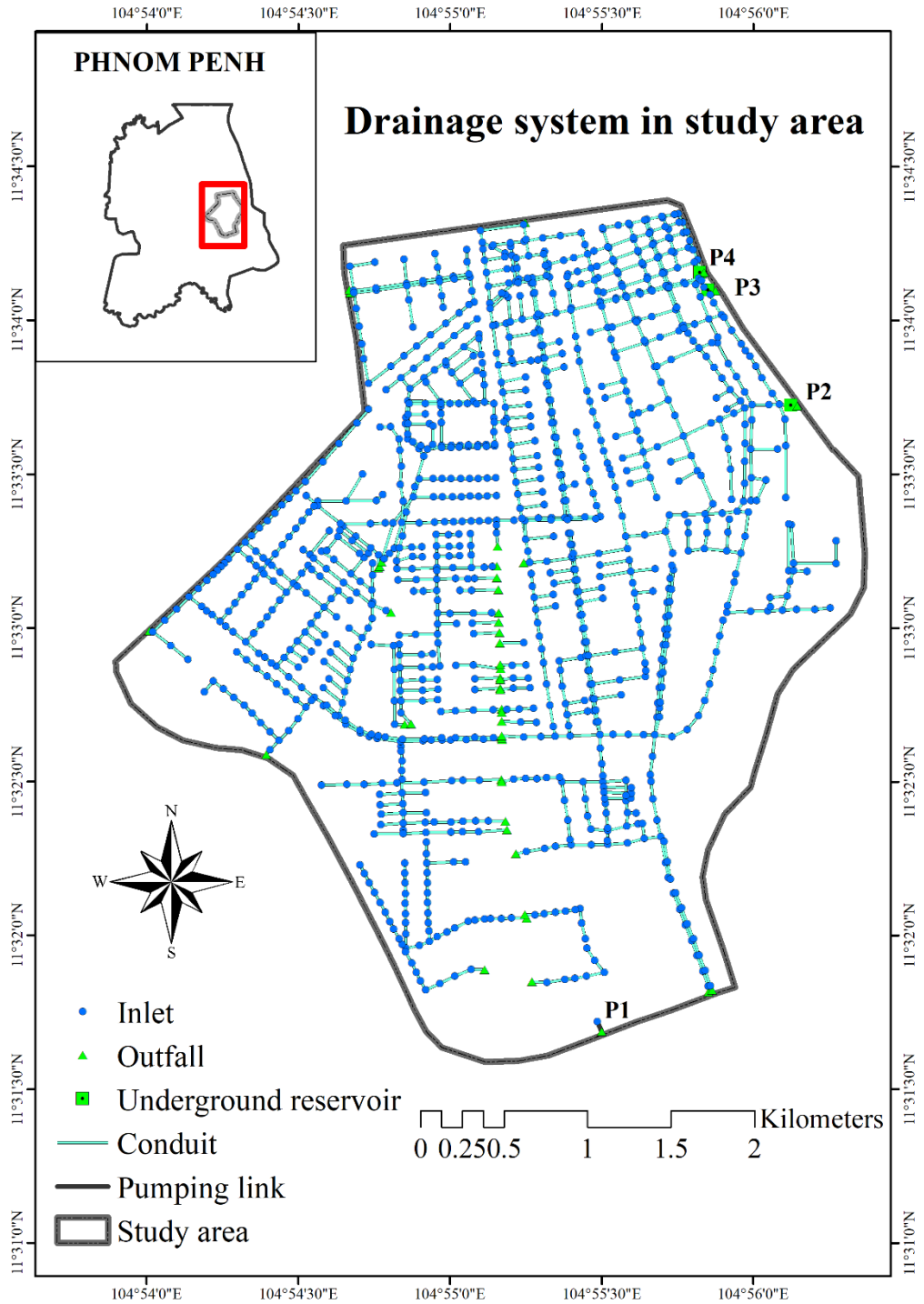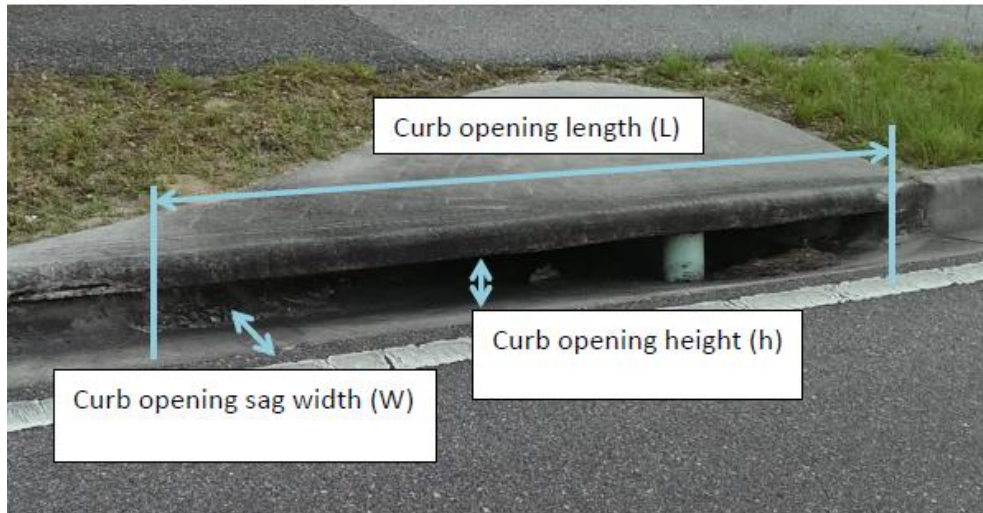
APPEXDIX B: Available inlet types allowed to set up in FLO-2D

Figure B-1: Type 2 - Curb opening inlet with sag

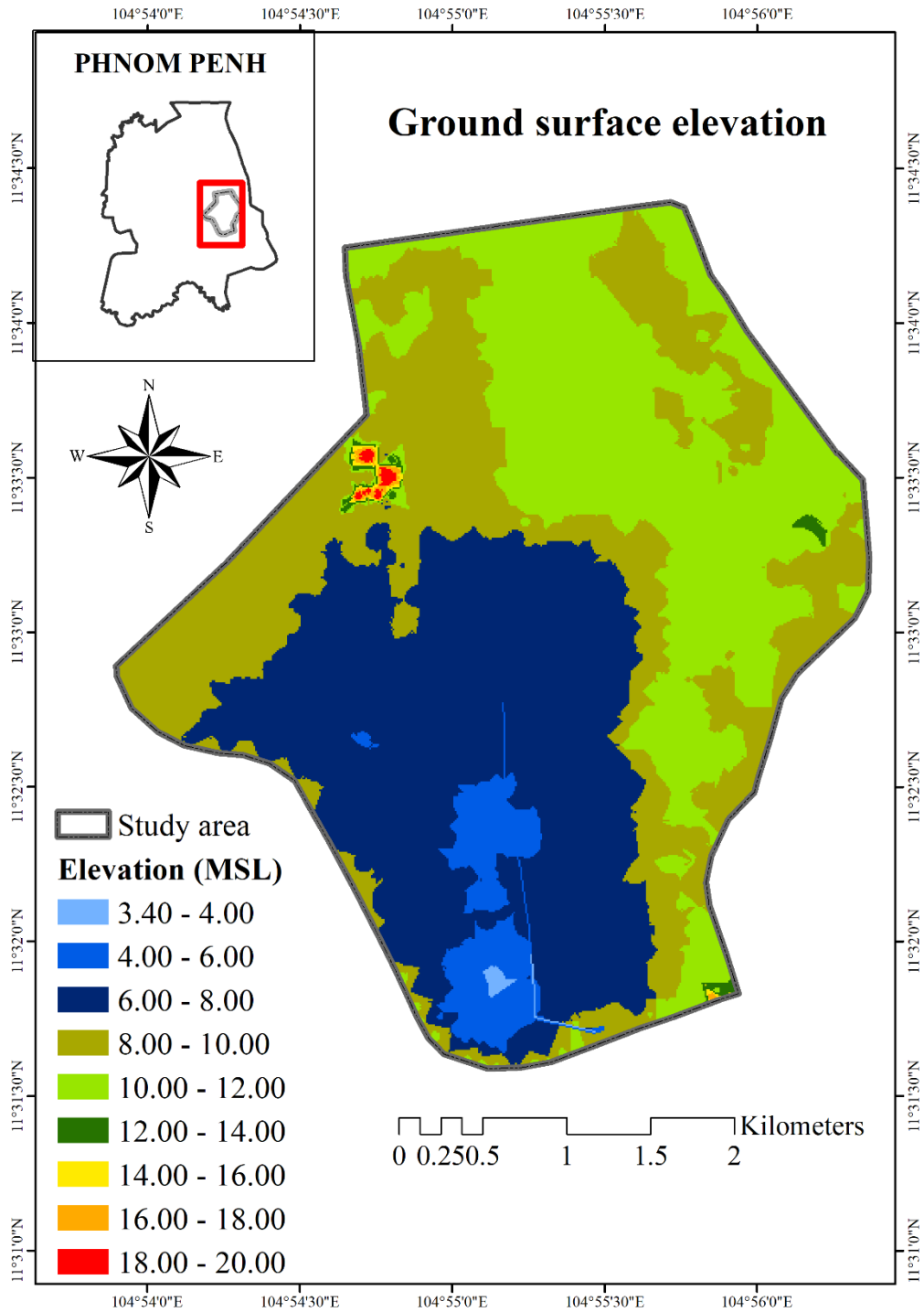Figure B-2: Type 3 - Grate inlet

Figure B-3: Type 4 - Unique inlet with stage-discharge rating table

Figure B-4: Type 5 – Manhole

APPEXDIX C: Ground surface elevation of the study area produced by GDS

Ground surface elevation

APPENDIX D: Referenced inundation photos collected from social media, Facebook

Figure D-1: The corner Monireth and Mao Tse Toung Blvd on 1st August 2015

Figure D-2: Preah Sihanouk Blvd (near Olympic stadium) on 1st August 2015

Figure D-3: Street 169 near Bak Touk High School on 1st August 2015

Figure D-4: Beoung Trabek on 3rd September 2015 at 5:20 PM

Figure D-5: Beoung Trabek (near Boeung Keng Korng market) on 3rd September
2015

Figure D-6: Boeung Trabek on 3rd September 2015

APPENDIX E: Chi square distribution table

Degree of Freedom	Probability of Exceeding the Critical Value								
	0.99	0.95	0.90	0.75	0.50	0.25	0.10	0.05	0.01
1	0.000	0.004	0.016	0.102	0.455	1.32	2.71	3.84	6.63
2	0.020	0.103	0.211	0.575	1.386	2.77	4.61	5.99	9.21
3	0.115	0.352	0.584	1.212	2.366	4.11	6.25	7.81	11.34
4	0.297	0.711	1.064	1.923	3.357	5.39	7.78	9.49	13.28
5	0.554	1.145	1.610	2.675	4.351	6.63	9.24	11.07	15.09
6	0.872	1.635	2.204	3.455	5.348	7.84	10.64	12.59	16.81
7	1.239	2.167	2.833	4.255	6.346	9.04	12.02	14.07	18.48
8	1.647	2.733	3.490	5.071	7.344	10.22	13.36	15.51	20.09
9	2.088	3.325	4.168	5.899	8.343	11.39	14.68	16.92	21.67
10	2.558	3.940	4.865	6.737	9.342	12.55	15.99	18.31	23.21
11	3.053	4.575	5.578	7.584	10.341	13.70	17.28	19.68	24.72
12	3.571	5.226	6.304	8.438	11.340	14.85	18.55	21.03	26.22
13	4.107	5.892	7.042	9.299	12.340	15.98	19.81	22.36	27.69
14	4.660	6.571	7.790	10.165	13.339	17.12	21.06	23.68	29.14
15	5.229	7.261	8.547	11.037	14.339	18.25	22.31	25.00	30.58
16	5.812	7.962	9.312	11.912	15.338	19.37	23.54	26.30	32.00
17	6.408	8.672	10.085	12.792	16.338	20.49	24.77	27.59	33.41
18	7.015	9.390	10.865	13.675	17.338	21.60	25.99	28.87	34.80
19	7.633	10.117	11.651	14.562	18.338	22.72	27.20	30.14	36.19
20	8.260	10.851	12.443	15.452	19.337	23.83	28.41	31.41	37.57
22	9.542	12.338	14.041	17.240	21.337	26.04	30.81	33.92	40.29
24	10.856	13.848	15.659	19.037	23.337	28.24	33.20	36.42	42.98
26	12.198	15.379	17.292	20.843	25.336	30.43	35.56	38.89	45.64
28	13.565	16.928	18.939	22.657	27.336	32.62	37.92	41.34	48.28
30	14.953	18.493	20.599	24.478	29.336	34.80	40.26	43.77	50.89
40	22.164	26.509	29.051	33.660	39.335	45.62	51.80	55.76	63.69
50	27.707	34.764	37.689	42.942	49.335	56.33	63.17	67.50	76.15
60	37.485	43.188	46.459	52.294	59.335	66.98	74.40	79.08	88.38

APPENDIX F: Referenced pictures of garbage and other obstruction of the flow in Beoung Trabek channel

Figure F-1: Garbage gathered in Beoung Trabek channel in Chamkarmon district's Phsar Doeum Thkov commune (Kimmarita, 2019b)

Figure F-2: Garbage and urban poor residents settled in the Beoung Trabek channel (Kimmarita, 2019a)

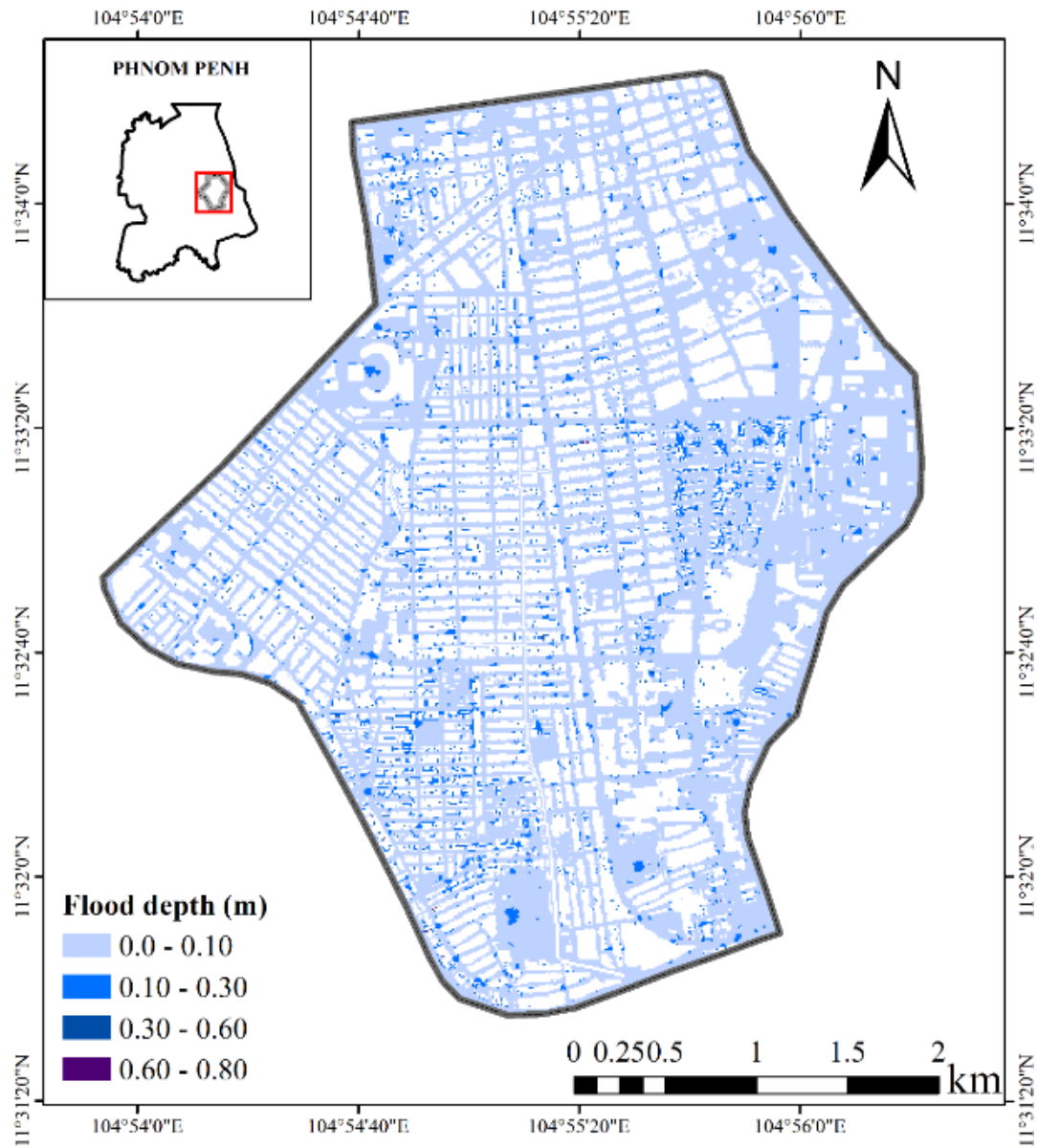**APPENDIX G: Flood depth of rising, peak, and receding flood for 2-year, 5-year, 10-year, and 25-year return period used to define the hazard of flood duration**

Figure G-1: Flood depth of rising flood for 2-year return period
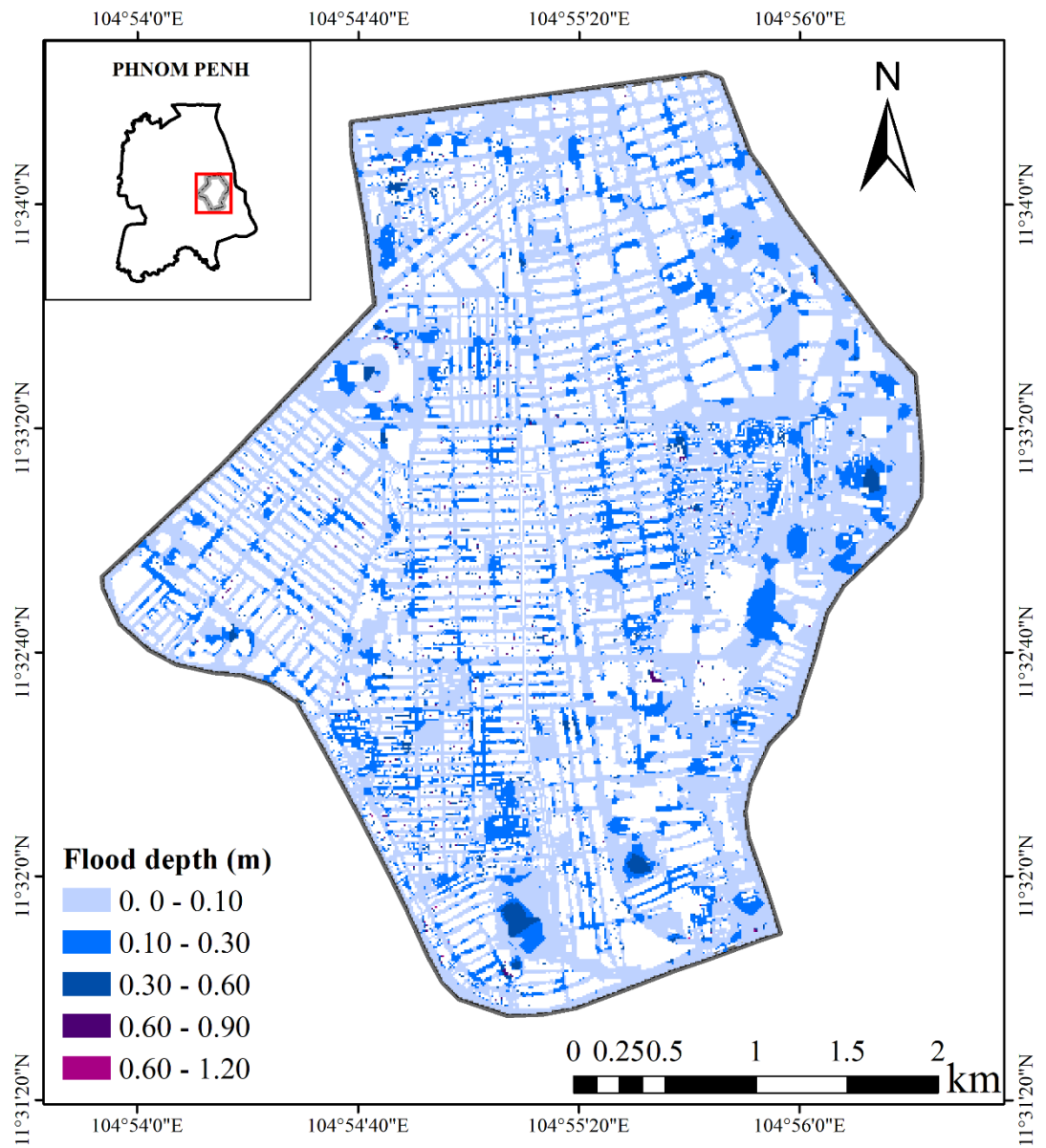
Figure G-2: Flood depth of peak flood for 2-year return period
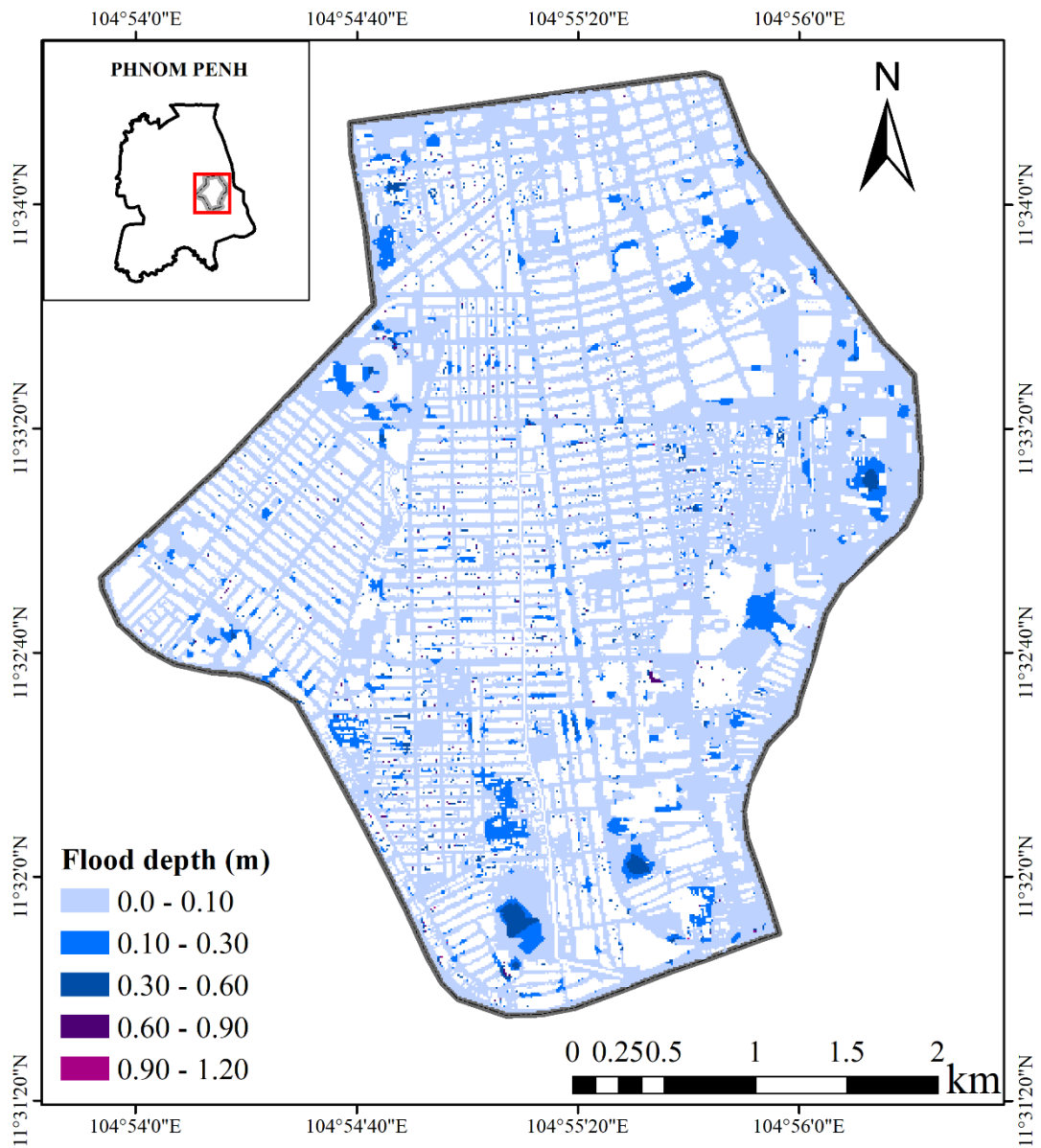
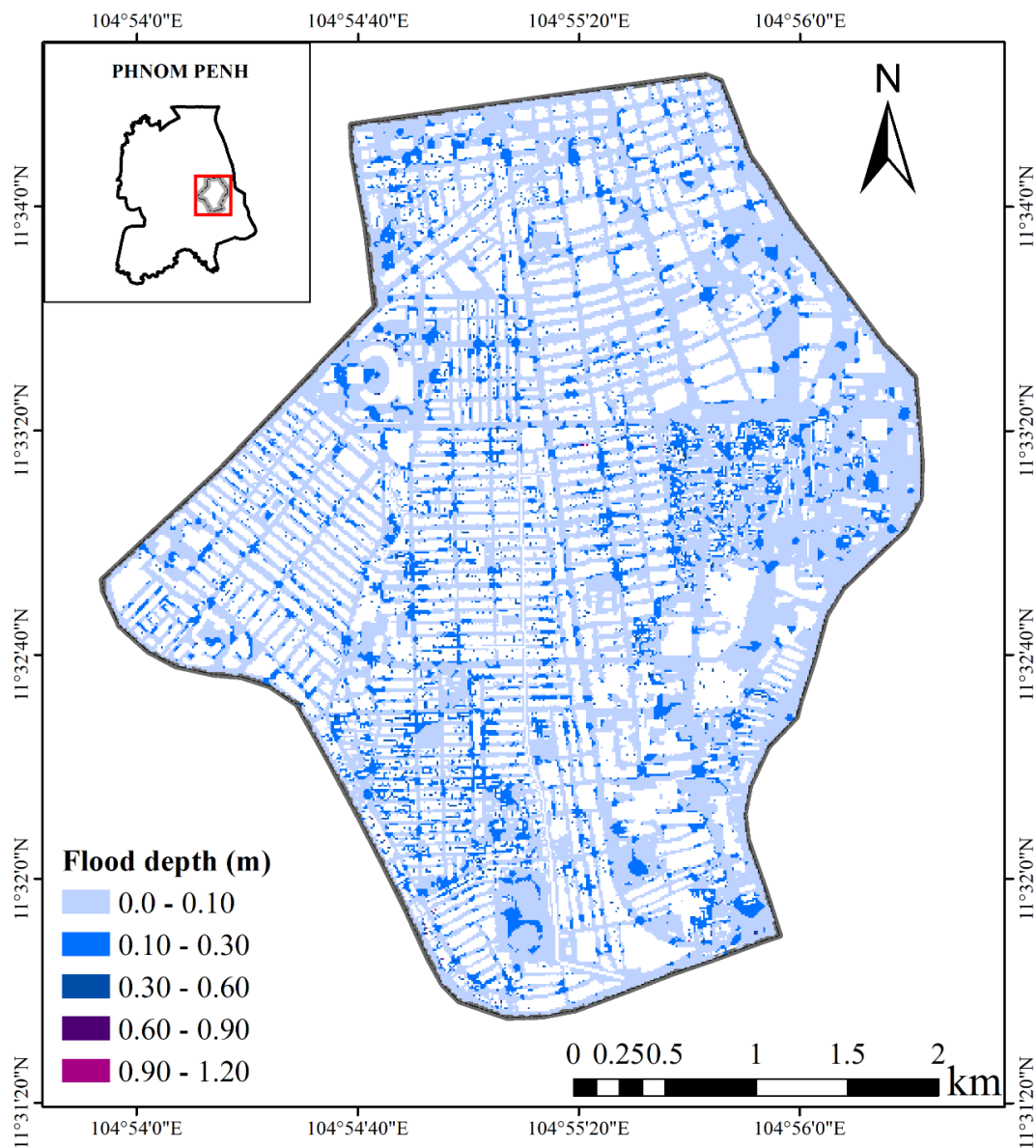Figure G-3: Flood depth of receding flood for 2-year return period
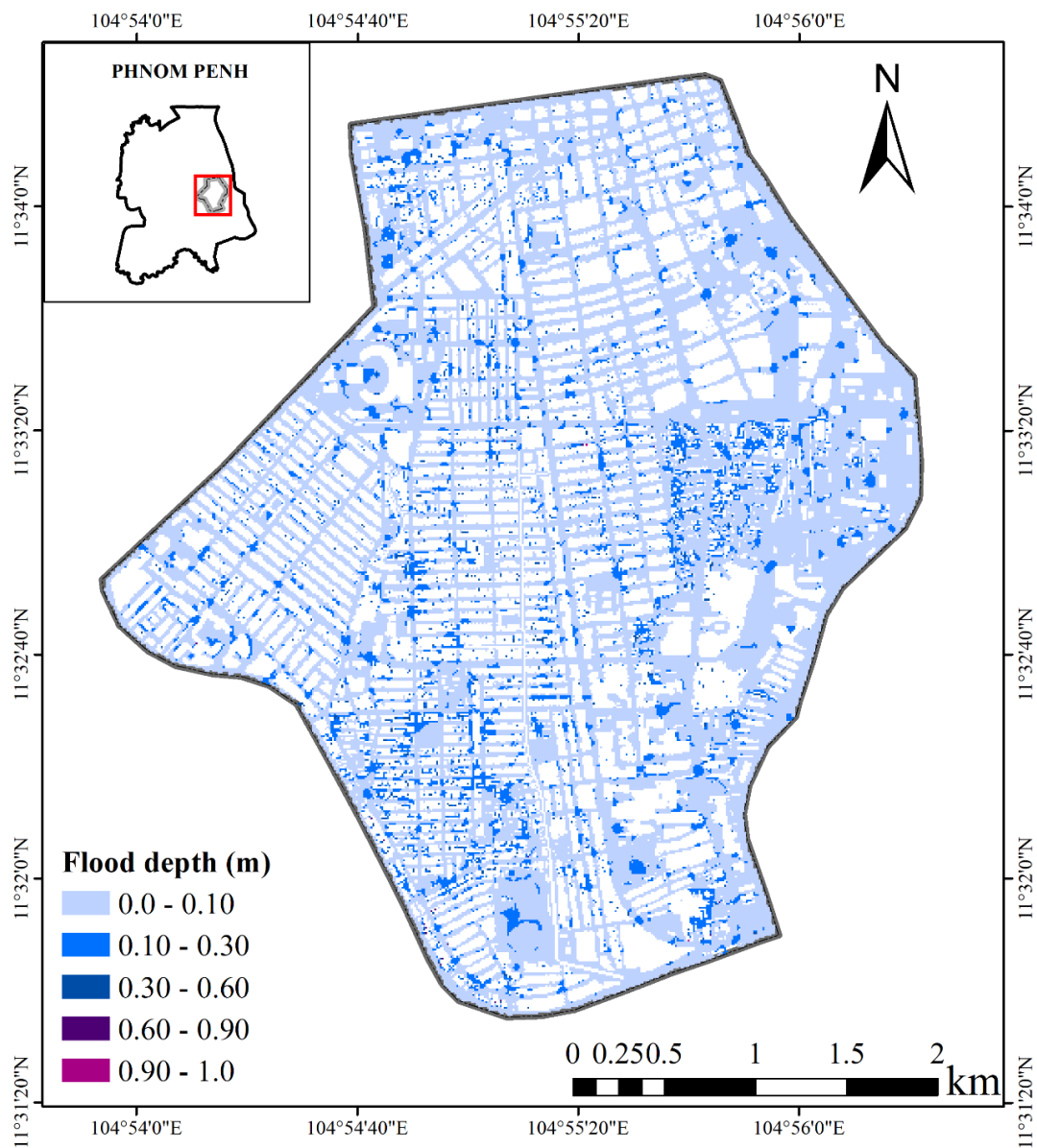
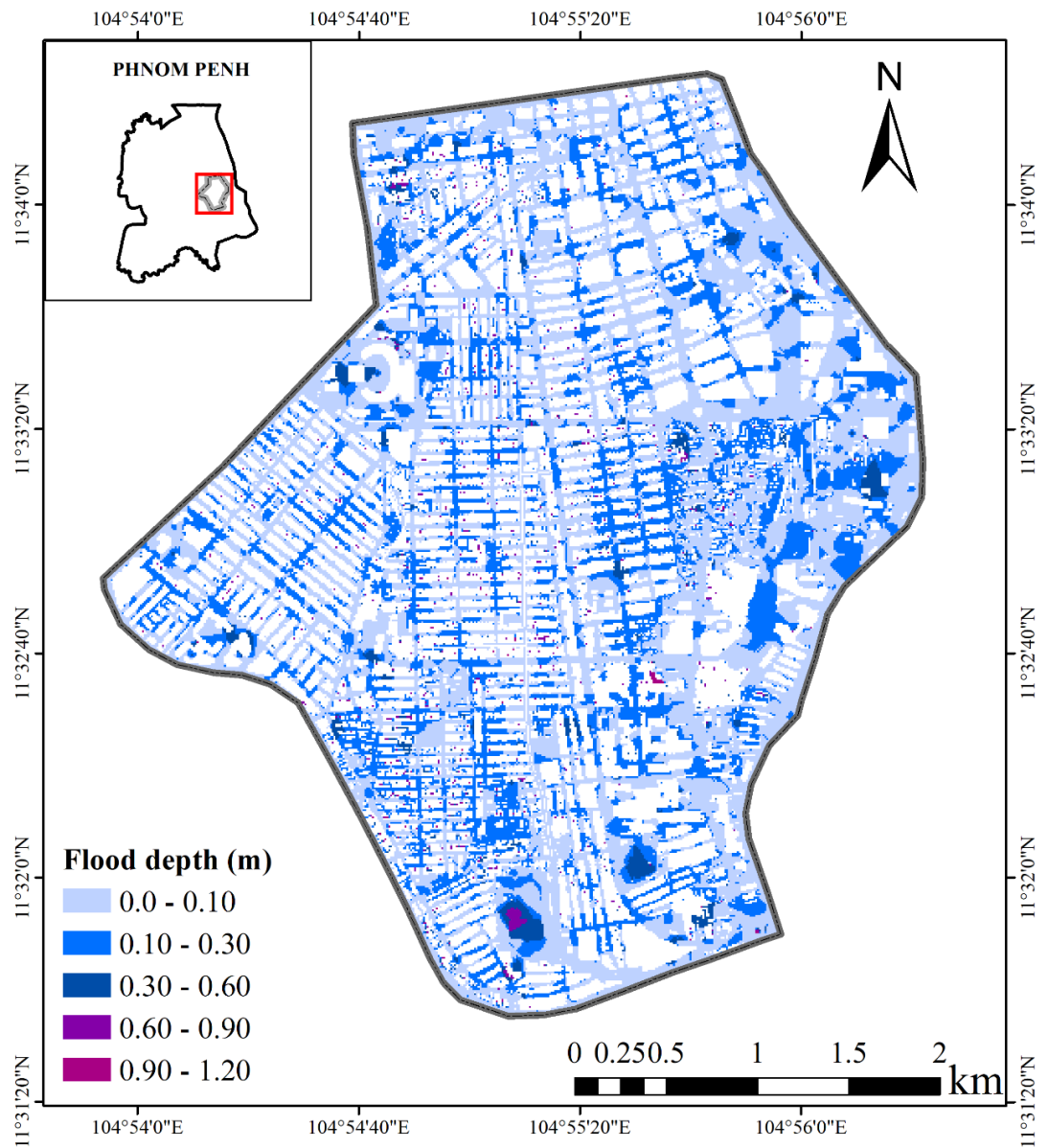Figure G-4: Flood depth of rising flood for 5-year return period
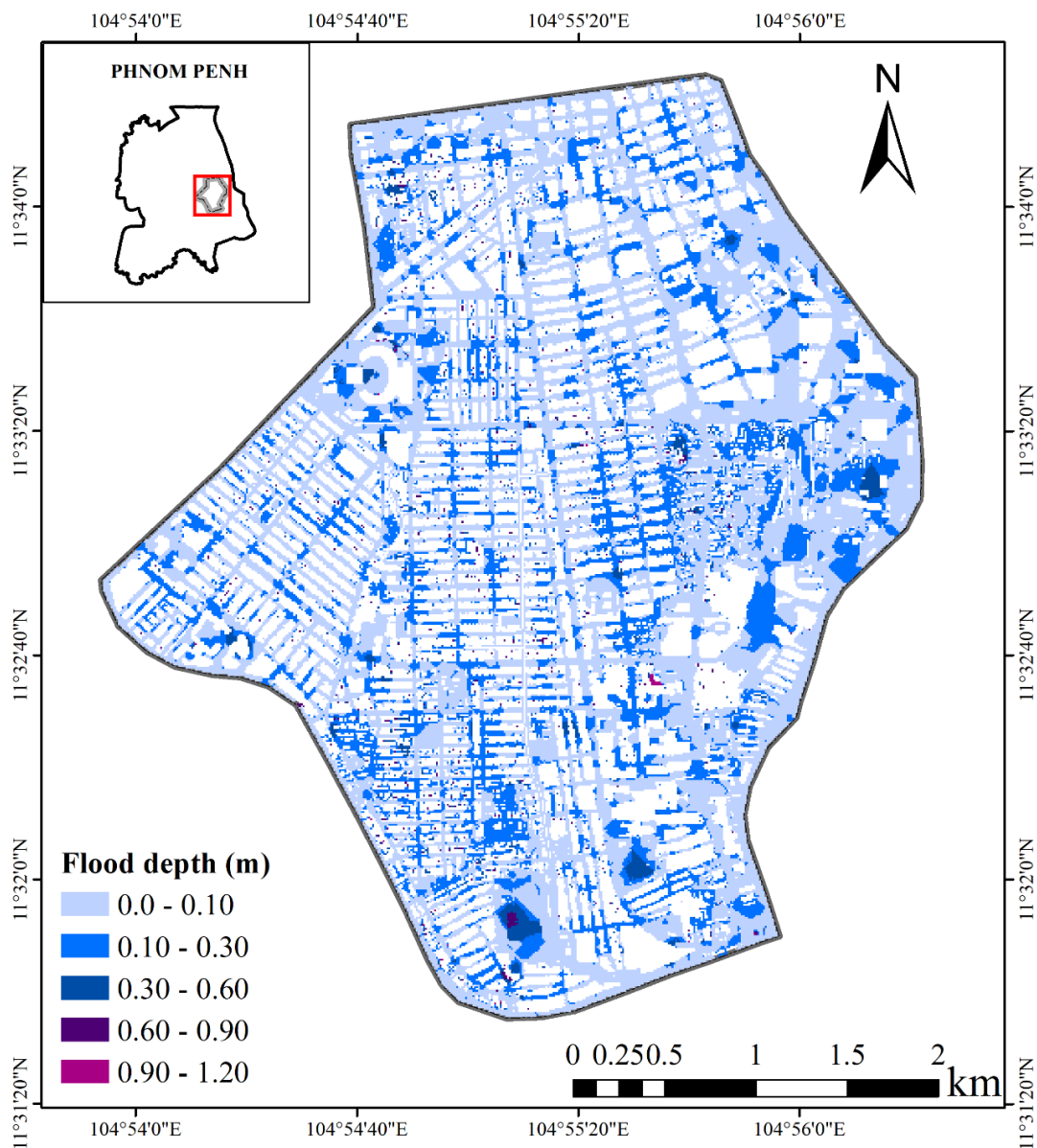
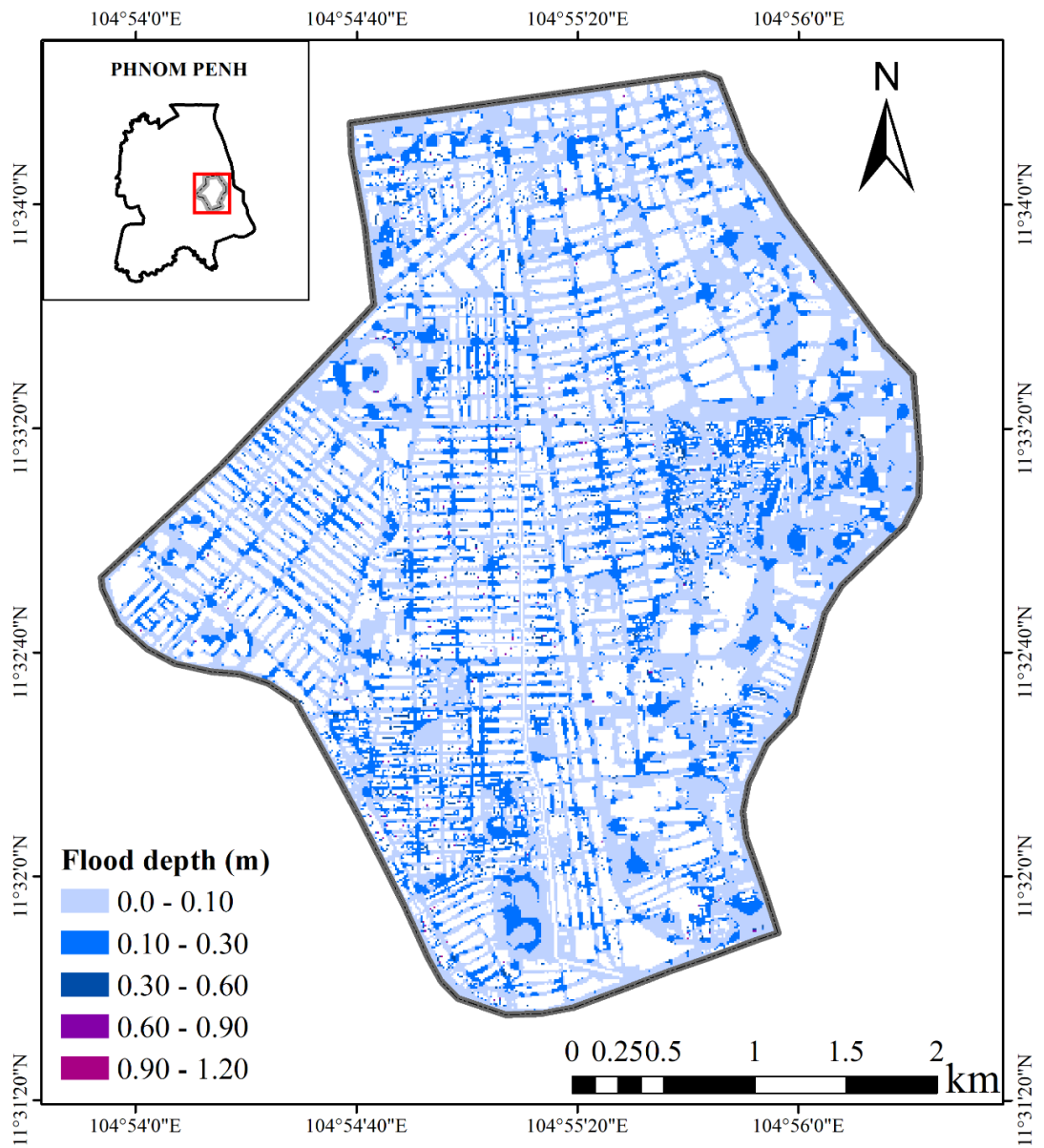Figure G-5: Flood depth of peak flood for 5-year return period
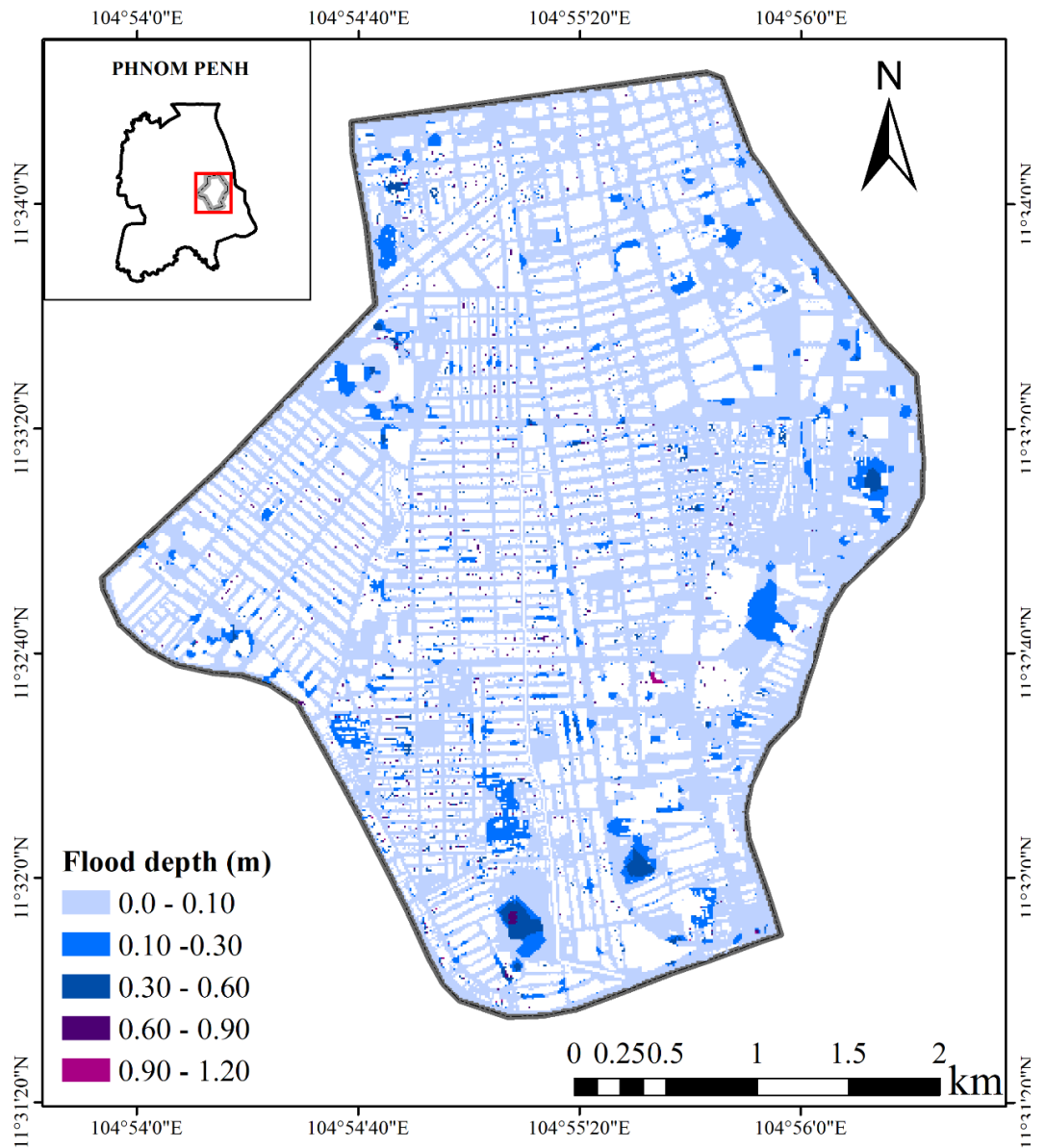
Figure G- 6: Flood depth of receding flood for 5-year return period

Figure G-7: Flood depth of rising flood for 10-year return period

Figure G-8: Flood depth of peak flood for 10-year return period

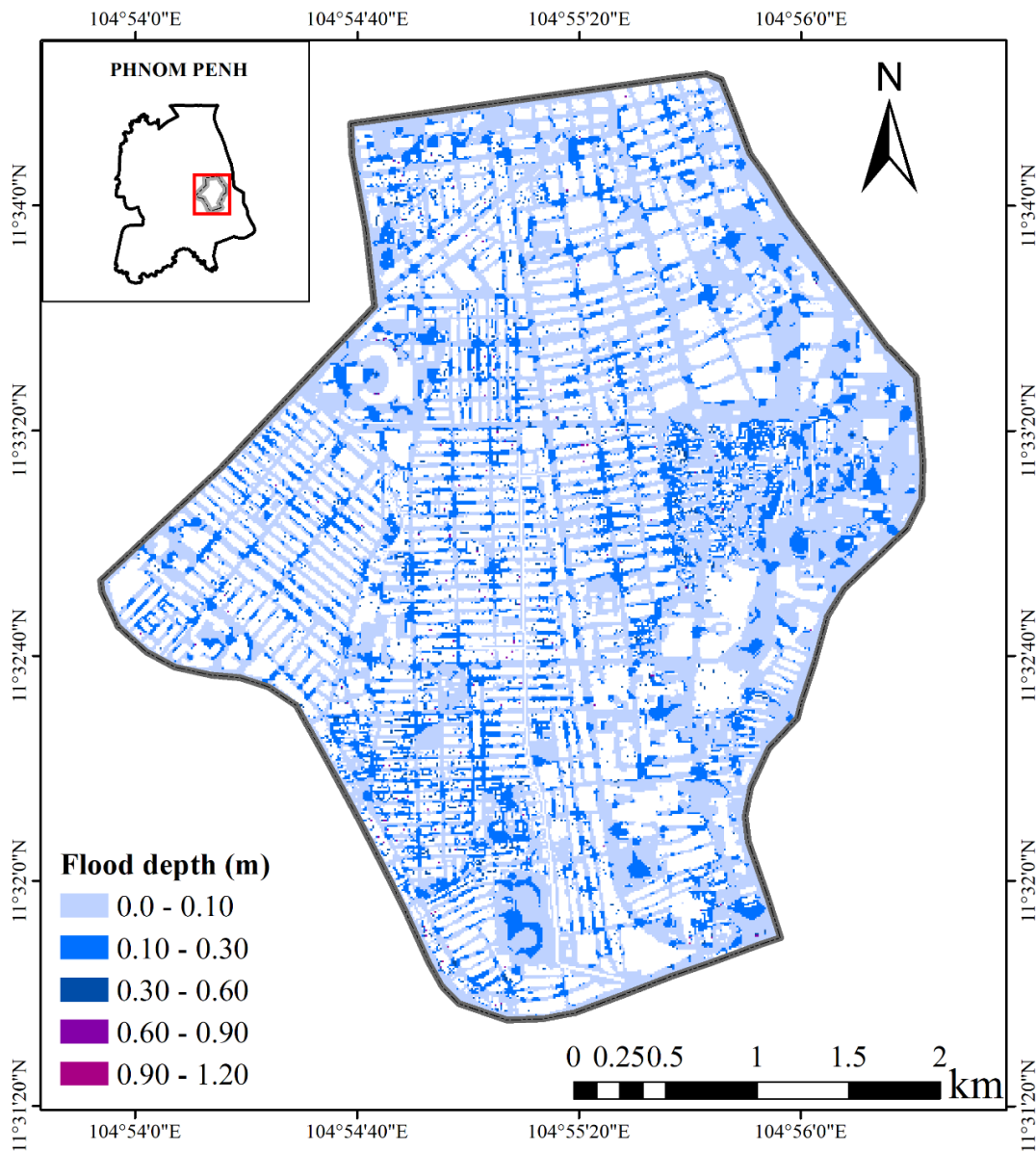Figure G-9: Flood depth of receding flood for 10-year return period

Figure G- 10: Flood depth of rising flood for 25-year return period
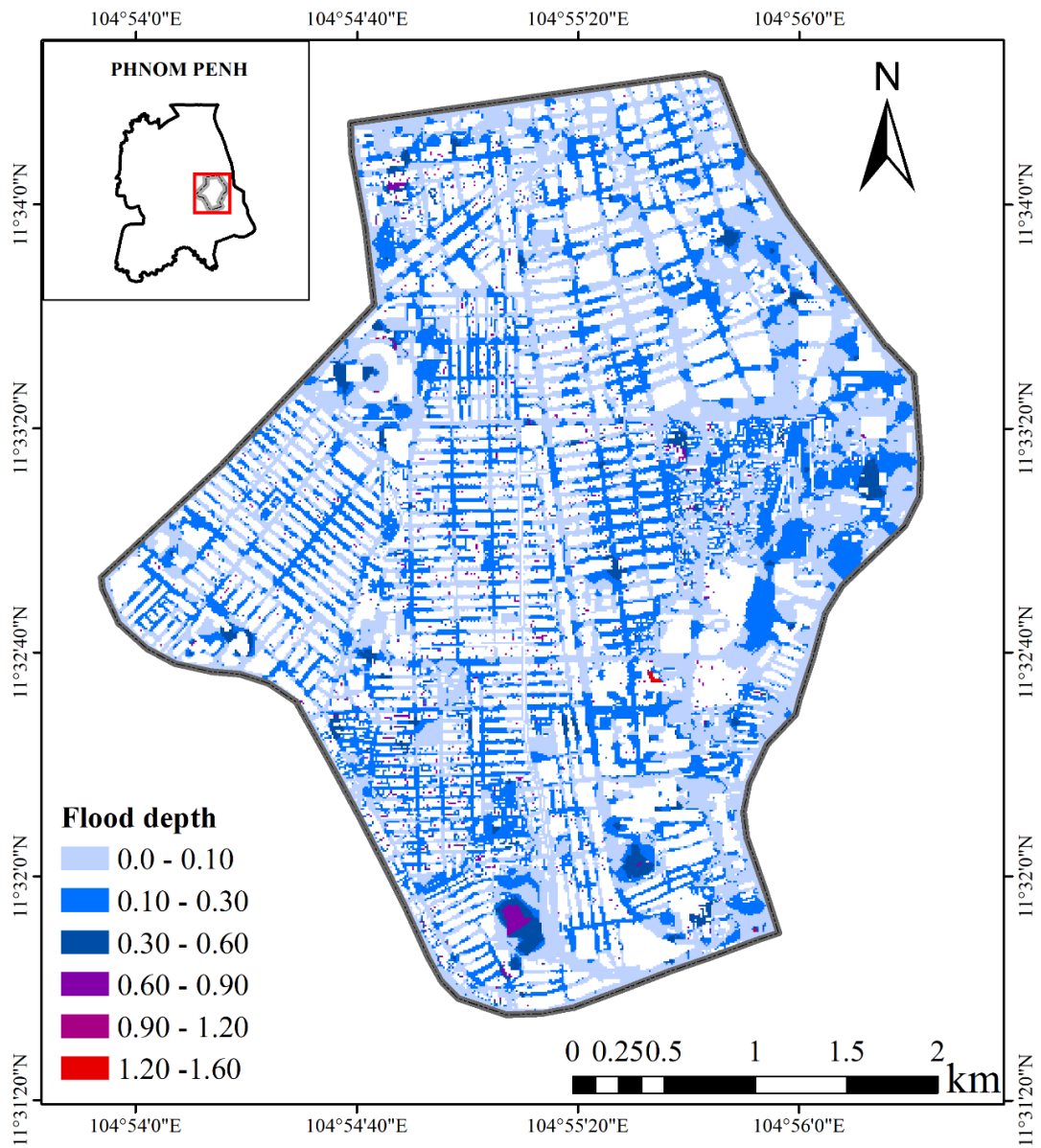
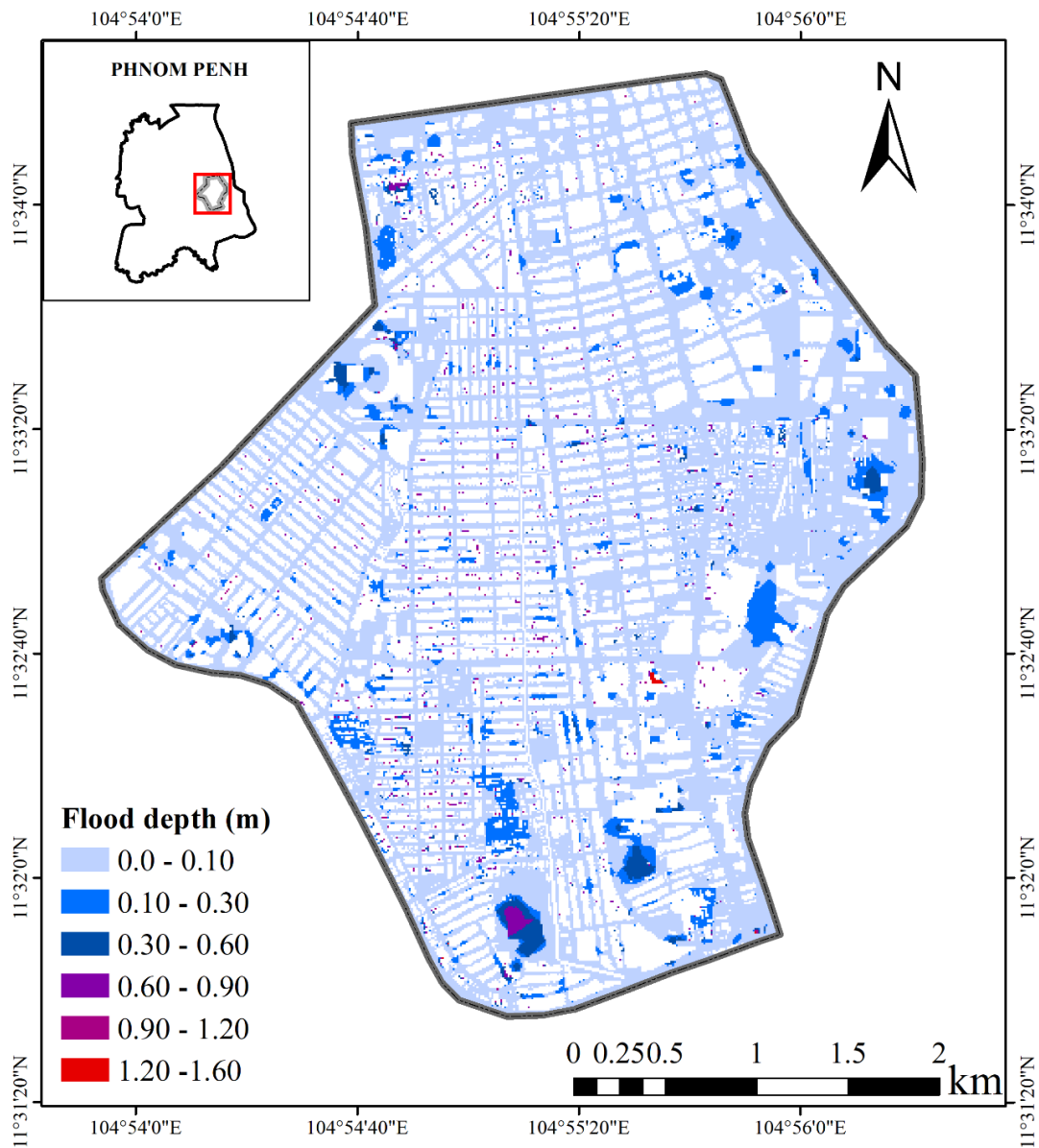Figure G-11: Flood depth of peak flood for 25-year return period

Figure G-12: Flood depth of receding flood for 25-year return period

VITA

NAME	Naichy Sea
DATE OF BIRTH	19 July 1992
PLACE OF BIRTH	Kompong Speu province, Cambodia
INSTITUTIONS ATTENDED	Institute of Technology of Cambodia
HOME ADDRESS	Trapangkhsang village, Tuol Ampil Commune, Barset District, Kompong Speu province, Cambodia
AWARD RECEIVED	Scholarship funded by Ministry of Water Resources and Meteorology and Asian Development Bank for Bechelor's Degree and scholarship Program for ASEAN Countries of Chulalongkorn University for Master's Degree

จุฬาลงกรณ์มหาวิทยาลัย
CHULALONGKORN UNIVERSITY